Carbon Nanotube Based Carbon Dioxide Gas Sensors for Respiratory Monitoring

A DISSERTATION
SUBMITTED TO THE FACULTY OF THE GRADUATE SCHOOL
OF THE UNIVERSITY OF MINNESOTA
BY

Shyam Sivaramakrishnan

IN PARTIAL FULFILLMENT OF THE REQUIREMENTS
FOR THE DEGREE OF
DOCTOR OF PHILOSOPHY

Adviser: Dr. Rajesh Rajamani

December 2009

Acknowledgements

My first thanks go to Prof. Rajesh Rajamani for making all this work possible. It is difficult to express my gratitude completely through words; but I wish to thank him particularly for rekindling my interest in scientific research. His faith and support at all times and in all ways during these five years turned me from a doubting undergraduate to a confident researcher. The innovations described in this thesis would not have happened without Prof.Rajamani's patience, guidance and motivation. Indeed, most of my learning has been outside the lab observing Prof. Rajamani at work. I feel very lucky to have experience doctoral study through the lens of Prof. Rajamani's lab.

I am also grateful to Prof. Arthur G. Erdman, Prof. Kim A. Stelson and Prof. William P. Robbins for sparing the time to serve on my thesis committee; especially knowing the limitations on their time imposed by academic responsibilities and services to the University.

We have been fortunate to collaborate with professors who have provided access to excellent research tools facilities. I am thankful to Prof. Bruce D. Johnson (Mayo Clinic, Rochester), Prof. William P. Robbins, Prof. Kent R. Mann, Prof. Ted M. Pappenfus (University of Minnesota, Morris) and Prof. Stephen A. Campbell for allowing us to use materials from their labs.

It is with great pleasure that I thank Lee Alexander for being such a wonderful resource and a great person. The final stages of this work were made possible through Lee's designs and manufacturing skills. At other stages, I have also been introduced to wireless and controller hardware by Lee. Lee has been a one-stop shop for all my design issues.

I have been very fortunate to have had great friends and colleagues in my lab-mates. My thanks go to all my labmates who have helped me at different stages of my work – Dr. Serdar Sezen, Dr. Michael Greminger, Dr. Xun Yu, Krishna Vijayaraghavan, Gurkan Erdogan, Peng Peng, Gridsada Phanomchoeng, Kalpesh Singal and Matthew Hildebrand.

A special word of thanks to Dr. Serdar Sezen who helped me make an early decision for pursuing doctoral study.

Throughout my stay in Minneapolis, I have also been fortunate to have a great group of friends. There are too many to thank; so I wish to specially mention my room-mates over the past years – Neelakantan Saikrishnan, Dr. Ramji T. Venkatasubramanian, Dr. Sriharsha Nagaraj and Krishna Vijayaraghavan. I am also extremely thankful to all friends at Chinmaya Balavihar that have treated me like a family member. All their support has been crucial to any success in this work.

Last, but not the least, I owe my biggest thanks to my family. I attribute my materials science knowledge to my brother's tutoring skills and true insight into this subject. I have been fortunate to receive all kinds of help from my parents – from career counseling, to market research and life skills. My parents and brother have been my biggest supporters and I definitely needed all their encouragement during doctoral study.

Dedication

To Prof. P. Sankaran and all my teachers

Abstract

The objective of this work is to create a new sensor for monitoring the concentration of exhaled CO_2 gas in human breath. Limitations such as high power, large size, lack of portability and undesirable use of sampling tubes are experienced currently during respiratory CO_2 monitoring. CO_2 being a very important biomarker, it is desirable to extend the scope of CO_2 monitoring beyond clinical use to home and ambulatory monitoring. Due to the vast amount of prior research effort put into currently used non-dispersive infra red (NDIR) CO_2 sensors, it was deemed unnecessary to further investigate this technique. The sensor development approach in this thesis has been creation of a solid-state CO_2 sensor through merging of state-of-the-art research in different disciplines - namely materials science, nanotechnology, chemistry, mechanical engineering and electrical engineering.

Early promise for development of such a sensor is shown by use of functionalized carbon nanotube (CNT) materials. Single-walled carbon nanotubes (SWNTs) functionalized with polyethylene imine (PEI) is used as the CO_2 sensitive material. A conductivity measurement technique using surface acoustic wave (SAW) sensors enables measurement of SWNT conductivity with very high resolution. While sensitive to CO_2, this embodiment is several times more sensitive to humidity in the environment. Since humidity variation happens simultaneously with CO_2 variation in exhaled breath, this is found not to be a viable technique for respiratory CO_2 measurement. This early failure suggested a need for a sensor that was equally or more sensitive to CO_2 than to other environmental analytes.

In looking for such an alternative sensor, a CO_2 sensor based on stiffness measurement of bare SWNTs was reported to be sensitive and selective to CO_2. However, current techniques used for film-stiffness measurement are too bulky, unreliable or expensive. Hence, a new stiffness sensing transducer is developed using an electret microphone. This stiffness measurement technique is based on the extreme sensitivity of an electret microphone’s capacitance to the stiffness of its membrane. A CO_2 sensor is obtained by

coating such a microphone with SWNTs. This embodiment shows good sensitivity to CO_2 but unpredictable response to humidity changes. While some microphones show excellent humidity resistance, others show large response to humidity. This behavior is traced to the fabrication of the microphones. Since commercial microphones are used in this work, it is not possible to control manufacturing specifications. Thus, practical difficulties with obtaining a reliable microphone are a major impediment. It was also judged that the sensitivity of stiffness changes to CO_2 might be insufficient for respiratory monitoring.

The above two sensor embodiments suggest the difficulty in obtaining a selective yet sensitive solid-state CO_2 sensor using carbon nanotubes. Hence, an alternative approach is tested using sensitive, selective but slow commercial CO_2 sensors. CO_2 sensors made using an electrolytic sensing technique are commercially sold for indoor air-quality monitoring. While reliable, such sensors are too slow for respiratory monitoring. But, development of a (second order) mathematical model for the sensor's slow response enables detection of fast CO_2 changes during breathing. This is achieved by inverting the mathematical model to predict the fast CO_2 input based on the sensor's slow output. The resulting embodiment is the first reliable respiratory CO_2 sensor developed in this work. Though better than NDIR sensors, the power requirements and size of electrolytic CO_2 sensors are still unacceptable for portable and wireless respiratory CO_2 monitoring.

Finally, based on research into CNTs and electrolytic CO_2 sensors, a new nanocomposite-material based CO_2 sensor is fabricated. This sensor combines advantages of high sensitivity and fast response of CNTs with the selectivity of metal carbonates to CO_2. The nanocomposite material is fabricated by attaching nanoparticles of calcium carbonate ($CaCO_3$) to SWNTs. CO_2 sensing is achieved by measuring the resistance of the SWNT film which changes due to the reaction between $CaCO_3$ and CO_2. Cross-sensitivity to humidity, while present, is small enough to be removed using a reference CNT sensor that does not respond to CO_2 but responds to humidity. While reliable in operation, this sensor however suffers from slow response due to chemisorption of CO_2 on some of the CNTs. Since resistance of the entire nanocomposite can be controlled by a few CNTs,

such slow-responding CNTs cause very poor overall response times (>100s). Model inversion techniques developed earlier are not effective with such response times to predict breath-by-breath CO_2 changes.

In order to enhance the response time, a capacitance based sensor is developed using a similar nanocomposite (SWNT-$BaCO_3$). This sensor's speed of response is found to be much better compared to the previous embodiment which results in the development of a low-power, small, fast and inexpensive CO_2 sensor. However, the sensor's capacitance is still found to be sensitive to environmental humidity. Further, the developed nanocomposites are also found to require humidity in the environment for sensing CO_2. Thus, the sensor needs constant humidity to respond to CO_2 reliably during breath sensing. This is achieved by completely removing humidity from the exhaled breath (using a molecular sieve) before it reaches the sensor. Simultaneously, humid air sampled away from the face is supplied using a low-power pump to humidify the sensing chamber. Using these designs, a reliable respiratory CO_2 sensor is fabricated that is compared with a NDIR CO_2 analyzer. Results show that the sensor reliably monitors CO_2 concentration in the breath. The developed embodiment could potentially be improved with drift-correcting techniques (hardware and software); but is currently unique in its ability to perform low-power, portable and low-cost respiratory CO_2 sensing.

Table of Contents

List of Tables

List of Figures

CHAPTER 1. INTRODUCTION

1.1 REVIEW OF CURRENT CAPNOGRAPHY SENSORS

Respiratory carbon dioxide (CO_2) gas analysis or capnography, has become a critical part of a number of diagnostic tests and monitoring devices used clinically. For example, monitoring respiratory gases has now become current standard of care for patients receiving general anesthesia [1]. After anesthesia, respiration can be depressed because of anesthesetic agents or additionally administered drugs (namely opioids) used to control pain leading to a rise in CO_2 concentration (hypercapnia). Breath analysis involving monitoring of the exhaled CO_2 concentration is therefore used in anesthesia [2-4].

Integration of respiratory gas analysis with measures of breathing pattern (e.g., tidal volume, respiratory rate) and ventilation to obtain measures of oxygen consumption (VO_2) and carbon dioxide production (VCO_2), can provide powerful prognostic information in a number of diseases [5]. In the case of hypercapnia (excess CO_2 in blood), breath analysis requires measurement of concentration of CO_2. Measuring exhaled CO_2 has also been used to confirm the correct placement of an endotracheal tube in the trachea and has saved many lives [6]. Several other applications such as monitoring patient breathing during treatment of cardiac arrest, asthma, dyspnea, pediatric trauma etc have also been reported [7].

Current measurement systems for CO_2 gas analysis include infra-red analyzers and mass spectrometers. Bedside infra-red analyzers are used for respiratory CO_2 gas analysis in anesthesiology [8]. Mass spectrometers have always been considered the gold standard for respiratory gas analysis for a number of reasons, including fast response time, ability to measure dry gases, accuracy and stability of measures [5]. In addition they have the advantage of measuring multiple gases simultaneously. These systems however have fallen out of favor due primarily to cost and size, as well as the need for ongoing preventive maintenance. When cost and space are not an issue, they remain the premier system for respiratory gas analysis. Several modifications can be made to mass spectrometers to further reduce gas delays and enhance response times.

A major limitation of both bedside infrared analyzers and mass spectrometers is the fact that they are expensive, bulky, cannot be used for ambulatory applications and for remote dynamic applications. In addition, the constant sample draw, temperature changes and water vapor pressure result in additional complications in these systems that need to be overcome (e.g., special lines or chemicals to dry the gas prior to analysis), which often causes delays in analysis or reduced response times.

Thus there is a need for new technology that would overcome many of these current obstacles. In particular, there is a significant need for small portable CO_2 sensor units that can be attached to the patient and used for ambulatory clinical applications [9, 10]. A small wireless respiratory CO_2 analysis system would allow for continual ambulatory measures. Having the potential for continual or intermittent wireless feedback on respiratory CO_2 measures could provide unique and important feedback for monitoring health status in several patient groups and has the potential to reduce emergency room visits and reduce health care costs [11, 12].

Early embodiments [13, 14] of respiratory monitors for non-intubated patients have been limited to measurement of respiratory rate alone. A more recently developed infra-red probe (PhaseIn Medical Technologies, Inc.) may be used to measure CO_2 at the nose of the patient. While such probes are more convenient to use compared to the bedside analyzers, they are still far too bulky to be attached to the body of the patient. Hence, they cannot be used for ambulatory or home monitoring applications (such as sleep apnea), where a small untethered sensor unit that can be mounted on the nose of the patient would be invaluable.

1.2 SOLID-STATE TECHNOLOGIES FOR CO_2 SENSING

Solid-state CO_2 sensors developed using responsive materials have the potential to be small, inexpensive and directly mountable beneath the nasal cavity, making them attractive for ambulatory monitoring. Several materials have been examined for realizing solid-state CO_2 sensors. Materials found responsive include polymers [15, 16], carbon nanotubes [17-19] and metal carbonates [20, 21].

Several material properties that respond to CO2 have been investigated. These include a material's resistance [22], mass [23], dielectric constant [24], elasticity [25], electrolytic properties [26] etc.

Further, several methods have been developed for the measurement of a single physical quantity itself. For example, resistance measurement has been performed using simple current measurement as well as using surface acoustic wave sensors [18] and field-effect transistors [17]. Similarly, dielectric constant measurement has been performed using capacitance measurement [16] as well as resonant sensors [27]. Researchers have used piezoelectric [28], thermal and magnetic actuation [29, 30] of resonance in cantilevers for measurement of elasticity. Piezoelectric, capacitive [31] and piezoresistive [32] monitoring of cantilever elasticity sensors have also been published. Similarly, chemical activity in carbonates has been monitored using electrolytic methods[20, 21, 33], field effect transistors[34], and capacitance and resistance electrodes[35].

However, most sensors have been reported to be unacceptably sensitive to other respiratory variables (like temperature, humidity and other gases), making them inadequate for respiratory CO_2 analysis. The following chapters detail research into novel carbon nanotube (CNT) based CO_2 sensors for respiratory monitoring. Different embodiments are developed to overcome multiple sensing challenges finally leading to a working prototype.

1.3 THESIS CONTRIBUTIONS

Chapter 2 details a surface acoustic wave (SAW) sensor coated with functionalized carbon nanotubes for CO_2 sensing. Earlier, SAW sensors have been used to monitor the mass of adsorbates on carbon nanotubes. The main contribution of this chapter is to develop a SAW sensor for monitoring conductivity of carbon nanotubes. Such conductivity-sensitive sensors are naturally more selective to adsorbates compared to mass-sensitive SAW sensors.

Chapters 3 and 4 describe an inexpensive and portable method for monitoring stiffness of thin films using electret microphones. This technique is used for CO_2 sensing by coating electret microphones with a CNT film that responds with changes in stiffness in the presence of CO_2. This method can be extended to measuring stiffness of a variety of thin films in other sensing applications. Compared to resonant techniques, this approach is naturally insensitive to the mass of adsorbed molecules. Further, it does not require sources of excitation, frequency sweeping or spectral analysis as required for resonant techniques.

Chapter 5 presents model-inversion techniques for extracting fast input data from the slow output of commercial CO_2 sensors. This is a first investigation into adapting CO_2 sensors developed for indoor air quality to respiratory monitoring. This method can help predict fast concentration variation (as observed during breathing) even with slow response times of solid-state sensors. While developed for a specific sensor, the techniques are equally applicable to any slow sensor.

Finally, Chapters 6 and 7 describe the development of a new nanomaterial for sensing CO_2. This new material is a nanocomposite of CNTs and metal carbonates like calcium carbonate and barium carbonate. The ability of CNTs to catalyze carbonate reactions with CO_2 is shown for the first time in these chapters. The resulting sensors show excellent sensitivity to CO_2. Using this new nanocomposite, an ultra low-power solid state respiratory CO_2 breath sensor is developed for the first time.

CHAPTER 2. CARBON-NANOTUBE COATED SURFACE ACOUSTIC WAVE SENSOR FOR CARBON-DIOXIDE SENSING

2.1 INTRODUCTION

In this chapter, carbon nanotube (CNT) coated surface acoustic wave (SAW) sensors are investigated for CO_2 sensing. Researchers in chemistry have long used the principle of resonant-frequency measurement of surface acoustic wave(SAW) devices, for observing extremely small changes in mass during gas chromatography [36]. A considerable body of literature also exists on using SAW devices coated with different chemicals for gas sensing [15, 37, 38]. Also, it has been reported independently that SAW devices can be operated in a batteryless wireless fashion [39-41] for a variety of sensing applications. Combined with their small size, low-cost and ease of manufacturing, SAW devices become attractive candidates for sensitive, portable gas sensing.

Researchers in chemistry have long used the principle of resonant-frequency measurement of surface acoustic wave(SAW) devices, for observing extremely small changes in mass during gas chromatography [36]. A considerable body of literature also exists on using SAW devices coated with different chemicals for gas sensing [15, 37, 38]. Also, it has been reported independently that SAW devices can be operated in a batteryless wireless fashion [39-41] for a variety of sensing applications. Combined with their small size, ease of manufacturing, SAW devices become attractive candidates for sensitive, portable gas sensing.

Briefly, SAW devices have a piezoelectric substrate excited by comb-like metal patterns called inter-digital transducers(IDTs) as shown in Figure 2.1. The IDTs convert incoming electrical radio frequency (RF) signals into mechanical waves which propagate along the surface of the device (surface acoustic wave – SAW). In a typical sensor, a set of receiving/load IDTs either reflect or collect the incoming SAW. The SAW characteristics such as amplitude and phase depend on the surface perturbations and have been used for

sensing. It has been shown that temperature, pressure, mass deposition, conductivity change, elasticity change affect the propagation characteristics of surface waves [42]. Perturbation theory has been used to predict changes in amplitude (attenuation) and phase by such physical disturbances [43]. Gas sensing, however, has predominantly been achieved by mass-sensitive SAW sensors since it is the most direct method of sensing [15, 38, 44].

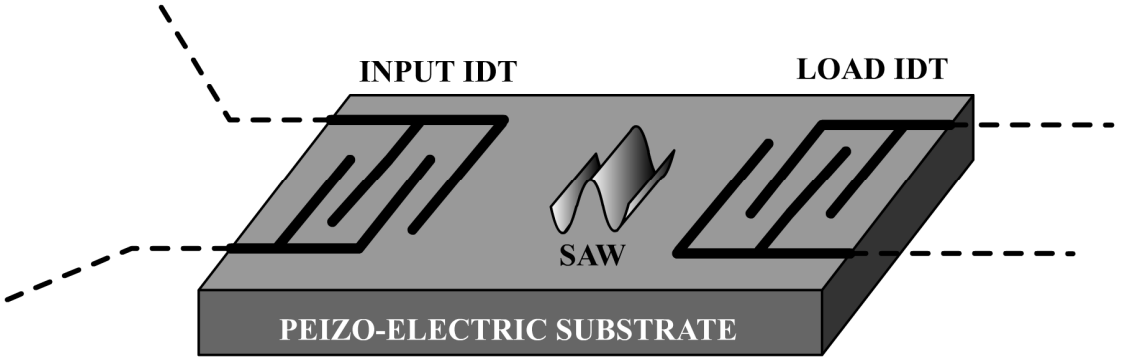

Figure 2.1. Surface acoustic wave (SAW) device with inter-digital transducers (IDTs)

In SAW based gas-sensing, coatings were typically used to enhance gas adsorption on the SAW substrate and thus cause a mass change proportional to the gas concentration on the substrate. The mass change was then observed as a frequency shift in an oscillator loop. Coatings used for CO_2 sensing in the past have typically been different kinds of polymers [15, 45]. While most SAW coatings tend to increase gas adsorption leading to a mass change, a few specialized coatings have also been shown to respond with a change in film conductivity upon gas adsorption [46, 47]. However, such film coatings have been extremely specialized being applicable to certain gases alone. Specifically, such coatings are not common for CO_2 sensing. In this work, a recently developed polyethyleneimine (PEI)-starch functionalized single walled nanotube (SWNT) coating is used which selectively changes its conductivity in the presence of carbon dioxide.

2.2 CARBON NANOTUBES AS GAS SENSING MATERIALS

It has been recently reported that the conductivity of carbon nanotubes (CNT) films is sensitive to a variety of gases [48-50]. Such conductivity-sensitive CNT films are thus attractive coatings for SAW devices. However, CNT films are typically sensitive to strongly reducing/oxidizing gases. CO_2 being a weakly reducing gas does not affect CNT film conductivity appreciably. It was reported in [51] that multiwall nanotube (MWNT)-silicon dioxide composite films changed their permittivity and conductivity upon exposure to CO_2. However, results presented in the paper showed that the change in conductivity for low CO_2 concentrations was not appreciable. This is believed to be due to the weakly reducing nature of CO2 and the reduction in sensitivity due to the presence of silicon dioxide nanoparticles in the exposed film area.

It was recently reported that conductivity of PEI-starch functionalized single walled carbon nanotubes (SWNTs) was sensitive to the concentration of CO_2 [17]. Hence, such a film was chosen as the selectivity-enhancing coating for CO_2 sensing in this work. A novel technique was used to assemble the SWNTs on the SAW substrate which eliminated the use of surfactants and maximized the exposed film area to the incoming gas. In earlier work [17], the change in CO_2 concentration was measured as a change in current of a MOSFET with the CNT film acting as its semiconducting layer. However, it has been reported [52] that the repeatability of such CNT-FETs is affected by oxygen adsorption at the metal-CNT film junctions which alters the work function of the contact, thereby altering the I-V characteristics of the FET. Hence, CNT-FETs cannot be deployed independently for repeatable gas-sensing. Researchers have subsequently explored polymer electrolytes [53] over metal-CNT contacts for atmospheric isolation in CNT-FETs; however, such methods also isolate the gas-sensitive CNT layer from the ambient rendering the design unsuitable for gas sensing.

CNT-coated SAW sensors used in this work monitor the gas concentration by detecting the change in acoustoelectric coupling between the piezoelectric SAW substrate and the CNT film deposited on the acoustic pathway. This sensing methodology eliminated the common problems of hysteresis and variability due to oxygen adsorption at the metal-

CNT junctions in the widely researched CNT-FETs. Combined with their small size and radio-frequency operation, CNT-coated SAW sensors show promise as a workable solution for portable, sensitive wireless gas monitoring.

Earlier work on SWNT coated SAW sensors utilized commercial SAW resonators for sensing trace quantities of organic vapors [23, 54]. The authors chose to utilize SWNT films as mass-sensitive coatings for SAW sensors. The additional sensitivity observed with a certain CNT coating [54] was attributed to the stronger acoustoelectric coupling between the film and the substrate. However, mass sensitive SAW sensors were found to be unsuitable for selective CO_2 sensing in respiratory monitoring due to the high likelihood of interfering gases and spurious solid particles. To overcome this disadvantage, the SAW sensor developed in this chapter measures changes in film conductivity alone. Further, to increase sensitivity, a custom-fabricated SAW delay line was chosen instead of a SAW resonator to increase the length of the acoustic propagation path exposed to the incoming gas.

To summarize the design, a SAW delay line sensor was chosen to achieve high sensitivity to conductivity changes of a PEI-starch functionalized SWNT film which responds selectively to CO_2 concentration changes. As explained later in Sec 2.3, a novel technique was used to assemble the SWNT films on the SAW delay line that maximized the exposed nanotube area to gases.

2.3 SENSOR FABRICATION

SAW delay lines were fabricated by patterning and lift-off of chromium and gold on 128^{o} XY-cut lithium niobate ($LiNbO_3$). The center frequency of the devices was 286 MHz, with a finger width, spacing of 3.15 μm and aperture of 50λ. The number of finger pairs was chosen to be 16. The IDT center to center spacing was chosen to be 3.98 mm to provide a net acoustic delay of 1 μs. Rubber cement was used as an acoustic absorber to absorb the SAWs behind the IDTs. The CNT film was assembled on the acoustic pathway subsequent to wire bonding of the SAW delay lines to a printed circuit board as shown in Figure 2.2.

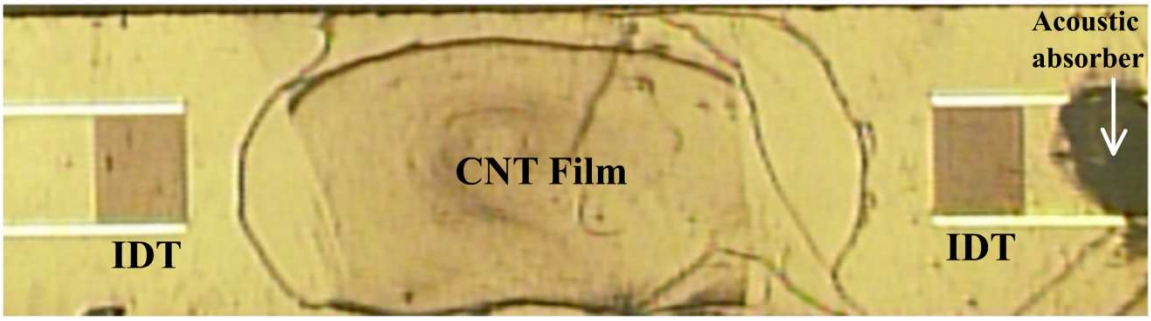

Figure 2.2. CNT coated SAW delay line

Though CNT films may be drop coated by utilizing ionic surfactants adsorbed on the nanotubes to uniformly disperse the CNTs in solution [55], such methods compromise the exposed nanotube area to incoming gases. Hence, surfactant-dispersed CNTs were not favored for this application. Since CNT films for gas sensing are required to have maximum surface area exposed to the incoming gas, a recently developed CNT coating technique for transparent thin film actuators [56] was utilized in this work. This procedure used oxidation of CNTs to achieve a dispersed negatively charged CNT suspension. Subsequent self-assembly on oppositely charged substrates allowed fabrication of uniform CNT films without interfering surfactant molecules in the film. This technique used as-grown CNTs sold by vendors which did not require fabrication expertise/expensive investment for growing CNTs. Such films without surfactants presented a higher ratio of nanotubes/substrate area to incoming gases, thereby increasing their sensitivity. The horizontal random network of CNTs was tens of nanometer thick and thus was not likely to trap gases as might be expected for vertically grown CNTs. Hence the response time of the film to gas sensing was likely to be higher. This film-coating technique was chosen for this study due to the promise of high sensitivity, ease of fabrication and control over film conductivity.

Acidified SWNTs in a stable suspension were prepared as described in ref. [56] by treating 100 mg of SWNTs from Timesnanoweb (Chengdu, China) with 30 ml of 96% H_2SO_4 and 10 ml of 69% HNO_3 at 110^oC for 70 min. The acid treated CNTs were subsequently diluted and filtered repeatedly to wash away the residual acids. Finally,

stable solutions of SWNTs were obtained by ultrasonication of the SWNT filtrate in solution for 3 h.

To assemble the SWNTs on the delay line, the acoustic propagation path of the SAW delay line was drop coated with poly(diallyldimethylammonium chloride) (PDDA) for 10 min followed by rinsing with de-ionized water and drying. The PDDA (Aldrich MW-20000-30000) solution was prepared as a 1.5 wt% solution with 0.5 M NaCl. The PDDA treatment introduced positive charges on the lithium niobate surface which later helped to bind the negatively charged carboxyl ($-COO^-$) ends of the SWNTs to the substrate. The SWNTs were drop coated onto the lithium niobate surface and allowed to dry. The sample was rinsed subsequently with de-ionized water and dried under heat. A solution of PEI and starch, prepared as described in ref. [17] was subsequently drop coated onto the SWNTs to completely cover the nanotube film. The PEI-starch film was allowed to dry and subsequently rinsed with de-ionized water and dried under heat. The PEI-starch film coating was found to be 30-40 nm thick. Thick films of PEI were found to attenuate the surface acoustic wave due to the viscoelastic nature of the polymer. Hence, this application necessitates the use of thin PEI-starch coatings. Such thin films also facilitate quick transport and response time during gas adsorption.

The PEI-functionalized SWNT film was observed to exhibit N-type behavior with a decrease in conductivity upon increasing gas concentration as shown in the results. This is consistent with the observation of N-type behavior of such films reported in ref. [17]. It has been explained in ref. [17] that the increase in carbon dioxide concentration results in increased formation of carbamate ions due to reaction of carbon dioxide with PEI in the presence of water. These ions being positively charged are known to reduce the electron donating effect of PEI and thereby decrease the conductivity of the SWNT film indicating N-type behavior. Figure 2.3 shows a summary of the sensor fabrication procedure.

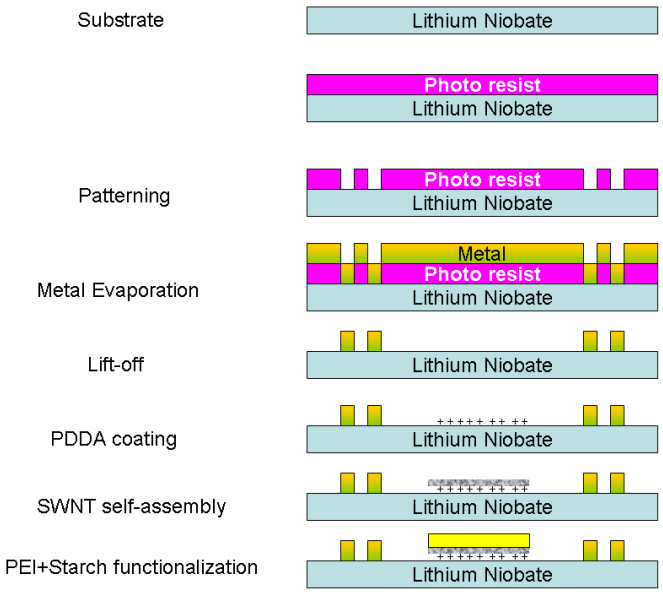

Figure 2.3. Fabrication sequence of SWNT coated SAW delay line

Rinsing after each step was found to be crucial to obtain a uniform film. It was also observed that large droplets when allowed to dry resulted in non-uniform film deposition. This is believed to be due to the accumulation of charges close to the droplet surface and subsequent deposition of the polymer/CNT ions around the periphery of the droplet, as shown in Figure 2.4(a). To avoid formation of big droplets, the entire surface was covered with a drop, as shown in Figure 2.4(b), such that the profile of the drop over the substrate was reasonably uniform. It was also observed that substrates with prior charges allowed formation of uniformly thick liquid films when coated with a oppositely charged liquid droplet.

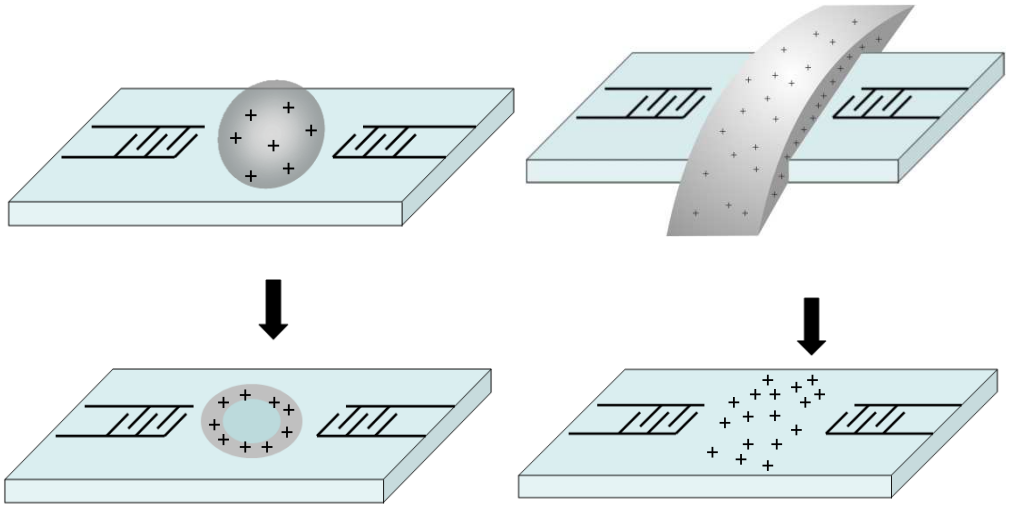

(a) (b)

Figure 2.4. Effect of drop shape on the deposited film structure. (a) Charges accumulated on the surface of a spherical drop resulted in concentric charge deposition. (b) Charges were distributed more uniformly with drying of an enveloping droplet

It has been reported independently [22] that PEI itself may be used for self-assembly of SWNTs since it is a positively charged polymer. However, in the above fabrication scheme, this positive charge was only used to bind the PEI coating to the SWNT film and not for self-assembly.

2.4 EXPERIMENTAL SETUP

The SAW delay line was placed inside a closed chamber with a gas inlet. Leakage out of the chamber acted as the gas outlet. Since gas always flowed into the chamber, it was expected that the leakage from inside the chamber to the outside due to forward pressure was much more than the leakage in the opposite direction. A humidity sensor placed inside the chamber showed that the humidity gradually decreased as the chamber was purged using pure nitrogen gas, indicating that the movement of gas was out of the chamber.

A 2-input fluid mixer was used to mix pure nitrogen and carbon dioxide. The supply to the mixer was controlled by flow control valves and on/off valves; the advantage of this setup being the complete isolation of the gas flow from the atmosphere. The humidity

was kept constant by bubbling the gas mixture through saturated salt solutions (NaCl, K_2CO_3) which maintain a constant relative humidity. Further, moist salt was also placed at the floor of the testing chamber to ensure uniform humidity in the chamber. A schematic of the gas sensing test-setup is shown in Figure 2.5.

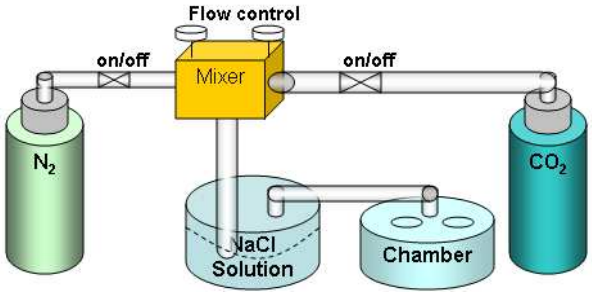

Figure 2.5. Gas sensing test setup

The change in reflected signal amplitude (attenuation) caused by gas adsorption on the PEI-starch functionalized SWNT film was measured using a pulse radar interrogation system. A RF square pulse was generated by mixing a square pulse from a pulse generator with the carrier signal from a RF generator and fed through a single-pole double throw Minicircuits ZYSWA-2-50DR transmit-receive switch into the SAW delay line. The pulse entered the SAW delay line through the input IDT traveled as a surface wave between the two IDTs and was reflected back from the load IDT. The propagation of the mechanical surface wave caused a finite time lag (2 μs in this case) between the transmitted and reflected signals, thereby allowing their separation in time domain for further processing, as shown in Figure 2.6.

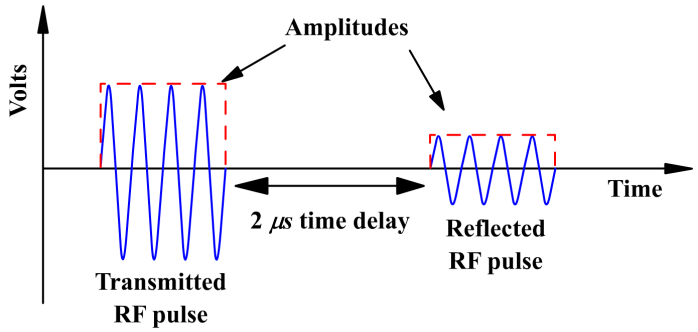

Figure 2.6. Time delayed transmitted, reflected RF pulses during SAW sensor operation

The reflected signal was routed through the switch into a quadrature demodulator to analyze the reflected signal strength. This interrogation technique has been commonly used in batteryless wireless SAW sensors [40, 41] to investigate the SAW sensor parameters remotely. Since the RF pulse propagates twice across the sensor path, the sensitivity of the attenuation to gas adsorption is doubled.

The demodulated in-phase, quadrature signals from the quadrature demodulator were viewed on a high-speed Tektronix oscilloscope which was controlled by a PC running Labview Signalexpress Tektronix-edition software. The software was used to calculate the amplitude of the reflected signals from the in-phase and quadrature components and simultaneously monitor voltage readings from a humidity sensor placed in the test chamber. A schematic of the pulse radar interrogation system is shown in Figure 2.7.

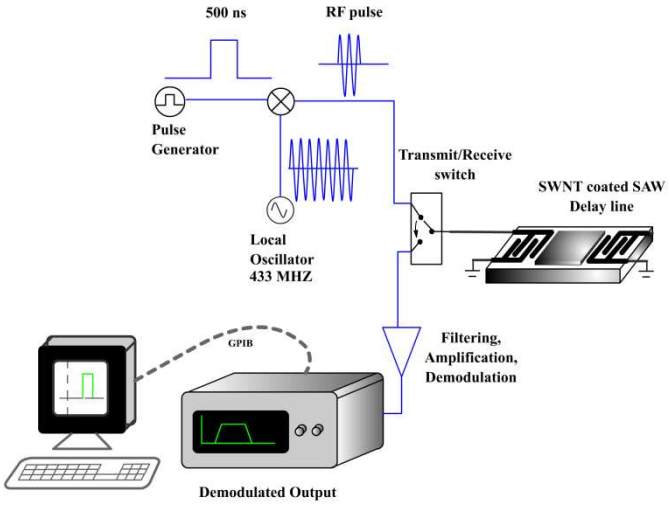

Figure 2.7. Pulse-radar type interrogation system for detecting attenuation change

2.5 RESULTS AND DISCUSSION

The changes in amplitude (attenuation) and phase of the reflected SAW signal were used to analyze the response of the sensor towards gases. The incoming gases altered the sheet conductivity of the film-coating which altered the amplitude and phase of the SAW. The

changes in phase, $\Delta\phi$ and attenuation, $\Delta\alpha$ of the surface acoustic wave are given by [47] :

$$\frac{\Delta\phi}{\phi} = \kappa\left(\underbrace{c_m f_0 \Delta\rho_s}_{mass} + \underbrace{\frac{K^2}{2}\Delta\left(\frac{\sigma_s^{\,2}}{\sigma_s^{\,2} + v_0^{\,2}C_s^{\,2}}\right)}_{conductivity}\right) \tag{1}$$

$$\frac{\Delta\alpha}{k} = \kappa\frac{K^2}{2}\Delta\left(\frac{v_0 C_s \sigma_s}{\sigma_s^{\,2} + v_0^{\,2}C_s^{\,2}}\right) \tag{2}$$

where c_m is the mass sensitivity coefficient, ρ_s is the mass per unit area, f_0 is the frequency of operation, K^2 is the electromechanical coupling coefficient, σ_s is the sheet conductivity of the film, C_s is the capacitance per length of the SAW substrate, κ is the fraction of the propagation path covered by the CNT film, and k (= $2\pi/\Lambda_{SAW}$) is the wave number. It is seen from Eq. (1) that the change in phase is a function of the change in mass as well as the change in conductivity. It has also been established that the phase is additionally affected by changes in temperature and elasticity of the substrate [42]. Since the change in attenuation was found to depend only on the film sheet conductivity, attenuation was chosen as the measurement parameter for the gas sensor.

The attenuation was measured indirectly through the insertion loss of the SAW sensor. The relation between the measured insertion loss (I.L) and attenuation per wavenumber is given by ref. [57] **:**

$$2\frac{\alpha}{k} = 0.0183\frac{I.L(dB)}{N_\Lambda} \tag{3}$$

where N_Λ is the number of wavelengths in the perturbed acoustic pathway. The factor of '2' in the left hand side of the Eq. (3) was used to account for the two-way propagation of the SAW before measurement of insertion loss. The measured changes in reflected voltage amplitude and insertion loss were observed to be roughly linear for the experiments reported in this work. Hence, the reflected voltage amplitude was directly used to characterize the response of the SAW sensor to CO_2 concentration.

The film deposition was tailored using the mathematical model of the system (Eq. (2)) to obtain high sensitivity as well as a high signal-to-noise ratio. It has been shown using Eq. (2) that attenuation change is most sensitive to sheet conductivity when $\sigma_s \approx v_0 C_s$ [42]. However, it was also shown that attenuation is maximum close to this, value thereby degrading the measured signal/noise ratio. As predicted by Eq. (2), the reflected signal was completely attenuated upon depositing the SWNT film over the entire acoustic pathway. The reflected signal became observable upon reducing the film coverage fraction to approximately 0.5. The film coverage fraction was further reduced to approximately 0.3 to enhance the signal/noise ratio. This reduction in coating area however reduced the sensitivity of the attenuation change to incoming gases. Thus, a trade-off was observed between the signal/noise ratio and sensitivity of the SWNT coated SAW delay line.

It was also observed that attenuation decreased after functionalizing the SWNT film with PEI and starch. Thus, PEI functionalization served dual purposes of enhancing sensitivity to CO_2 and improving the signal/noise ratio. This is believed to be due to the decrease in SWNT film conductivity upon functionalization with PEI. The decrease in SWNT conductivity upon functionalization was subsequently verified on larger CNT films, thereby confirming the above assumption. Figure 2.8 shows the reflected signal from a bare SAW delay line.

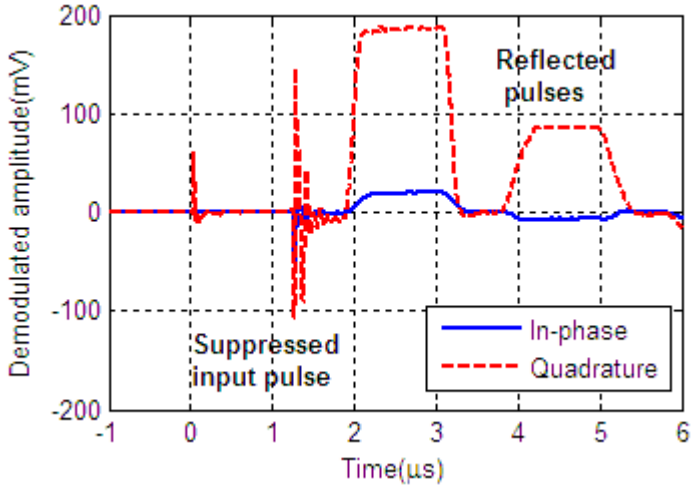

Figure 2.8. Reflected square pulses from bare SAW delay line

The edges of the input pulse and the demodulated envelope of the reflected signals are observable in Figure 2.8. It may be observed that the open IDT on the load side of the bare SAW delay line allows multiple reflections. However, the signals were attenuated upon coating with the SWNT film and functionalizing with PEI and starch, as shown in Figure 2.9.

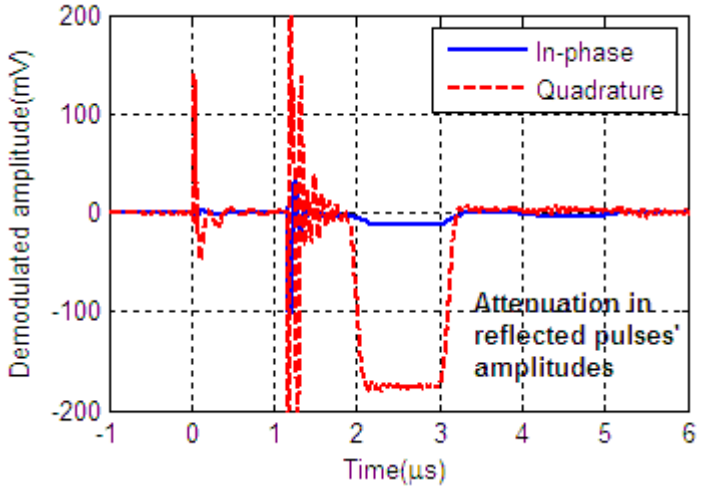

Figure 2.9. Decrease in reflected signal amplitude upon film coating

2.5.1 RESPONSE TO CO_2

Figure 2.10 shows the response of the coated SAW delay line towards 3.5% CO_2. The introduction of CO_2 resulted in a decrease in film conductivity, as explained in ref. [17].

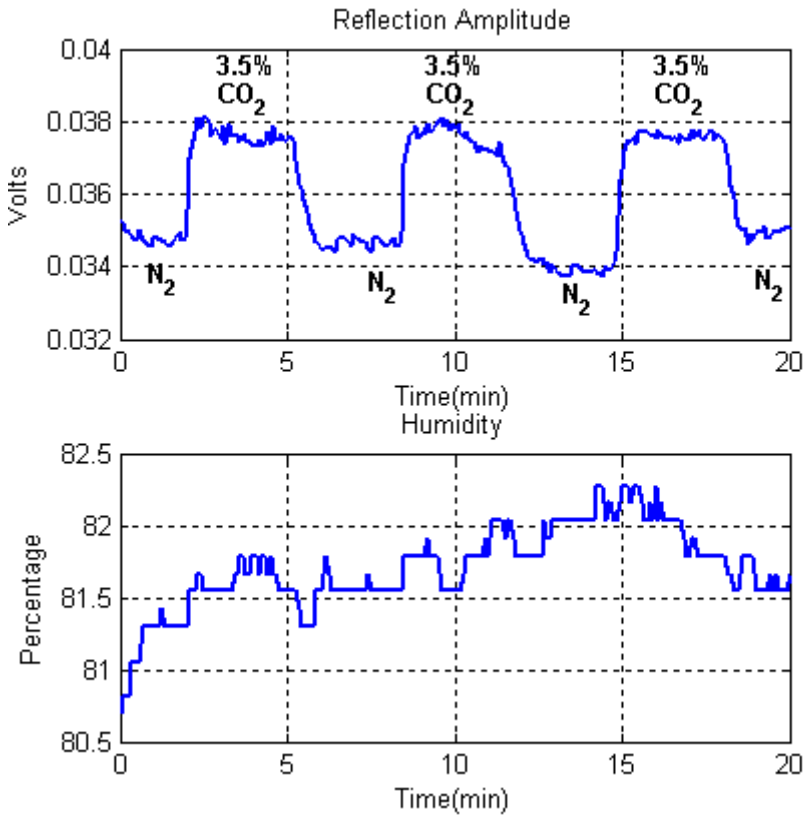

Figure 2.10. Change in reflection amplitude of the PEI-starch functionalized SWNT coated SAW delay line

Thus the attenuation was observed to decrease with an increase in CO_2 concentration. A small gradual increase in signal strength may be observed from the figure over the different cycles. This is believed to be due to the decrease in humidity during the experiment, as shown in Figure 2.10. It was described in ref. [17] that humidity was required for carbamate ion formation in the presence of CO_2. Thus, humidity was required for this sensor to function. It may also be observed from Figure 2.10 that the signal response to CO_2 is a function of the humidity level. Thus a complementary humidity measurement would be required for estimating the concentration of CO_2 accurately in the presence of humidity variation.

Figure 2.11 further demonstrates effect of humidity on the sensor response over three cycles of increasing and decreasing exposure to CO_2. In this experiment, the CO_2 concentration was changed every 48 min; stepping from 0%, 2.5%, 10%, 20%, 40% and

back using the same concentration steps. The observed response to humidity was expected due to the sensitivity of the uncoated areas of the SAW substrate and the PEI functionalized SWNT film towards humidity [58]. Figure 2.12 shows the corrected amplitude response to CO_2 over a single cycle, after subtracting the scaled humidity response. In this experiment, a scaling factor of '400' was used to correct the humidity interference.

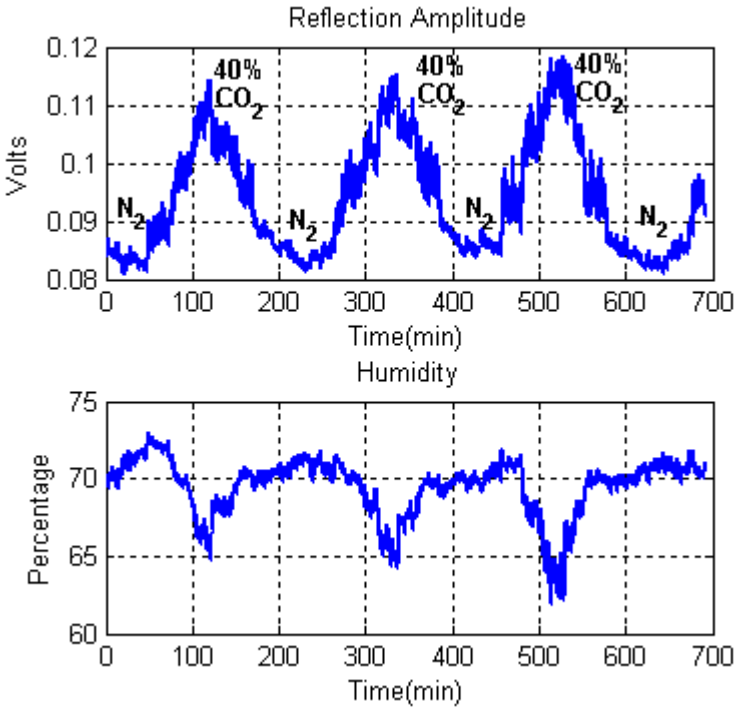

Figure 2.11. Raw response of the CNT coated SAW sensor with varying humidity

(a)

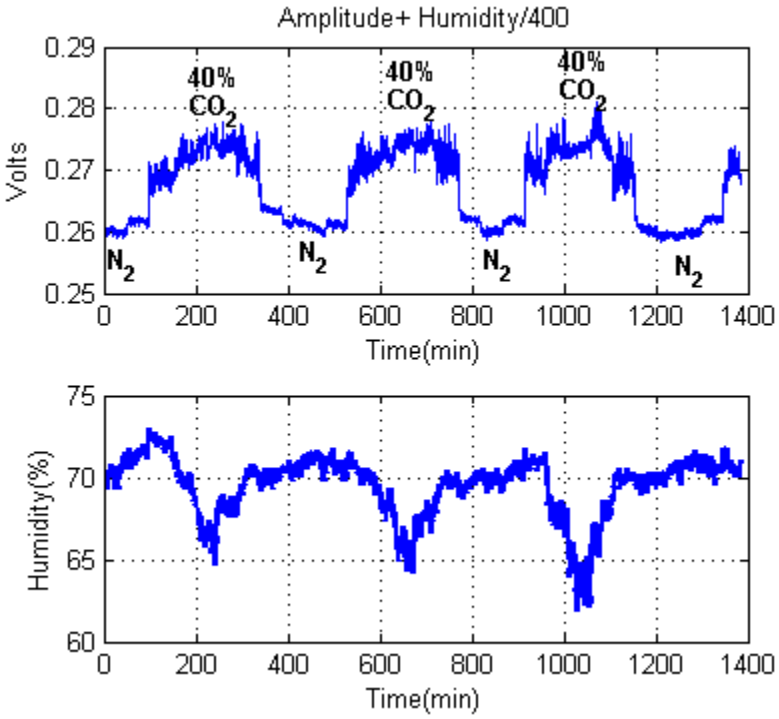

(b)

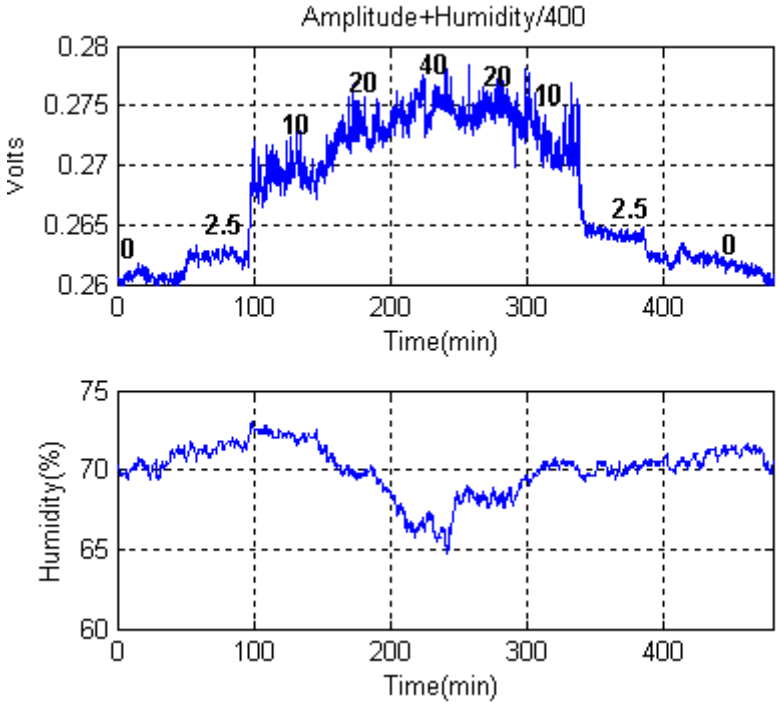

Figure 2.12. Corrected amplitude response to CO_2 over (a) three cycles and (b) a single cycle

These results indicate that the sensor is inherently cross-sensitive to humidity due to the chemistry of carbamate ion formation. However, a complimentary humidity measurement is shown to be adequate to predict the effect of humidity. Further testing of such films on SAW sensors will need to be performed to understand the cross-sensitivity of the CNT-coated SAW sensors to respiratory gases such as oxygen and nitrogen dioxide.

2.5.2 EFFECT OF FILM SHEET CONDUCTIVITY ON GAS-RESPONSE

It was observed that the response to CO_2 could be altered by tailoring the SWNT film sheet conductivity. This is due to the non-linear relation between the attenuation response of the SAW sensor and the sheet conductivity of the film coating. It has been shown in ref. [42] that the attenuation change follows a curve similar to that shown in Figure 2.13 with change in sheet conductivity. The sheet conductivity values shown in Figure 2.13 are appropriate for $LiNbO_3$ SAW sensors. As seen from Figure 2.13, the direction and magnitude of attenuation change with increasing CO_2 can be altered by the film nominal sheet conductivity. In Figure 2.10, the SAW delay line was coated with a film with low nominal sheet conductivity. Hence, a decrease in sheet conductivity upon CO_2 adsorption caused a net decrease in attenuation.

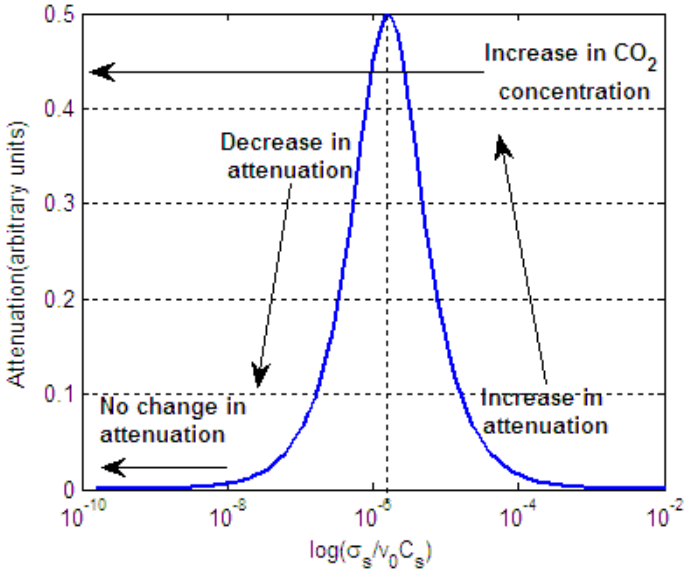

Figure 2.13. Change in attenuation with normalized sheet conductivity for lithium niobate

2.5.3 REVERSAL OF AMPLITUDE RESPONSE

While the direction of amplitude response in multiple experiments was predominantly similar to Figure 2.10 and Figure 2.12, the response was observed to reverse direction with certain films. Figure 2.14 shows the response of a SAW delay line with a CNT film of high nominal sheet conductivity. The high nominal sheet conductivity causes a shift to the right side of the curve shown in Figure 2.13. Thus, a decrease in sheet conductivity due to CO_2 adsorption resulted in greater attenuation contradictory to the decrease in attenuation shown in Figure 2.10 and Figure 2.12.

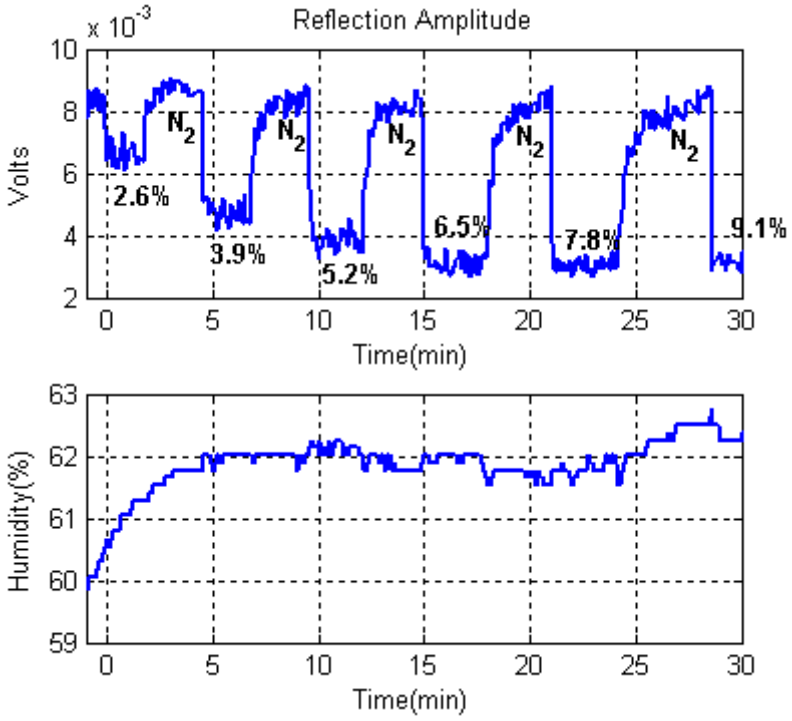

Figure 2.14. Increase in attenuation with CO_2 concentration due to a coating with high sheet resisitivity

Considerable variation in amplitude response was observed in other preliminary experiments, indicating the critical importance of a standardised SWNT coating process. A process of SWNT film assembly was subsequently developed to guarantee a response similar to that shown in Figure 2.10 and Figure 2.12. This was achieved by reducing the number of nanotubes assembled on the substrate to yield a low nominal sheet conductivity. To reduce the number of assembled nanotubes, the SWNT film was washed

after drop coating on the PDDA-functionalized substrate and prior to drying. This variation from the procedure suggested in ref. [56] was necessary to guarantee precision in tailoring the sheet conductivity and hence the amplitude response.

While the direction of response to CO_2 can be controlled using the above fabrication procedure, the magnitude of response would still vary depending on the exact value of the film sheet conductivity. Indeed, the control of sheet conductivity of CNT films is complicated by the random assembly of metallic and semi-conducting nanotubes during film growth. The resulting repeatability of the current sensor along with the achieved resolution of 5000 ppm compares unfavorably with existing low-cost portable infra-red based gas analyzers. However, the slow response of such analyzers (eg: Bacharach CO_2 monitor 2800) prevents breath-by-breath monitoring of gas concentration. In contrast, the instantaneous response of the developed SAW-CNT sensors permits the tracking of gas concentration in individual breaths. The slow change in gas concentration shown in the results is an effect of the chamber flow dynamics. The sensor itself was tested to show sub-second rise and fall times with gas concentration. Combined with low sensor cost and wireless operation, conductivity-based SAW-CNT sensing is an attractive technique for breath monitoring. However, challenges related to repeatability and resolution will need to be addressed to realize a feasible SAW-CNT based breath monitor.

2.6 CONCLUSIONS

Small gas sensors have been developed by coating functionalized SWNT films on SAW delay lines. The change in conductivity of a PEI-starch functionalized SWNT film was detected by coating the film on the acoustic propagation path of a custom-fabricated SAW delay line and measuring the change in attenuation with gas concentration. This technique may be easily extended to other types of gas sensing by appropriate functionalization of the SWNT sensors.

Compared to existing optical infra-red based sensors, these sensors exhibit cross-sensitivity to humidity which needs to be estimated using a complimentary humidity

measurement. This aspect of cross-sensitivity is common to all chemistry-dependent sensors including capacitive, resistive and resonant carbon dioxide sensors. Hence, other alternatives need to be examined to achieve a portable and low-cost respiratory CO_2 analyzer comparable to bulky optical non-dispersive infrared (NDIR) analyzers.

CHAPTER 3. ELECTRET MICROPHONES FOR SWNT FILM STIFFNESS AND CO_2 MEASUREMENT

3.1 INTRODUCTION

The CO_2 sensitive film (recognition layer) was chosen to be one of SWNTs functionalized with PEI in the previous chapter. While sensitive to CO_2, it was shown that the film conductivity shows unacceptable cross-sensitivity to humidity. Thus, it is not a suitable choice for respiratory CO_2 sensing. In a later report, it was shown that the stiffness of SWNT films changes selectively with CO_2 adsorption [59]. In particular, the stiffness of SWNTs was also reported to be insensitive to humidity and oxygen. Hence, a sensor based on stiffness detection of SWNTs is investigated for respiratory CO_2 sensing. However, unlike physical properties such as conductivity, dielectric constant and mass; techniques for portable and sensitive measurement of stiffness changes are not well-developed. For example, the conventional method of stiffness measurement requires optical methods for detecting cantilever deflection in the presence of an analyte [60, 61]. While the solid-state sensing element itself is small, the use of large optical systems complicates their use in portable apparatus. Indeed, a chief motivation behind solid-state sensing research is the reduction in cost. However, optical analyzers typically increase the system cost unacceptably.

Apart from the disadvantages of optical sensing, the cantilever design of conventional stiffness sensors also suffers from a few other drawbacks. Cantilever based methods typically have the disadvantage of non-specific analyte adsorption on the uncoated surface in liquid environments [62]. In gaseous environments, capacitive measurements of cantilever deflection are affected by gas seepage due to change in dielectric constant between the electrodes. Further, cantilever actuation and position measurement require development of independent mechanisms. Most techniques also require frequency sweeping for resonant frequency identification. Such analyzers increase the power requirement of the final sensor. Researchers have used piezoelectric [28], thermal and magnetic actuation [29, 30] of resonance in cantilevers. Piezoelectric, capacitive [31] and

piezoresistive [32] monitoring of cantilever motion have also been published. However, all these methods suffer from the one or more of the drawbacks discussed above.

Attempts have been made to find alternate methods of stiffness sensing for the above reasons. Metal oxide semiconductor (MOS) transistors have been used to detect changes in stiffness of piezoresistive films [63]; but such methods apply only to large changes in surface stress measurement of mechanical members. Also, the measurement of resistance change used in these techniques is not suitable for analyte sensing, when the recognition layer changes its resistance along with its stiffness in the presence of analytes (as seen in carbon nanotubes). Other techniques using SAW sensors [64] too are not suitable for monitoring elastic property changes of recognition layers because of their extreme sensitivity to conductivity changes in such films.

Recently, Satyanarayana et al [62], Rodriguez et al [65] and Tsouti et al [66] have suggested capacitive measurement of curvature changes in surface micromachined membranes for measurement of stiffness variations in the presence of analytes. While such capacitive techniques eliminate the need for optical measurement and membrane vibration, the sensitivities of proposed sensors are limited by the membrane stiffness post micro-fabrication. This work develops a capacitive stiffness sensor using electrically stretched capacitive membranes. Electrostatic stretching of membranes is used to augment their sensitivity to stiffness changes as discussed in the following section. Subsequently, an electret sensor with a precharged membrane is shown to be an excellent solution for self-actuated stiffness measurement. Finally, one embodiment of the sensor coated with single walled carbon nanotubes (SWNTs) is shown to track changes in carbon dioxide (CO_2) concentration.

3.2 SENSITIVITY ENHANCEMENT USING ELECTROSTATIC ACTUATION

This section describes the sensing principle for stiffness measurement using electrically stretched capacitive membranes. As mentioned earlier, capacitive stiffness measurement techniques permit realization of miniature analyte sensors. Micromachined capacitive membranes are typically pre-stressed during microfabrication due to the high temperature

deposition of the membranes and its subsequent cooling down to room temperature. A change in the capacitance of the sensor is effected by the change in membrane curvature upon stiffness change in the recognition layer. However, this response to stiffness change in the composite membrane is affected by the pre-stress in the membrane. Indeed, in the absence of any curvature, a change in membrane stiffness would not alter its vertical position. This becomes important for larger membrane sensors which are not micro-fabricated.

Conversely, it can be shown that electrostatic actuation can be used to enhance any membrane's response to stiffness changes. Pulling of the membrane initiated by an electric field can be used to induce a curvature to the membrane. Subsequent change in the membrane stiffness would then cause the membrane to appropriately alter its curvature to compensate for the applied electrostatic force. This change in membrane curvature can then be measured as a change in capacitance. Apart from inducing curvature, the strength of the electric field can also be used to control the sensitivity of the response to stiffness changes. This is shown below. The force balance equation for a membrane subjected to a voltage potential V_{DC} shown in is given by,

$$\frac{\varepsilon A V_{DC}^2}{2x^2} = k(d_0 - x) \tag{1}$$

where ε is the dielectric constant of the medium, A is the metallic electrode area, V_{DC} is the voltage between the membrane and back-plate, k is the membrane-stiffness, d_0 is the original vertical separation between the membrane and the back plate, and x is the actual vertical separation between the membrane and the backplate.

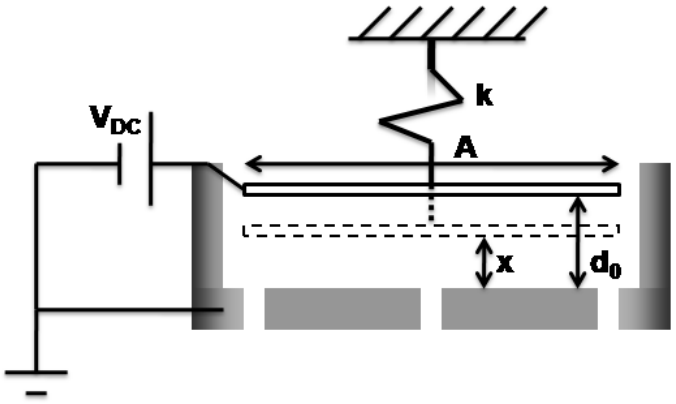

Figure 3.1. Schematic representation of electrostatically acutated membrane capacitor

Simplifying,

$$x^3 - 2d_0x^2 + \frac{\varepsilon AV_{DC}^2}{k} = 0 \tag{2}$$

$$\Rightarrow \frac{\partial x}{\partial k} = -\frac{\varepsilon AV_{DC}^2}{k^2(4xd_0 - 6x^2)} \tag{3}$$

Now, the sensitivity of the capacitance change to the stiffness change is given by

$$\frac{\partial C}{\partial k} = \frac{\partial C}{\partial x}.\frac{\partial x}{\partial k} \tag{4}$$

where $C = \frac{\varepsilon A}{x}$ is the measured capacitance. Now, $\frac{\partial C}{\partial x} = -\frac{\varepsilon A}{x^2}$

Substituting in Eq. (4)

$$\frac{\partial C}{\partial k} = \frac{\varepsilon^2 A^2 V_{DC}^2}{6k^2x^3(x - \frac{2}{3}d_0)} \tag{5}$$

Thus the sensitivity of the capacitance measurement to the stiffness change $\frac{\partial C}{\partial k}$ varies with x and V_{DC}. However, the vertical separation x itself is dependent on the bias voltage V_{DC} and the membrane's nominal stiffness k. At a given V_{DC} and k; x is obtained as the unique real root of Eq. (2). The value of x decreases with increasing V_{DC} due to increasing attractive force between the membrane and the backplate. Further, the term

$(x-\frac{2}{3}d_0)$ also decreases as the vertical separation x decreases. Indeed, x can never be lower than $\frac{2}{3}d_0$ for a membrane in stable equilibrium. Below this critical separation distance, the membrane snaps into the backplate due to an unbalanced increase in the electrical attractive force [67]. Thus, with increasing V_{DC}, the numerator of Eq. (5) increases while the denominator decreases. Hence, the sensitivity of the capacitance measurement to the stiffness change $-\frac{\partial C}{\partial k}$ increases with V_{DC}.

Figure 3.2 shows the change in sensitivity with increasing bias. The constant parameters were chosen to be $\varepsilon = 8.85e^{-12}$, $A = \frac{\pi}{4}(5mm)^2$, $d_0 = 10\mu m$ $k = 2000\,Nm^{-1}$ for the simulation. The sensitivity can be seen to increase dramatically by stressing the membrane using electrostatic forces. This is the working principle behind the developed sensor.

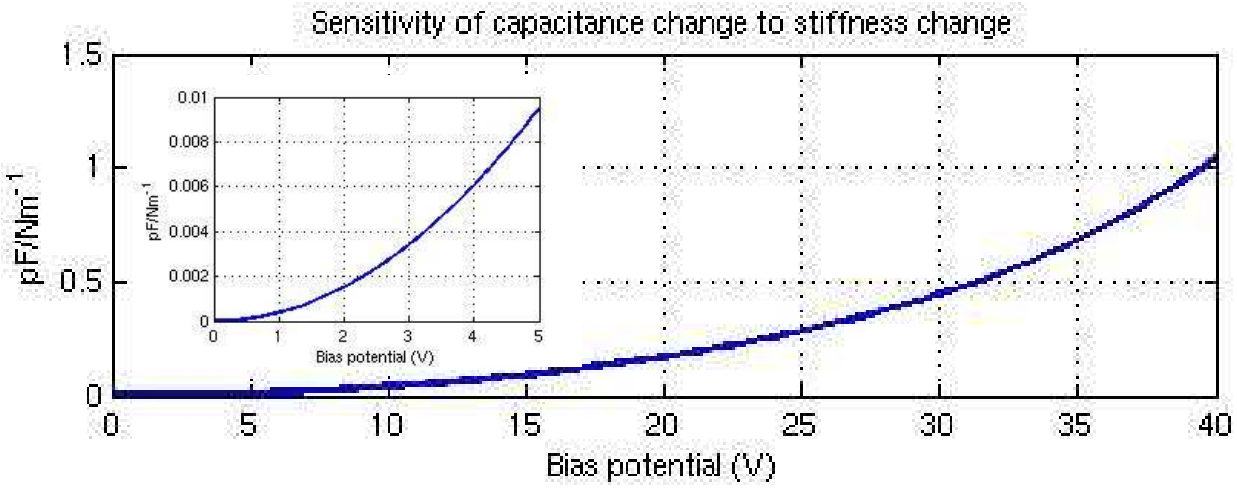

Figure 3.2. Change in sensitivity with bias voltage V_{DC}

3.3 DESIGN OF STIFFNESS SENSOR

Membranes with high stiffness require large bias voltages to increase the sensitivity. Indeed, Eq. (5) suggests that sensitivity reduces with increasing membrane stiffness for a given bias potential. Hence, it is beneficial to use a membrane with low nominal stiffness.

A membrane with low nominal stiffness is also required for studying stiffness changes in mechanically soft recognition layers. This is because the stiffnesses of the membrane and the recognition layer act in a parallel configuration to resist deflection. It is well-known that the net deflection of such parallel springs is predominantly controlled by the change in stiffness of the harder spring. Figure 3.3 shows a spring-mass representation of the membrane and the recognition layer. In this representation, the stiffness of the metal film-electrode coating the membrane is considered together with the membrane.

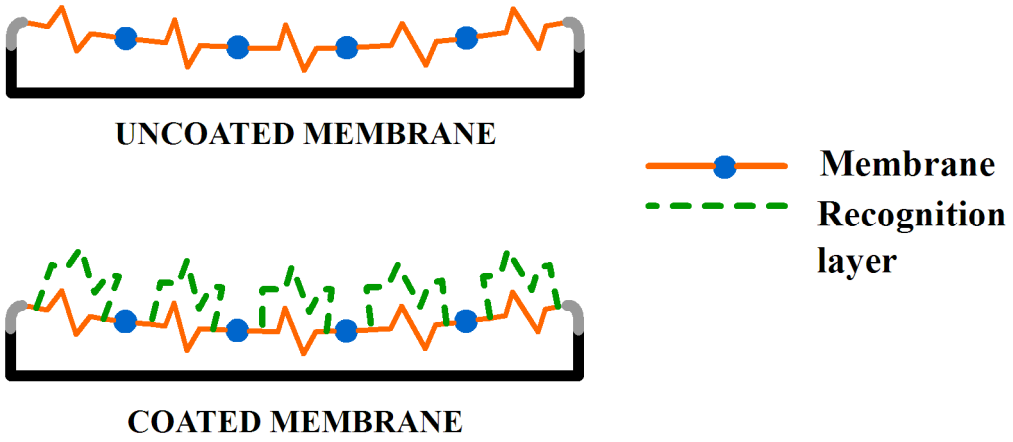

Figure 3.3. Parallel addition of stiffnesses upon coating membrane with recognition layer

Apart from the membrane stiffness, the bias voltage supply is also a factor in the final sensor design. It is known that micro-machined capacitors tend to have a large stiffness due to the small membrane area and require a large bias voltage. To overcome complications arising due to bias voltage supply, an electret element is used for the first time as a stiffness sensor in this work. Electret microphones use membrane materials that are capable of trapping and storing charges. These charges are embedded into the membrane during fabrication itself thus eliminating the need for an external bias voltage. The charged electret membrane induces an opposite charge on the metallic backplate resulting in an electrostatic pulling force on the membrane. Electret microphones are used commonly for audio applications where the electret membrane shows enhanced sensitivity to sound. Figure 3.4 shows a schematic representation of the developed electret stiffness sensor coated with a carbon nanotube recognition layer for carbon dioxide gas sensing.

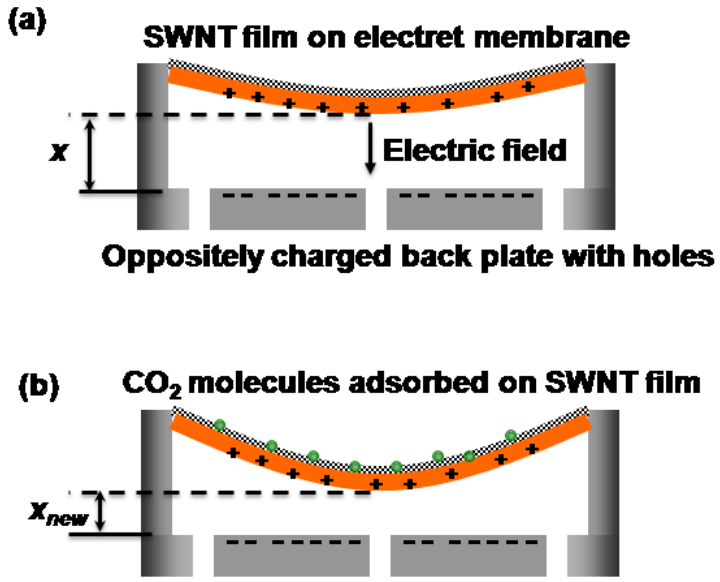

Figure 3.4. Schematic representation of the developed electret stiffness sensor

In contrast to resonant sensors, the intrinsic electric field of the electret sensor is used to cause a static deflection of the membrane and capacitance measurement is used for monitoring stiffness change in films. This design eliminates cumbersome instrumentation for independent excitation and measurement and the need for frequency sweeping, which results in a small sensor package and a large speed of response respectively. Further, typical electrets use a polymer membrane (polytetrafluoroethylene) whose stiffness is not expected to be substantially larger than recognition layers like carbon nanotubes, zeolites, oxides, polymers etc. Hence, the final sensor is expected to be sensitive to the changes in film stiffness of the recognition layer in the presence of analytes. Finally, the capacitance measurement circuit being the only powered constituent results in a very low power sensor package (<30mW).

3.4 EXPERIMENTAL SETUP

MEO96PD-00-604-NF FET-less omnidirectional electret condenser microphones obtained from ICC Intervox are used as stiffness sensors in this work. The nominal capacitance of these microphones is measured to be around 10pF. Other no-FET microphones such as the TSB-1460,160,165 etc. from Transound International could also

be used equally. Capacitance measurement is achieved using MS3110 universal capacitive readout IC from Irvine Sensors Corporation. The capacitance readout IC provides a resolution of 4aF/√Hz and a voltage output proportional to the capacitance change, which can be directly acquired into a computer. A custom fabricated printed circuit board (PCB) is used to achieve a small sensor package with the IC and electret microphone along with reference and decoupling capacitors as shown in Figure 3.5. It may be observed from Figure 3.5 that the developed sensing platform is smaller than a 9V battery and requires only three electrical connections viz. supply voltage, ground reference and capacitance output.

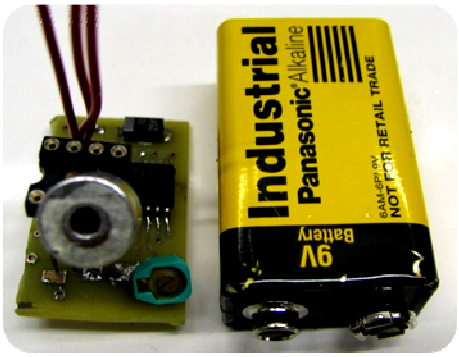

Figure 3.5. Size comparison of the electret stiffness sensor and measurement electronics with a 9V battery

Wireless data readout is achieved using an eZ430-RF2500 development kit based on the ultra low-power MSP430 microcontroller from Texas Instruments. This development kit permits acquisition of signals from the capacitance readout chip, averaging of the data and wireless transfer to a receiving unit connected to a USB port of a laptop. The wireless data transfer utilizes the SimpliciTI® protocol, operates at 2.4 GHz and provides telemetry distances up to 100 feet. Indeed, the MSP430 microcontroller also permits direct capacitance measurement without the additional MS3110 chip; but its resolution is found unsuitable for this work.

Special techniques need to be employed to deposit SWNT films on the electret membrane of the sensor since they tend to aggregate together due to strong Van der waal's forces

and inhibit uniform film deposition. In this work, a SWNT dispersion technique developed in Ref [68] is used to coat SWNTs with poly(3-hexylthiophene) (P3HT) and disperse the resulting SWNTs in chloroform. P3HT was prepared in a similar manner as described by Loewe et al [69]. Briefly, the SWNT dispersing procedure involves ultrasonicating SWNTs together with P3HT and chloroform and subsequent filtration to remove excess dissolved P3HT. The final P3HT coated SWNTs disperse stably in chloroform and may be drop coated from the solution. Chloroform evaporates upon drop coating to yield a SWNT film on the electret membrane. The drop coating procedure is done carefully to avoid excess deformation and consequent pull-in of the electret membrane into the backplate. Hence, the drop coating is done in small successive steps without adding substantial weight to the membrane. Figure 3.6 shows a scanning electron microscope (SEM) image of a film fabricated using this procedure.

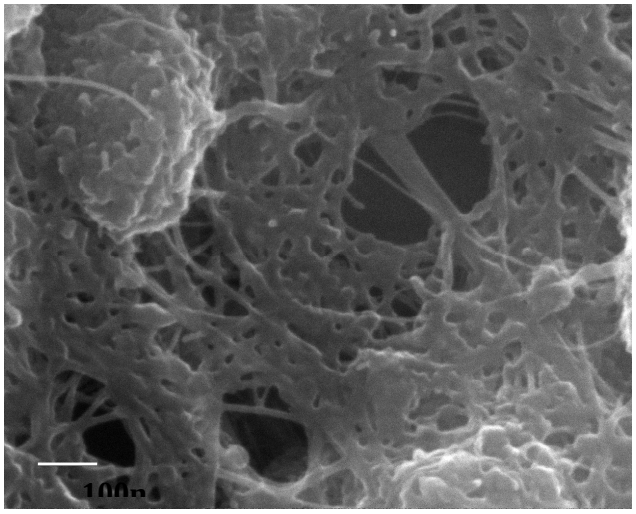

Figure 3.6. SEM image of SWNT-P3HT film

The microphones are sealed in a plastic chamber with the sensing membrane alone exposed to the incoming gas. This is necessary to prevent gas seepage between the measurement leads of the microphone which causes a change in the measured capacitance. Varying humidity, in particular, is found to alter the capacitive readout due to the varying dielectric constant of water vapor. A humidity sensor inside the sealed chamber is hence used to monitor humidity seepage during the experiment as shown in Figure 3.7.

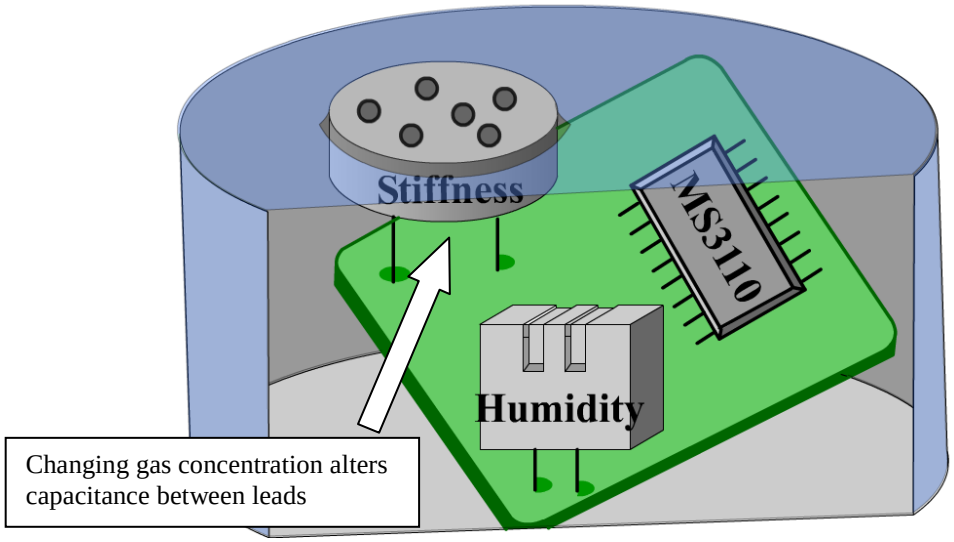

Figure 3.7. Schematic of sealed sensor-leads and electronics

The stiffness of the composite membrane is also expected to be sensitive to temperature changes. However, the temperature during experiments is found to be substantially constant. Hence, temperature compensation is not adopted in the experiments. However, in the presence of large temperature variations, measurement of the capacitance of an uncoated electret sensor is required for reference.

3.5 RESULTS AND DISCUSSION

The measured change in the microphone's capacitance is almost entirely due to the stiffness change of the SWNT coated electret membrane. The effect of mass change due to CO_2 adsorption is found to be negligible upon estimating the force exerted on the membrane due to mass change. The approximate force is computed by assuming an average diameter of 453pm for a CO_2 molecule [70]. Given that the diameter of the microphone's electret membrane is less than 1 cm, it is possible to calculate the maximum number of CO_2 molecules that can be adsorbed on the membrane. Since surface adsorption is predominant, only a monolayer of CO_2 molecules is assumed for the calculations. However, the values obtained below show that the mass change due to even 100s of CO_2 layers would not appreciably contribute to membrane deflection.

Upon computing the maximum number of CO_2 molecules that can be adsorbed on the membrane surface and taking the molecular weight of CO_2 molecules as 44 g/mol, the maximum force due to CO_2 adsorption is calculated to be approximately $8.9x10^{-11}$N. However, an applied sound pressure level of 60dB, corresponding to a force of $4x10^{-7}$N, much larger than the weight of an adsorbed monolayer of CO_2 molecules, is found to negligibly affect the membrane capacitance (indeed, a no-FET electret microphone is used to deliberately decrease sensitivity to sound). Thus, the microphone capacitance shows orders of magnitude higher sensitivity to the gas induced stiffness variations in the SWNT film than to the weight of adsorbed CO_2 molecules.

Figure 3.8 shows the change in capacitance with the CO_2 gas concentration. The humidity data presented in Figure 3.8 are measured by a humidity sensor placed inside the gas chamber and does not reflect the humidity leakage into the sealed sensor chamber. The data shows that the stiffness of the sensor drifts slowly with time indicating possible chemisorption. This artifact possibly arises from the cutting of the SWNTs during ultrasonication. It has been established that open ends and defects in CNTs are locations for hydrogen bond formation and water/oxygen adsorption [71]. This is believed to be the reason for the observed drift. On the other hand, the humidity inside the sealed sensor chamber also showed a slow gradual increase indicating slow seepage of humid air between the microphone's leads. This could also be a cause for the observed drift in the data. Repeated experiments with the sensor gave similar results confirming the usability of this approach. Figure 3.9 shows a repeated run of the same experiment on a different day. It may be seen that the drift varies between the two experiments while the absolute magnitude of the response to CO_2 concentration remains similar. This suggests the need for dynamic drift compensation for utilizing the developed carbon dioxide sensors in practical applications.

It is noted that analyte sensing applications seldom require calculation of absolute film stiffness values. The results presented also suggest that calibration of the measured capacitance with the gas concentration is sufficient to develop a practical analyte sensor. However, the same techniques could be extended to absolute film stiffness

measurements. This would require identification of the electret sensor's parameters such as the nominal capacitive gap d_0, membrane area A and stiffness k, as well as the voltage potential V_{DC} due to the charge embedded in the electret membrane. The techniques for measuring and estimating these parameters will be developed in future work.

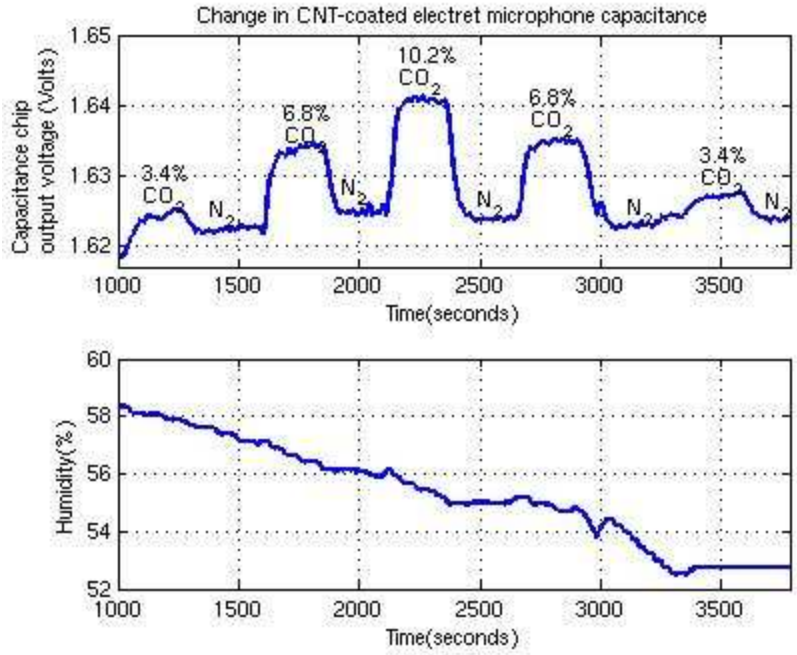

Figure 3.8. Change in capacitance with CO_2 concentration (initial run)

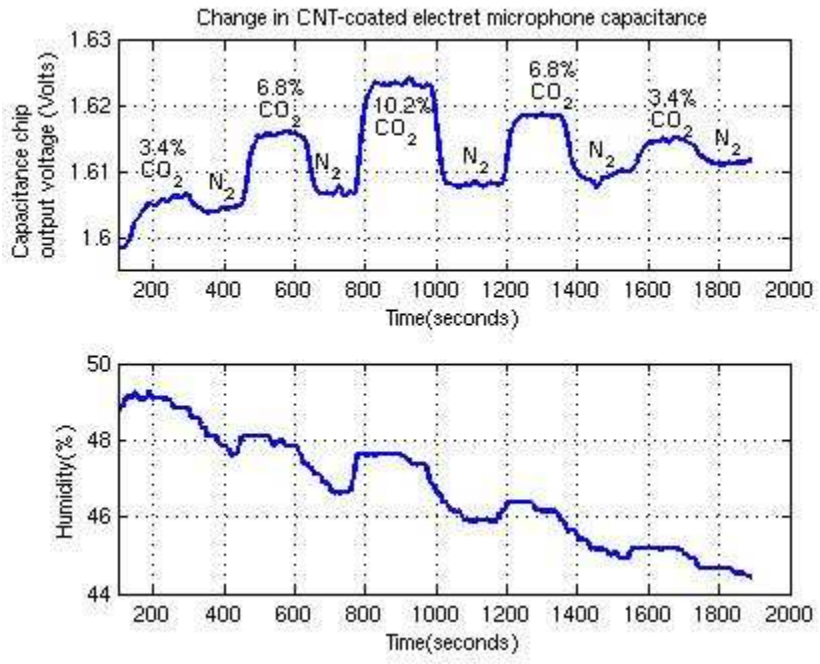

Figure 3.9. Change in capacitance with CO_2 concentration (repeated run)

3.6 CONCLUSION

This chapter presents the application of a stiffness monitoring technique using an electret microphone for portable CO_2 gas sensing. Compared to earlier resonant frequency techniques, the presented method greatly simplifies measurement, reduces size and cost and improves the ease of use. While results obtained with this sensor make it attractive for respiratory CO_2 sensing, several practical problems with microphone design and specifications necessitated an alternate approach. These issues are discussed in the next chapter.

The key idea behind the developed sensor is to augment the sensitivity of capacitive membranes to stiffness changes using electrical stretching. Further, the intrinsic electric field of electret capacitors is used to enhance the sensitivity to stiffness changes without any external voltage biasing. Capacitance measurement allows miniaturization of the measurement electronics thereby resulting in a portable and low-power sensor package. The techniques described above are easy to scale for array-based stiffness measurements

and pattern recognition methods. A wide variety of possible applications are envisioned for the developed stiffness sensing technique.

CHAPTER 4. EVALUATION OF SENSING PROPERTIES OF ELECTRET MICROPHONES

This chapter presents an evaluation of the sensing properties of a thin-film stiffness sensing technology developed in the previous chapter that utilizes commercial electret microphones. The analysis is used to obtain both quantitative and qualitative information on sensor selection for stiffness sensing applications. The sensing properties examined include sensitivity, selectivity and the effect of microphone's electric field. Specifically, a mathematical method to estimate the stiffness sensitivity of a commercial microphone from its acoustic sensitivity is presented. This method utilizes direct measurements of the microphone's parameters to compute sensitivity to thin-film stiffness changes. The discussion on selectivity focuses on undesired cross-stiffness changes in the microphone membrane in the presence of changes in unrelated environmental analytes.

The chief advantage of this sensing technology is its simplicity and low cost. However, as described later in this chapter, certain constraints prevent use of this technology for respiratory CO_2 sensing using commercially manufactured microphones. These constraints are brought out in this chapter and key design issues discussed. These design issues would need to be addressed in designing custom sensors for sensing applications.
Chiefly, two sensing properties need to be evaluated before use of electret microphones for CO_2 sensing. These include sensitivity, selectivity and effect of electric field.

(a) Sensitivity is the most important property to be quantified for use of these sensors in an application. Clearly, it is most beneficial to achieve maximum sensitivity within the choice of available commercial electret microphones. A mathematical analysis is provided to predict stiffness sensitivity of commercial microphones based on manufacturer's specifications of acoustic sensitivity and a few simple measurements on a microphone.
(b) Selectivity refers to the inherent response of electret microphones to other respiratory variables. The evaluation of selectivity is more qualitative requiring field testing of microphones to determine their cross-sensitivity to changes in unwanted environmental

analytes. Evaluation of these properties helps understand the applicability of microphones for CO_2 sensing.

4.1 SENSITIVITY TO STIFFNESS CHANGES

The first property of relavance is sensitivity of electret microphones to film-stiffness changes. In this chapter, it is assumed that commercial retail microphones would be used in sensing applications. However, the theory presented would also enable characterization and comparison of custom fabricated electret microphones with commercial ones.

As described in the previous chapter, sensitivity to stiffness changes can be expressed as

$$\boxed{\frac{\partial C}{\partial k} = \frac{\varepsilon^2 A^2 V_{DC}^2}{6k^2 x^3 (x - \frac{2}{3} d_0)}} \tag{1}$$

Eq (1) provides an analytical expression for sensitivity, constants V_{DC} and k in this equation are typically unknown for commercially manufactured microphones. A numerical value for sensitivity to stiffness changes cannot be computed without prior knowledge of these constants. Constants A and d_0 can be estimated simply by physical measurements on a microphone. Separation distance x could possibly be calculated from the microphone's capacitance. To eliminate the need for knowledge of constants V_{DC} and k, an alternate expression will be derived that utilizes the expression for acoustic sensitivity (provided by microphone manufacturer) and capacitance of the microphone.

To begin this derivation, the expression for acoustic sensitivity, a commonly specified parameter, is first considered. Acoustic sensitivity of an electret microphone is given by the change in voltage across a load resistor for a given change in acoustic pressure. Acoustic sensitivity is proportional to the voltage across the microphone's capacitance; the proportionality constant depending upon supply voltage, load resistance and amplification factor of pre-amplifier (these parameters are standard for many microphones making the proportionality constant same for such microphones).

The acoustic sensitivity is then given by:

$$Acoustic\ sensitivity\ \alpha \frac{dV}{dP} = \frac{d\left(\frac{Q}{C}\right)}{dP} \tag{2}$$

where V is the voltage across the microphone, P is the acoustic pressure acting on the microphone membrane and Q is the approximately constant charge on the microphone whose magnitude depends upon the supply voltage. It can be absorbed into the proportionality constant γ to express the acoustic sensitivity as

$$Acoustic\ sensitivity = \gamma.\frac{d\left(\frac{1}{C}\right)}{dP} = \gamma.\frac{d\left(\frac{x}{\varepsilon A}\right)}{dP} = \gamma.\frac{1}{\varepsilon A}.\frac{dx}{dP} \tag{3}$$

To derive an expression for $\frac{dx}{dP}$, consider the force balance equation in an acoustic microphone,

$$\frac{\varepsilon A V_{DC}^2}{2x^2} + A.P = k(d_0 - x) \tag{4}$$

(electrical force + acoustic force = mechanical restoring force)

Differentiating,

$$-\frac{\varepsilon A V_{DC}^2}{x^3} dx + A.dP = -k.dx \tag{5}$$

$$\Rightarrow \frac{dx}{dP} = \frac{A}{\left(\frac{\varepsilon A V_{DC}^2}{x^3} - k\right)} \tag{6}$$

To eliminate unknown V_{DC} from this equation, substitute from Eq. (4)

$\frac{\varepsilon A V_{DC}^2}{2x^2} \approx k(d_0 - x)$ (assuming that force due to electrical attraction is much larger than that due to acoustic pressure)

$$\Rightarrow \frac{dx}{dP} = \frac{A}{\left(2\frac{k(d_0 - x)}{x} - k\right)} \tag{7}$$

$$\Rightarrow \frac{dx}{dP} = \frac{Ax}{3k\left(\frac{2}{3}d_0 - x\right)} \tag{8}$$

Thus,

$$\boxed{Acoustic\ sensitivity = \gamma . \frac{x}{3\varepsilon k\left(\frac{2}{3}d_0 - x\right)}} \tag{9}$$

Now, Eq. (1) can be rewritten as

$$\frac{\partial C}{\partial k} = \frac{\varepsilon^2 A^2 V_{DC}^2}{6k^2 x^3 (x - \frac{2}{3}d_0)} = \left(\frac{\varepsilon A}{x}\right).\left(\frac{\varepsilon A V_{DC}^2}{2x^2}\right).\left(\frac{x}{3\varepsilon k(x - \frac{2}{3}d_0)}\right).\frac{\varepsilon}{kx} \tag{10}$$

Substituting from Eqs. (4), (9)

$$\frac{\partial C}{\partial k} = C.\left(k(d_0 - x)\right).\left(\frac{Acoustic\ sensitivity}{\gamma}\right).\frac{\varepsilon}{kx} \tag{11}$$

Thus the final expression for sensitivity can be written as

$$\boxed{\Rightarrow \frac{\partial C}{\partial k} = \varepsilon . C\left(\frac{d_0}{x} - 1\right)\left(\frac{Acoustic\ sensitivity}{\gamma}\right)} \tag{12}$$

Eq. (12) suggests that a microphone with a larger nominal capacitance, larger acoustic sensitivity and smaller vertical separation x would be more sensitive to stiffness changes.

4.1.1 COMPARISON OF $\left(\frac{d_0}{x} - 1\right)$ FOR DIFFERENT MICROPHONES

All terms in Eq. (12) are known or measureable except $\left(\frac{d_0}{x} - 1\right)$. While d_0 can be measured accurately by measuring the thickness of the dielectric spacer, the value of x has to be computed using the capacitance of the microphone. The authors have observed that it is difficult to obtain a precise value of x due to the bending of the membrane which results in a non-linear equation between the capacitance C, electrode area A, and the separation distance x. It is noted that the equation $x = \frac{\varepsilon A}{C}$ is an approximation since the membrane is curved and not parallel to the backplate as assumed in the equation. Hence, it is not possible to obtain accurate estimates of x by measuring the capacitance and area of a microphone.

The following method is proposed to make comparisons of the term $\left(\frac{d_0}{x}-1\right)$ between microphones. The ratios of the separation distances of different microphones can be obtained more accurately by taking the ratio of $\left(\frac{\varepsilon A}{C}\right)$ for different microphones. It is noted that the value of x will always be lesser than the nominal separation distance d_0, since the membrane is always attracted towards the backplate. Also, if $x<\frac{2}{3}d_0$, then the membrane would snap into the backplate due to a non-linear increase in electrical attraction [67].

Thus,

$$\boxed{1<\left(\frac{d_0}{x}\right)<\frac{3}{2}}$$

for an electret membrane. With the above condition, it can be shown that

$$\boxed{\left(\frac{d_{01}}{x_1}-1\right)>\left(\frac{d_{02}}{x_2}-1\right)\Leftrightarrow\frac{d_{01}}{x_1}>\frac{d_{02}}{x_2}} \tag{13}$$

(Note that condition (13) holds for all $\left(\frac{d_0}{x}\right)>1$).

This implies that the term $\left(\frac{d_0}{x}-1\right)$ can be compared using the value of $\left(\frac{d_0}{x}\right)$ alone.

Now,

$$\frac{d_0}{x}=\frac{d_0 C}{\varepsilon A}\Rightarrow\frac{\left(\frac{d_0}{x}\right)_1}{\left(\frac{d_0}{x}\right)_2}=\frac{\left(\frac{d_{01}C_1}{A_1}\right)}{\left(\frac{d_{02}C_2}{A_2}\right)} \tag{14}$$

All the terms in Eq. (14) are measureable thus implying that the term $\left(\frac{d_0}{x}-1\right)$ can be compared between microphones using the ratio of $\left(\frac{d_0}{x}\right)$. It can further be shown that the ratio of $\left(\frac{d_0}{x}-1\right)$ between microphones will always be larger than the ratio of $\left(\frac{d_0}{x}\right)$.

Let $y_1 = \left(\frac{d_{01}}{x_1}\right)$, $y_2 = \left(\frac{d_{02}}{x_2}\right)$ be two numbers greater than '1' such that $y_1 > y_2$.

Let $\left(\frac{y_1}{y_2}\right) = p$, where $p > 1$. Then,

$$\frac{\left(\frac{d_{01}}{x_1} - 1\right)}{\left(\frac{d_{02}}{x_2} - 1\right)} = \frac{y_1 - 1}{y_2 - 1} = \frac{py_2 - 1}{y_2 - 1} = p + \frac{p-1}{y_2 - 1} \tag{15}$$

Since, $y_2 = \left(\frac{d_{02}}{x_2}\right) < \frac{3}{2}$

$$\frac{1}{y_2 - 1} > 2 \tag{16}$$

. Thus,

$$\boxed{\frac{\left(\frac{d_{01}}{x_1} - 1\right)}{\left(\frac{d_{02}}{x_2} - 1\right)} > 3p - 2} \tag{17}$$

Since the minimum value of $\left(\frac{y_1}{y_2}\right)$ is '1', the ratio of $\left(\frac{d_0}{x} - 1\right)$ will always be larger than the ratio of $\left(\frac{d_0}{x}\right)$ or the ratio of $\left(\frac{d_0 C}{A}\right)$ as shown in Figure 4.1. Since relatively small deflections are created by electret charges, typically $\frac{1}{y_2 - 1} >> 2$ or

$$\frac{\left(\frac{d_{01}}{x_1} - 1\right)}{\left(\frac{d_{02}}{x_2} - 1\right)} >> p \tag{18}$$

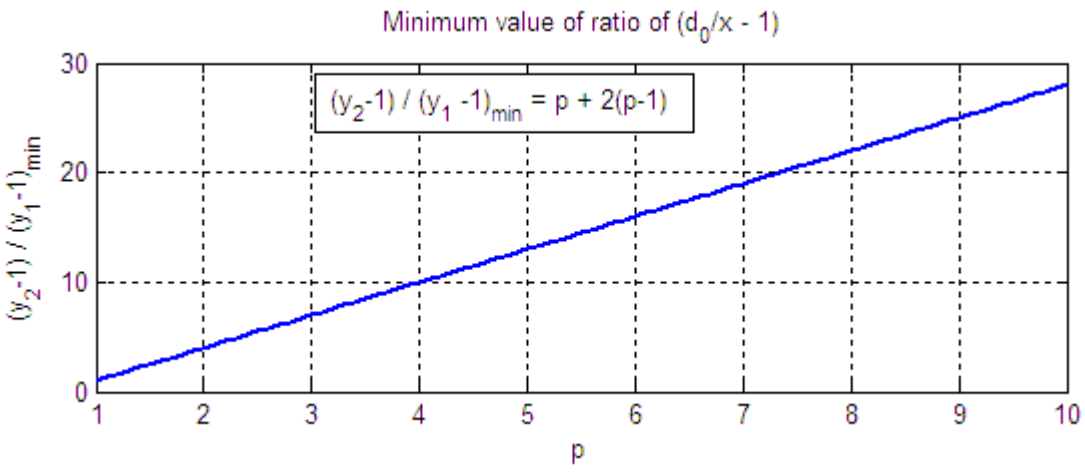

Figure 4.1. Plot of minimum value of ratio of (d_0/x - 1) vs the ratio of (d_0/x).

Summarizing, the sensitivities of microphones to stiffness changes can be compared using the product of the ratio of three terms viz.

1. Capacitance

2. Acoustic sensitivity (assuming similar load resistance, supply voltage and pre-amplification)

3. $\frac{d_0 C}{A}$ (and using Eq (17) to predict the minimum value of ratio of $\left(\frac{d_0}{x}-1\right)$)

4.2 SELECTIVITY TO STIFFNESS CHANGES

The other important property in choosing commercial electret microphones is their inherent cross-sensitivity to unwanted respiratory variables. In a sensing application, the microphone's membrane would be coated with a SWNT thin film that responds to changes in CO_2 concentration. An ideal microphone membrane should show no change in stiffness upon exposure to changing concentration of other environmental analytes. Frequently, this is not the case; since most microphones tend to use polymers with thin metal electrodes as the membrane, as shown in Figure 4.2. Different polymers tend to alter their elasticity in the presence of different analytes. A highly sensitive microphone may be unsuitable for a sensing application if the membrane exhibits cross-sensitivity to unwanted analytes. Clearly, this aspect of a sensor can only be predicted by field testing.

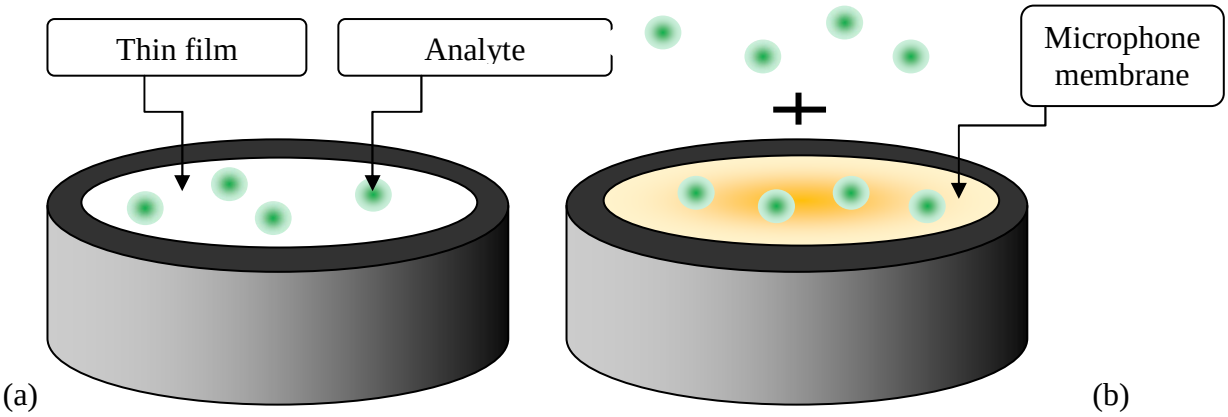

Figure 4.2. Schematic of analyte molecules interacting with (a) thin film and (b) microphone membrane.

An important environmental variable to which a microphone could show cross-sensitivity is humidity. Since environmental humidity can change significantly during the time scale of measurement, it is important that a sensor does not show cross-sensitivity to humidity. Sec 4.3.2 evaluates a number of commercial microphones for their cross-sensitivity to humidity. The inherent response to humidity observed in experiments could also be due to slow seepage of analytes into the dielectric gap of the microphone. However, the initial speed of response of microphones suggests a variation in the membrane's properties rather than seepage into the dielectric gap. Seepage into the dielectric gap could be a possible explanation for long-term drift in the sensor's response.

4.3 ILLUSTRATIVE EXAMPLES

4.3.1 COMPARISON OF SENSITIVITY

An illustrative example using commercially available microphones is used to show the application of the above techniques to compare the sensitivities of two microphones for stiffness sensing. Two commercially available no-FET electret microphones are chosen for this purpose. The ICC-MEO-96PD-00-604-NF is a front-electret while the Transound TSB 160A is a back-electret microphone. Table 4.1 provides a comparison of relevant parameters for these two no-FET electret microphones. As described in Sec 4.1.1, these include (a) capacitance, (b) acoustic sensitivity and (c) $\frac{d_0 C}{A}$.Since membrane area is

proportional to the square of diameter $\frac{d_0 C}{D^2}$ is used instead of $\frac{d_0 C}{A}$, where D is the diameter of the membrane.

Table 4.1. Comparison of parameters for ICC Intervox and Transound no-FET electret microphones

Parameter	**ICC – MEO-96PD-00-604-NF**	**Transound – TSB 160A**
d_0	20 μm	20 μm
Membrane diameter (*D*)	9.7 mm	16 mm
Capacitance	16.8pF	23.19pF
Acoustic Sensitivity	10 mV/Pa	5 mV/Pa
$\frac{d_0 C}{D^2}$	3.57 (arbitrary units)	1.81 (arbitrary units)
Capacitance * Acoustic Sensitivity * $\frac{d_0 C}{D^2}$	**599.76** (arbitrary units)	**209.87** (arbitrary units)

Figure 4.3 shows the scanning electron microscope images of the spacer cross section of above two microphones indicating that the spacers have a similar thickness, close to 20 μm.

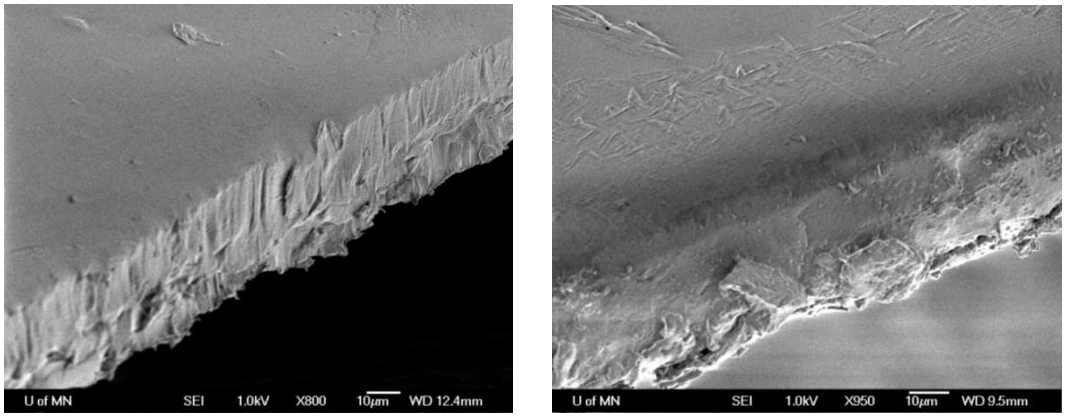

(a) ICC Microphone (b) TSB Microphone

Figure 4.3. Scanning electron microscope images of spacer cross-section of (a) ICC Intervox microphone (b) Trasound microphone.

Table 4.1 shows that ICC electret microphones are nearly 3 times as sensitive to stiffness changes as TSB microphones. It must be noted that the simplified term $\left(\frac{d_0}{x}\right)\alpha\left(\frac{d_0 C}{D^2}\right)$ is

used in the above table instead of the original term $\left(\frac{d_0}{x}-1\right)$ in Eq. (12). Based on Eq. 17, the sensitivity of ICC electret microphones to stiffness changes can be predicted to be atleast more than 7 times that of the TSB 160 microphones. Eq. 18 suggests that a much larger sensitivity can be expected for ICC electret microphones in practice. Indeed, this was found to be the case when the two microphones were used to monitor stiffness changes in thin films.

To compare the sensitivity of microphones, similar SWNT films were coated on the two microphones and carbon dioxide gas was introduced to alter their stiffness. SWNTs were purchased from Timesnano, China. Acid-treated negatively charged single walled CNTs (SWNTs) [56] were drop coated onto the microphone membranes and allowed to dry. Experiments on SWNT stiffness sensing were performed by sealing the electronics and microphone leads away from the environment. This ensured that measured capacitance changes were not affected by gas seepage between leads connecting the microphones to the electronics. Capacitance measurement for ICC microphones was performed using programmable chips (MS3110) from Irvine sensors and that for TSB microphones using programmable chips (AD7746) from Analog Device Inc. Labview™ software was used for acquiring and storing data. Ultra pure CO_2 and N_2 gas were mixed and bubbled through a saturated salt solution of sodium chloride (to maintain constant relative humidity). The concentration of CO_2 was altered by changing the relative flow rates of the gases. This synthetic mixture ensured that no unwanted gas species existed in the sensing chamber. This helped eliminate spurious stiffness changes due to adsorption of unknown gases.

Figure 4.4 shows that the capacitance of SWNT coated ICC microphones varied with CO_2 gas concentration (earlier tests confirmed that similar uncoated ICC microphones were unresponsive to CO_2 gas). Figure 4.5 shows that SWNT-coated TSB microphone showed no changed in capacitance upon introduction of CO_2 gas. The long-term drift observed in Figure 4.5 is believed to be due to slow seepage of humid air into the microphones' dielectric gap. These results show that ICC microphones respond to

stiffness changes in SWNT films deposited on their membranes while TSB-165 microphones show little or no response. Since similar SWNT films were coated on both microphones, it is concluded that ICC microphones display much higher sensitivity to SWNT film-stiffness changes. These results are in agreement with the evaluation that ICC microphones are at least 7 times more sensitive than TSB microphones.

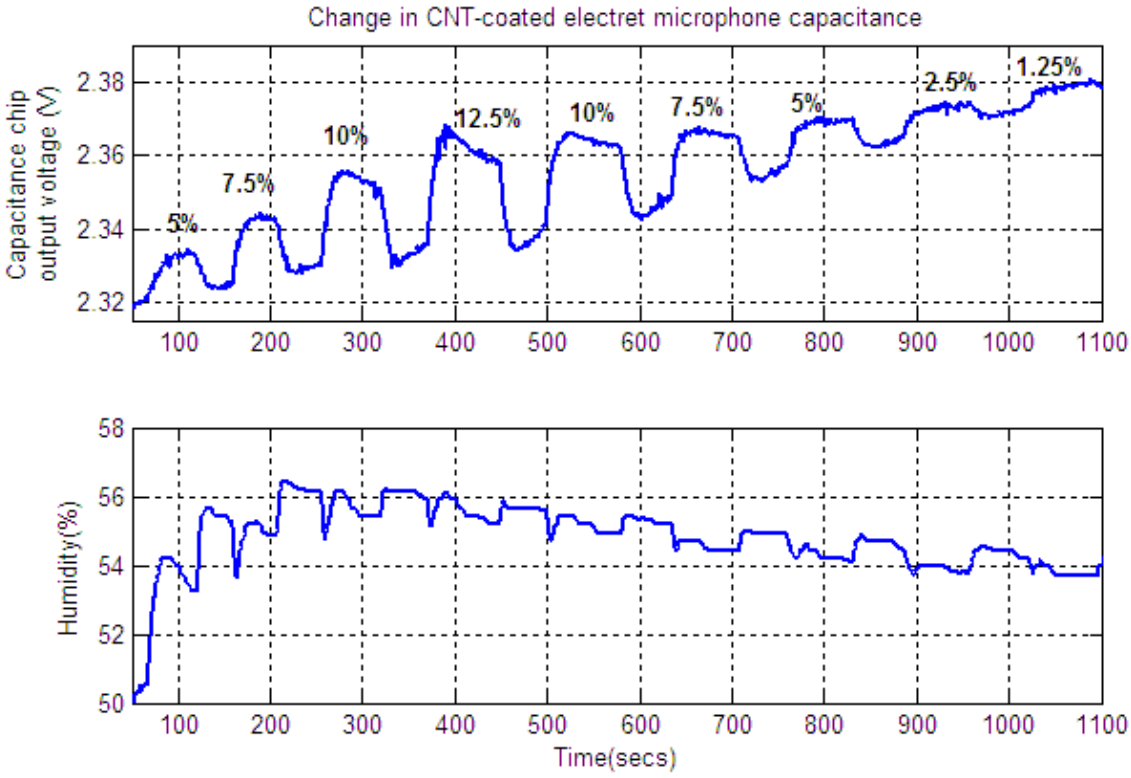

Figure 4.4. Response of SWNT coated ICC microphone to humidity and CO_2 gas

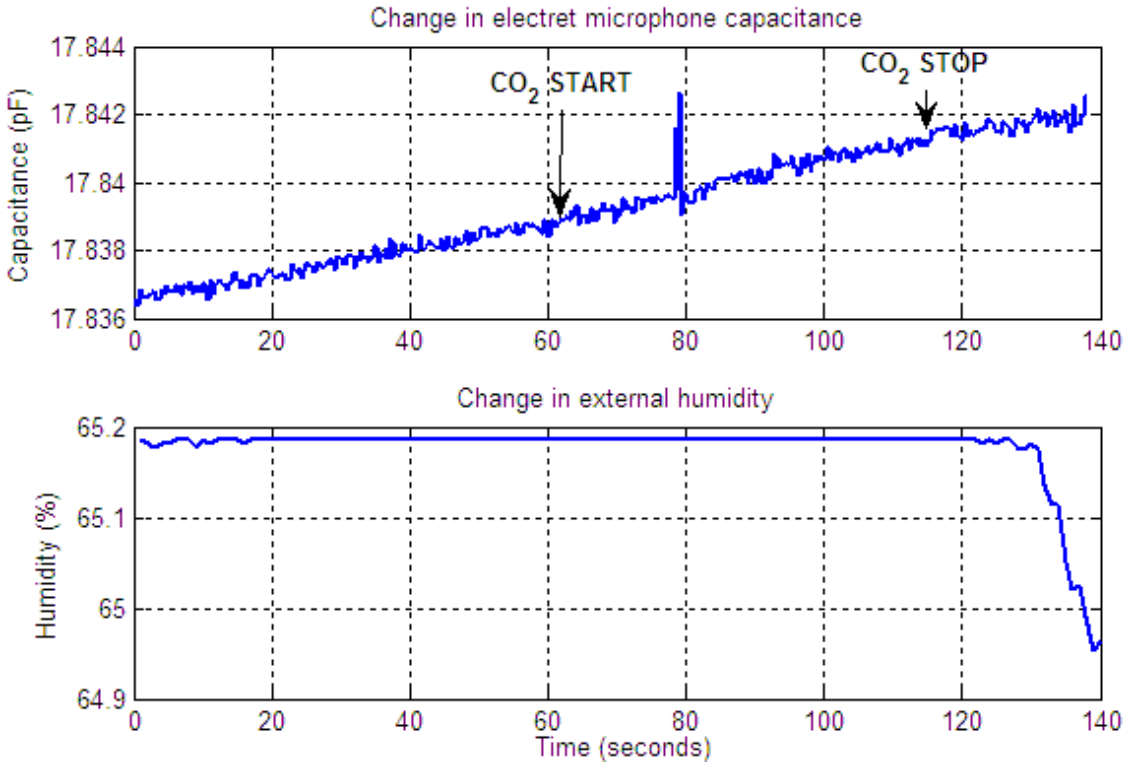

Figure 4.5. Response of SWNT coated TSB 165 microphone to CO_2 gas.

4.3.2 EVALUATION OF SELECTIVITY

This section presents an illustrative example of humidity cross-sensitivity of uncoated commercial microphones. Humidity is a common variable in most environmental sensing scenarios. Gas sensors made using commercial microphones need to be selective in their response to target gases and not respond to humidity. However, polymeric microphone membranes may be expected to undergo change in stiffness with varying humidity. Hence, uncoated microphones need to be tested for their humidity response to determine their inherent cross-sensitivity to humidity. Similar tests would also be required for other interfering analytes that could vary in large concentrations.

A batch of ICC electret microphones was chosen for testing their cross-sensitivity to humidity. This batch was chosen because of observed interference due to humidity during CO_2 gas sensing experiments. Experiments were performed with sealed sensors as described in Sec 4.3.1. Ultra pure N_2 gas was bubbled through a sodium chloride salt

solution to increase humidity in the sensing chamber from room level to 50%. The N_2 flow rate and temperature were kept constant throughout the experiment. Figure 4.6 shows the variation in capacitance of two different ICC electret microphones with increasing humidity. The change in the uncoated microphone's capacitance with humidity was found to be greater than 0.005pF for 10% change in relative humidity. This response was much larger than that of SWNT coated microphones to room-level changes (100s of ppm) in CO_2 gas concentration (<0.001pF). Hence, such a microphone would be unsuitable for indoor CO_2 gas monitoring. Similar interference from humidity may be expected for sensing other types of gases as well. However, such microphones would be a suitable alternative for thin film monitoring in interference-free environments such as vacuum chambers.

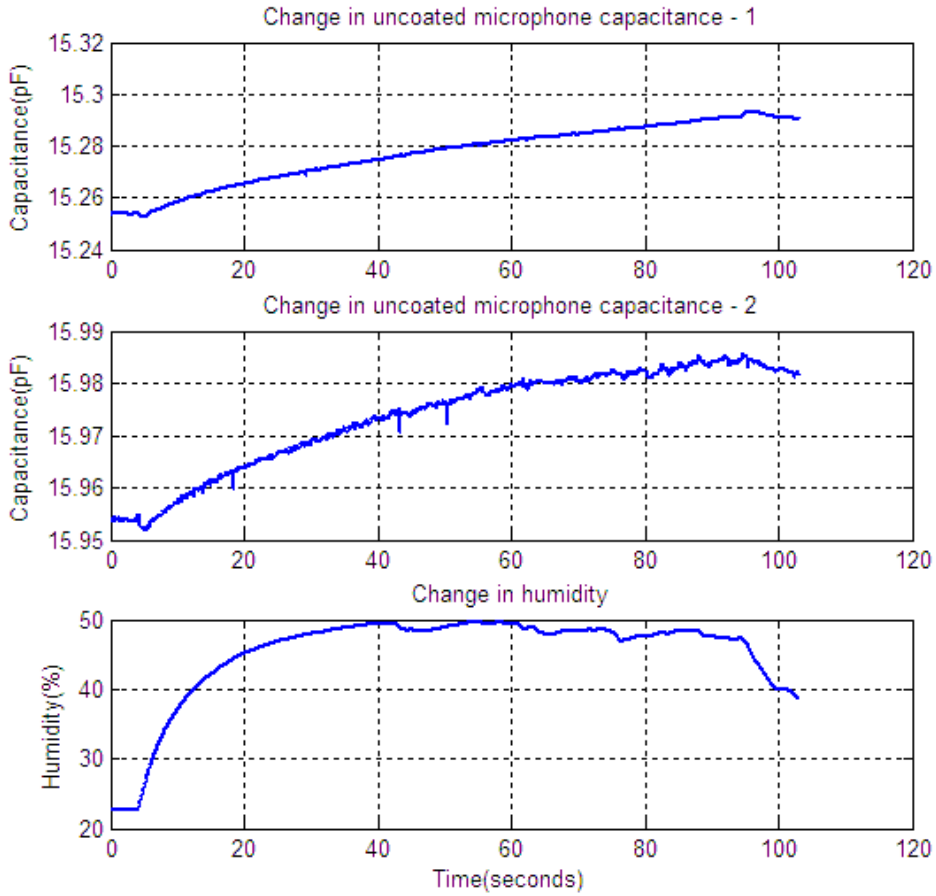

Figure 4.6. Change in capacitance of uncoated ICC microphones with varying humidity (electronics sealed away from humidity change).

The above example illustrates that certain microphones may be unsuitable for CO_2 sensing applications. It is noted that some samples of microphones used in the previous chapter were found sufficiently insensitive to humidity. Thus, testing is required to predict the cross-sensitivity of microphones to unwanted analytes. The reason for the inherent insensitivity of few tested microphones is not clear. Some possible reasons could be the insensitivity of membrane material and good isolation of membrane from analytes by the top metallic electrode and mechanical construction.

4.4 CONCLUSION

A mathematical method has been provided to compare the relative sensitivities of different commercial microphones. This method requires physical measurements on microphones and would need testing for determination of sensitivities.

Membrane material and microphone construction are shown to affect selectivity of microphones. Hence, it is not possible to predict selectivity apriori and field testing is required to identify potential interferers during sensing. Humidity is a frequent interferer during gas sensing and found to alter the capacitance of most types of microphones. An ideal electret microphone for CO_2 sensing applications should use an inert membrane material; but repeated tests showed poor selectivity in all tested models. Certain samples from different batches of the ICC Intervox microphone showed good selectivity, but this performance was not repeatable in other models. Thus, the fabricational variations of commercial microphones make them unsuitable for repetable CO_2 sensing. It is conceivable that custom-fabricated microphones with tightly controlled membrane properties could yield repeatable results. But, such fabrication was deemed infeasible and hence not pursued.

CHAPTER 5. MODEL INVERSION TECHNIQUES FOR BREATH-BY-BREATH MEASUREMENT OF CO_2 FROM LOW BANDWIDTH SENSORS

5.1 INTRODUCTION

As described in previous chapters, novel carbon nanotube-based sensors show promise for development of inexpensive and wearable respiratory CO_2 sensors. However, sensor embodiments based on stiffness/conductivity measurement of functionalized carbon nanotubes are not sufficiently insensitive to other environmental variables making them unsuitable for reliable CO_2 sensing. This chapter develops techniques to enable use of selective but slow CO_2 sensors for breath-by-breath tracking of CO_2 concentration. This is achieved by mathematically modeling the sensor's dynamic response and using model-inversion techniques to predict input CO_2 concentration from the slowly-varying output.

A relatively selective solid state sensing technology has been that of metal-carbonate electrolytic sensors. Electrolytic carbonate sensors possess sensitivity and selectivity suitable for respiratory monitoring. One embodiment [21] based on Li_2CO_3-$CaCO_3$ was shown to be particularly selective. This embodiment was later commercialized by Figaro Engineering, Japan [72]. Figure 5.1 shows a picture of a commercial solid-state CO_2 sensor system from Figaro Engineering.

Figure 5.1. Photograph of CDM4160 CO_2 sensing module from Figaro Engineering

However, such sensors show response times that are orders of magnitude higher (10's of seconds) than that required for respiratory monitoring (100ms). Hence they have been traditionally used for slow CO_2 monitoring applications like indoor air quality and greenhouse monitoring. However, it is possible to use such slow sensors for monitoring fast CO_2 concentration changes using a mathematical model of its time-response. This is shown in this chapter using a Figaro electrolytic sensor.

The developed algorithm allows commercial electrolytic CO_2 sensors to be used for monitoring fast changes in respiratory CO_2 gas concentration. The estimation algorithm which could be easily implemented on a micro-controller or a base-computer is not expected to substantially add to the size and cost of electrolytic CO_2 sensors. Thus, this technique heralds the use of low-cost electrolytic CO_2 sensors for ambulatory respiratory monitoring.

The following section discusses algorithm development and signal processing techniques for estimation of fast varying CO_2 concentration input from a slow Figaro electrolytic sensor. Then, details of the experiments with the Figaro sensor are provided followed by experimental comparisons with an infra-red respiratory CO_2 analyzer. Corrections to the initially assumed dynamic model are proposed based on observed results. Finally, a robust second-order cascaded model is found to be sufficient for predicting respiratory CO2 input. Figure 5.2 summarizes the modeling procedure and results obtained from using different models.

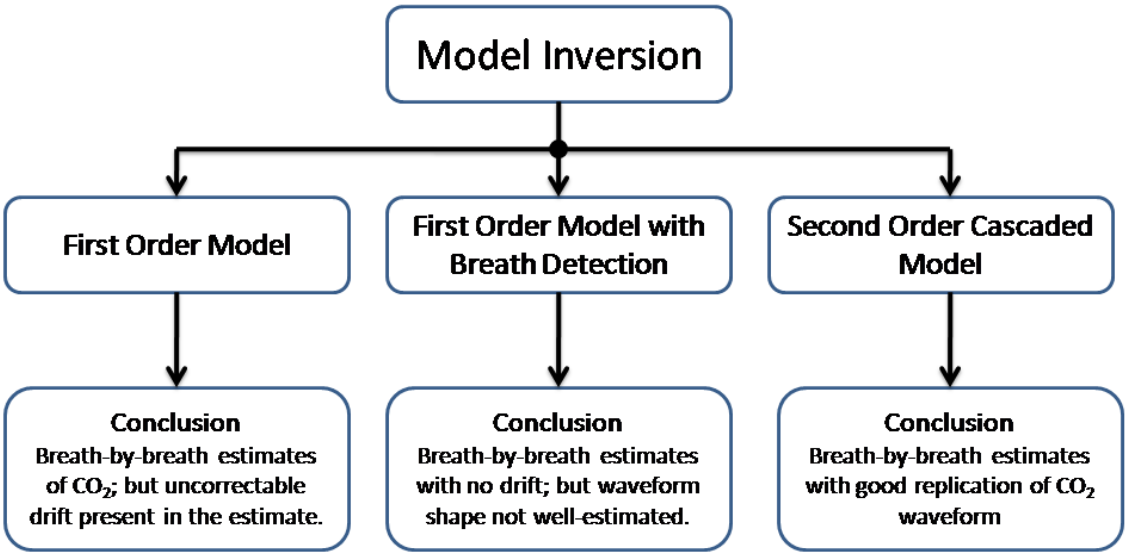

Figure 5.2. Summary of dynamic models for Figaro sensor used for estimating respiratory CO_2 concentration

5.2 Model Inversion Using First Order Model

The development of an estimation algorithm requires a mathematical model of the slow sensor's dynamic response. Using a model, it would be possible to understand the relation between the actual input (respiratory CO_2 concentration) and the observed output from the sensor. In this work, the sensor is initially modeled as a first order transfer function of the form:

$$y(t) = x(t) - \tau \dot{y}(t) \tag{1}$$

where y is voltage from the sensor, x is the respiratory CO_2 concentration and τ is the time constant. This model is chosen because the first order response closely resembles that of an electrolytic CO_2 sensor's response. Figure 5.3 shows the time response of a first order system (τ = 90) and Figure 5.4 shows the observed response from a Figaro CO2 sensor. Since the sensor's response was similar to a first order system's response, the above model initially seems adequate.

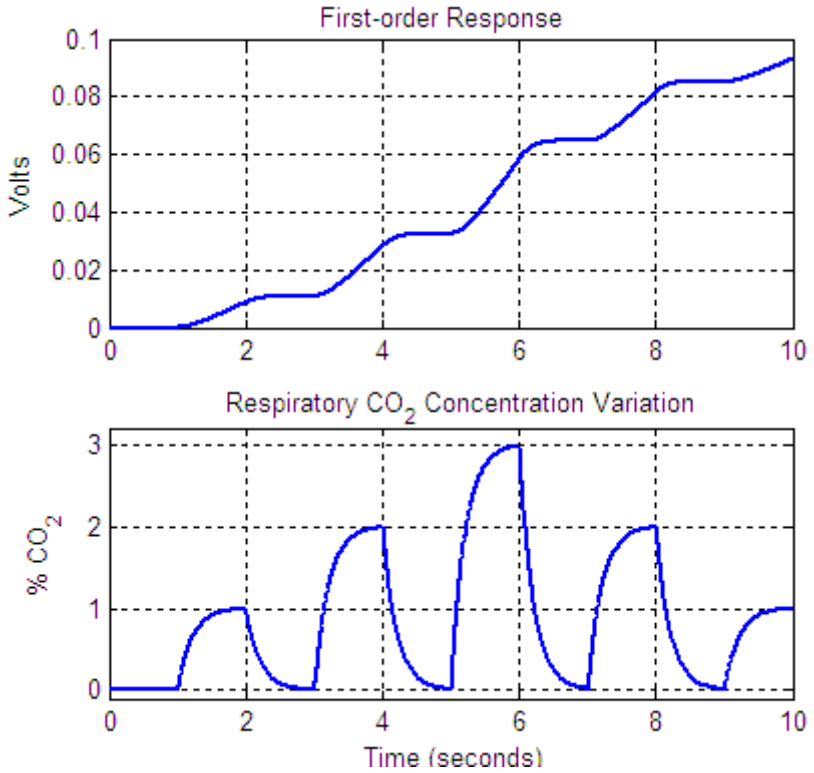

Figure 5.3. Expected output from a CO_2 sensor showing a first-order response to respiratory CO_2 input

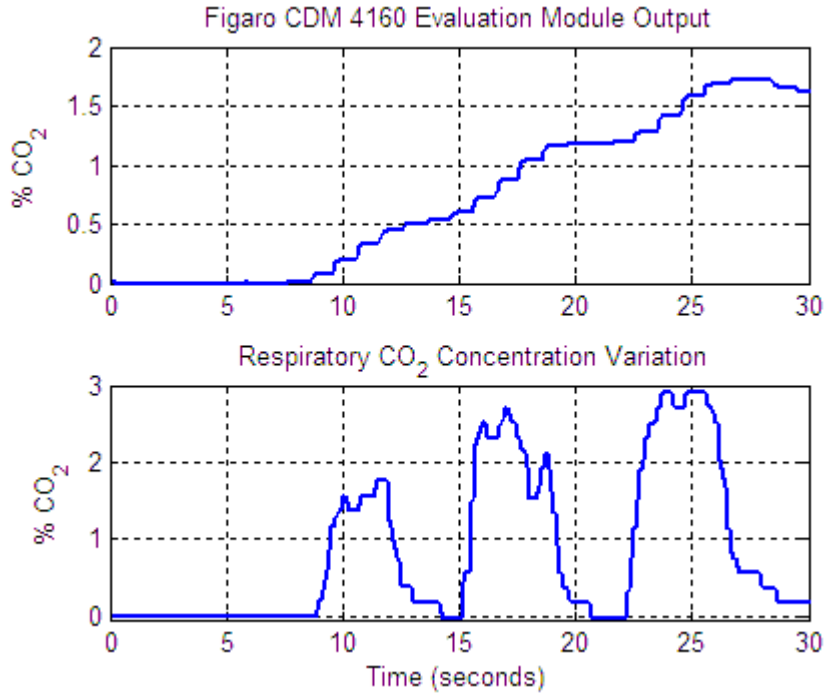

Figure 5.4. Observed response of Figaro CO_2 sensor to real breathing

An inverse first-order equation will then be used to predict the fast varying input provided the time constant τ of the system is known (the time constant itself can be determined by experiments). In this work, further signal processing was also used to remove the effect of noise and in the data. The complete procedure is summarized below:

1. Filter output data to decrease noise
2. Perform inverse first-order transformation to get noisy estimate of input
3. Filter noisy estimate to obtain a smooth estimate of input

5.2.1 ESTIMATION ALGORITHM

Let the respiratory CO2 input and sensor output (as functions of time) be denoted by $x(t)$ and $y(t)$ respectively. Eq. 1 can be rewritten as:

$$y(t) + \tau \dot{y}(t) = x(t) \tag{2}$$

Substituting $\dot{y}(t) = \frac{y[n] - y[n-1]}{\Delta t}$, Eq. 2 can be written in discrete-time domain as:

$$x[n] = y[n] + \tau . \frac{y[n] - y[n-1]}{\Delta t} \tag{3}$$

where $x[n]$, $y[n]$, $y[n-1]$ denote present input, present output and output at previous time-step respectively. τ and Δt are sensor's time constant and data acquisition system's sampling time respectively. Eq. 3 can be used to estimate the input $x[n]$ by measurement of the output $y[n]$ over time.

The above technique assumes that the sensor's time constant τ is known *apriori*. Time constant τ is defined as the time taken for the sensor's response to reach 63% of its final value. The time constant can be calculated by calibration experiments.

5.2.2 NOISE REMOVAL

As Eqs. 2, 3 involve differentiation of a measured signal, high frequency measurement noise will be amplified greatly. Hence the estimate of the input $x[n]$ will be noisy. To reduce the effect of noise, the measured signal $y[n]$ is filtered through a low-pass filter

before using Eq. 3. However, such filtering does not completely eliminate noise in the measurement. Hence, the input-estimate $x[n]$ is further filtered through a low-pass filter to remove noise and make the signal readable.

5.2.3 RESULTS

The above procedure was used to estimate the breathing input to a Figaro CDM 4160 evaluation module. A calibrated NDIR capnograph (Nonin LifeSense with analog voltage output) was used to compare estimates with true respiratory CO_2 concentration. The capnograph drew breath samples using an internal pump through a 21" nasal pressure cannula (Medcare #1420002) which was stuck on the outer wall of the Figaro CO_2 sensor as shown in Figure 5.5. Note that delays due to transport through sampling tube are not compensated in this work as they do not affect comparison between estimated and measured CO_2 concentrations.

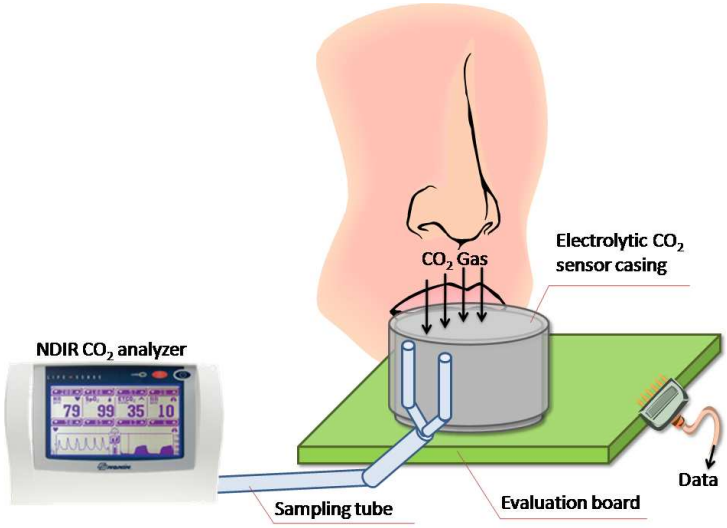

Figure 5.5. Schematic diagram of showing sampling tube stuck on Figaro CO_2 sensor's wall (not to scale)

Initial estimates (with τ = 17) using the first order model for the Figaro sensor resulted in drift in the estimate. This is shown in Figure 5.6. The drift observed in the estimate could not be corrected by altering the value of τ used in Eq. 3 indicating that the first-order model could not completely capture the dynamic response of the sensor.

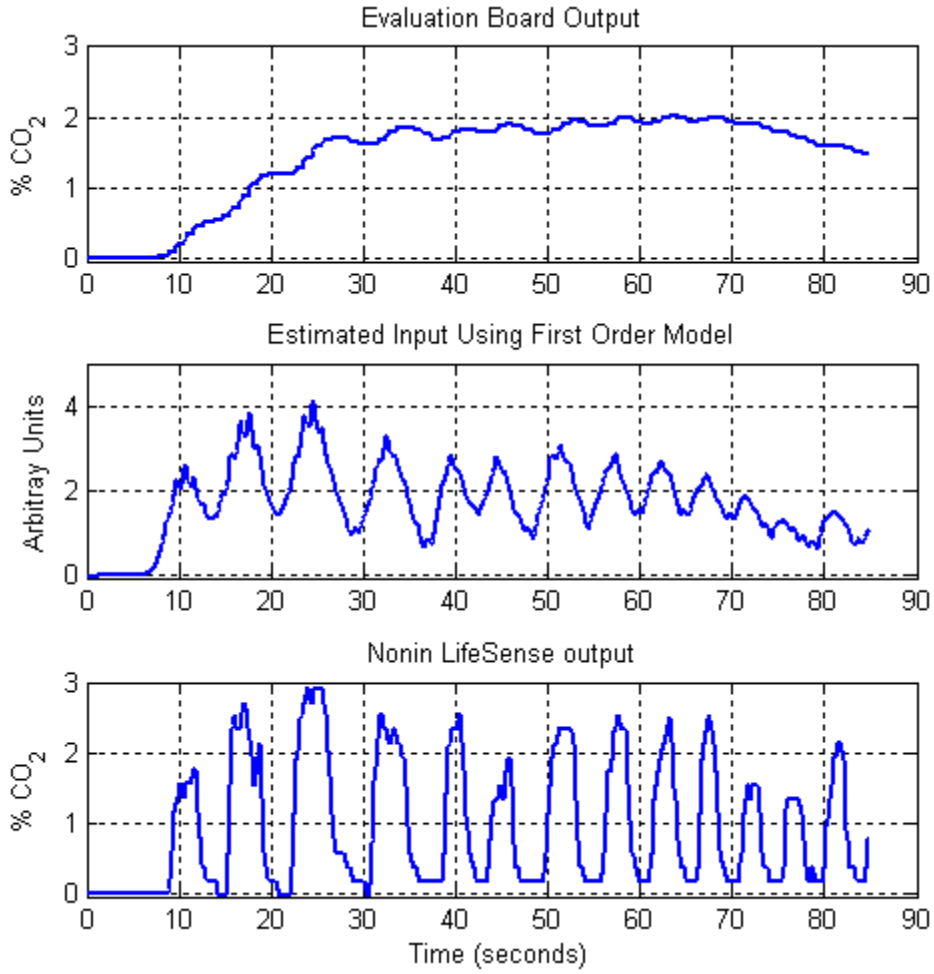

Figure 5.6. Drifting estimate using first order model for CO_2 sensor

5.2.4 BREATH DETECTION

One technique to remove the baseline drift observed in Figure 5.6 is breath detection and compensation. This technique involves detecting breaths and setting the CO_2 concentration at the start and end of breaths to zero. The estimated input is then correspondingly subtracted by the line equation between the two boundary points as shown in Figure 5.7. Breath detection itself is achieved by filtering the estimated input to a smooth curve and tracking the change in sign of the slope. Filtering is important to eliminate false slope changes due to noise in the estimated input. The filters used in this work are chosen to cause no change in phase. The obtained starting and ending time stamps of each breath are then used to correct drift in the unfiltered estimate.

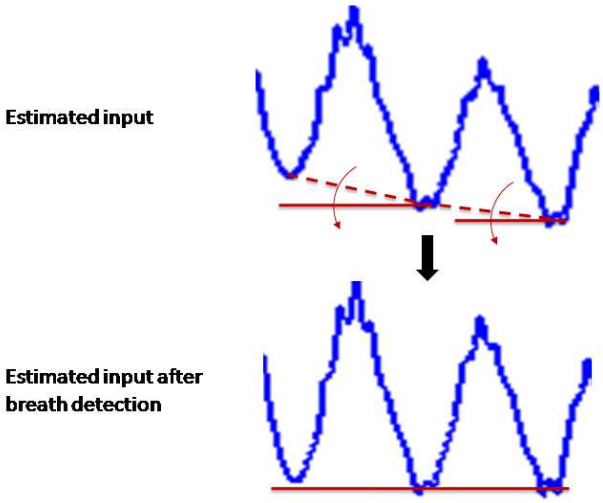

Figure 5.7. Drift removal between individual breaths in estimated input

This technique over-rides inaccuracies in system modeling using prior knowledge of the input. However, it suffers from two key limitations; (a) it cannot accurately track the shape of the true capnogram because of wrong system model and (b) it is likely to be erratic when CO_2 concentration settles to non-zero values at the end of each breath. Figure 5.8 shows that breath detection using the first-order model is capable of eliminating drift in estimation; but does not track the shape of capnograms.

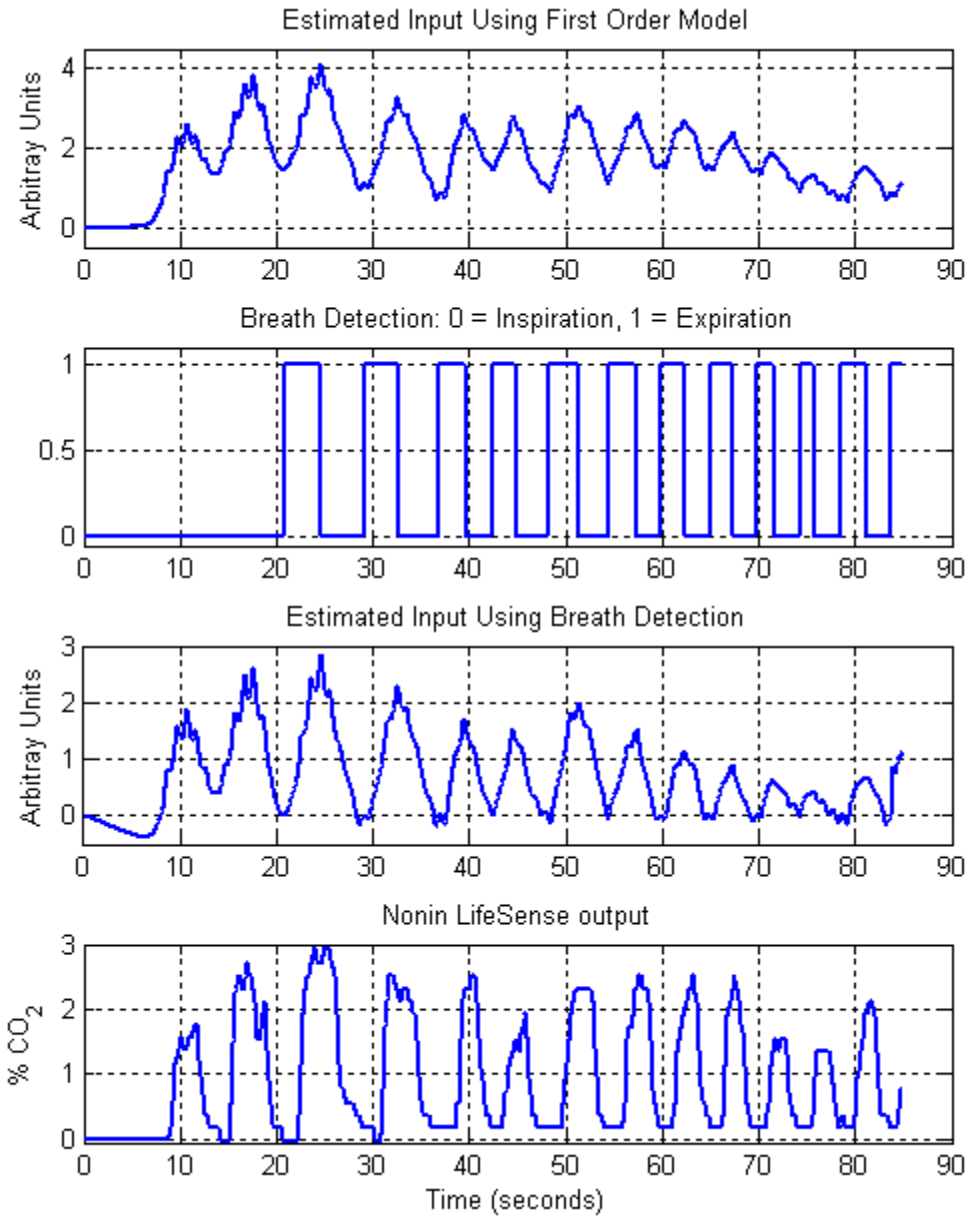

Figure 5.8. Drift-corrected estimate using first order model for CO2 sensor and breath detection

5.3 SECOND ORDER CASCADED MODEL

Since the first order model does not provide a completely accurate estimate of the capnogram, a more accurate model is developed to directly remove drift, while simultaneously correcting the shape of estimated input. The assumption behind the first order model was that the slow response was due to the inherent speed of the electrolytic sensor. The effect of the zeolite filter covering the sensor [21] was ignored in the model. Zeolite filters are typically used to absorb certain interfering gas species that could

corrupt the sensor's output. However, gas transit through such filters reduces the speed of response of the sensor. Thus zeolite filters enable robust sensing sacrificing speed of response.

In order to investigate the effect of this filter, a new experiment was designed to annul the delay due to gas flow through the filter. This was accomplished by drilling holes on the sensor assembly's walls close to the base and the electrolytic sensor. The tube from the capnograph was inserted through these holes close to the electrolytic sensor and beneath the zeolite filter, as shown in Figure 5.9.

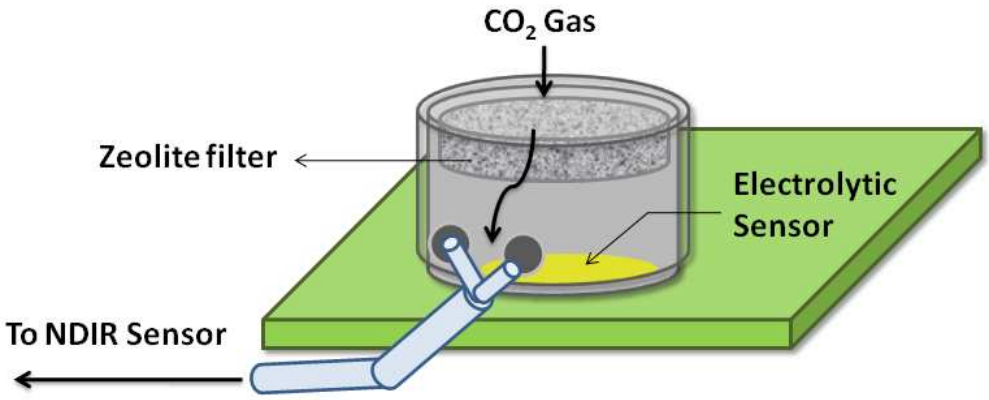

Figure 5.9. Schematic diagram of experimental setup to inspect delay due to zeolite filter

This ensured that the electrolytic and NDIR sensors experienced similar delays due to flow through the filter. Indeed, it was observed (Figure 5.10) that the delay through the filter was eliminated due to suction exerted by the NDIR sensor's pump. Figure 5.10 shows the estimated CO_2 concentration using a first-order model with a much smaller time constant (τ = 4) to compensate for the inherent delay in the electrolytic sensor.

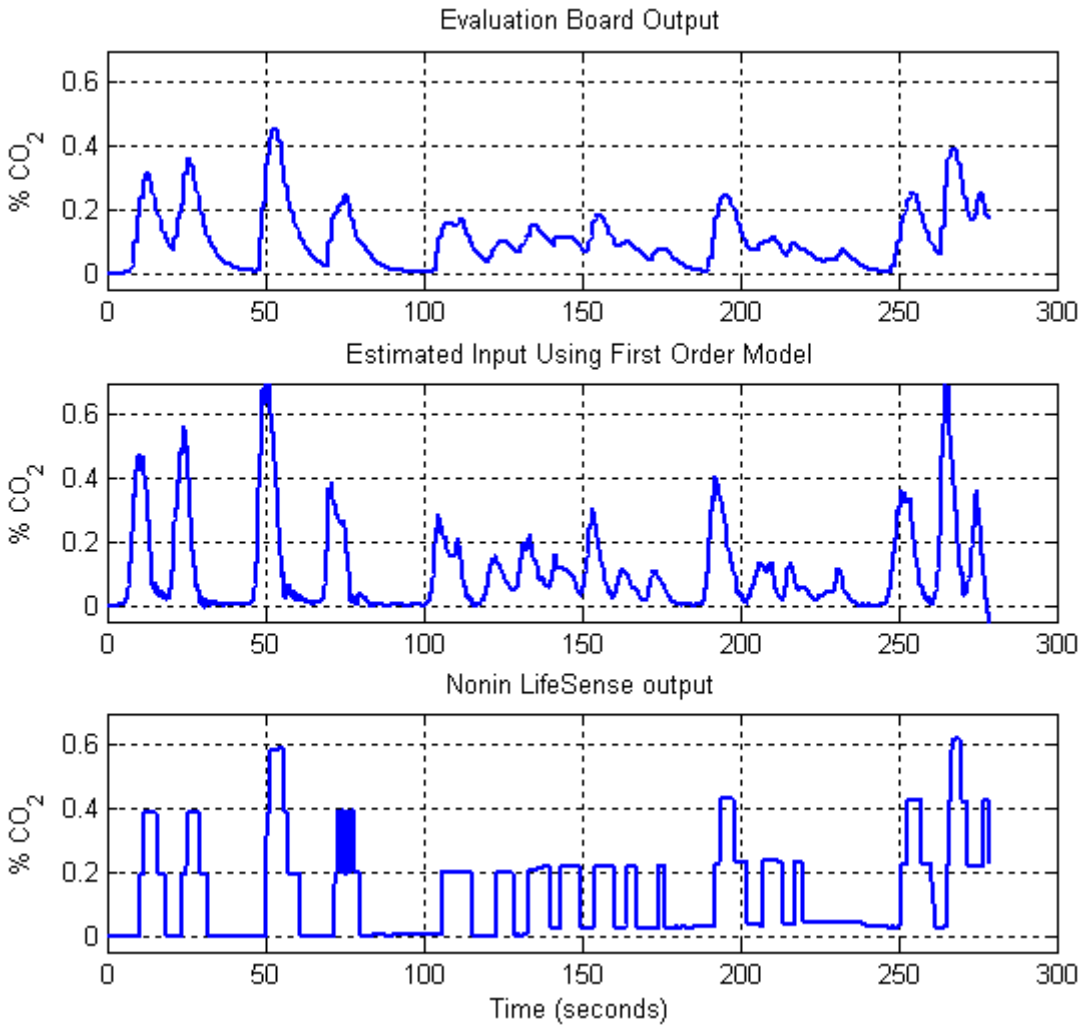

Figure 5.10. Estimation of CO_2 gas concentration after eliminating delay due to zeolite filter

It can be seen from Figure 5.10 that accurate estimation of respiratory CO_2 concentraion is possible when a pump draws air through the electrolytic sensor. In itself, this experiment shows that an additional pump would enable use of electrolytic sensors for respiratory CO_2 sensing. However, the goal of this chapter is to develop a light-weight sensor that would be wearable and inexpensive. Hence, addition of pump hardware would not be suitable.

However, it can be concluded using the above experiment that the observed speed of response in is largely dominated by gas transit through the zeolite filter. Further, the first order model is also found to be inadequate because of the presence of two first order

responses in the system (due to zeolite filter and electrolytic sensor respectively). Hence, a second order model is chosen for the system and the input estimation algorithm changed appropriately. The second order model is chosen as a cascade of two first order models:

$$y(t) = y_f(t) - \tau_s \dot{y}(t),\ y_f(t) = x(t) - \tau_f \dot{y}_f(t)$$

where y_f is unmeasured CO_2 concentration of outflow from zeolite filter, τ_f and τ_s represent time constants for filter and sensor respectively. Following the derivation in the previous section,

$$y(t) + \left(\tau_f + \tau_s\right)\dot{y}(t) + \tau_f \tau_s \ddot{y}(t) = x(t) \tag{4}$$

Substituting $\ddot{y}(t) = \dfrac{y[n] - 2y[n-1] + y[n-2]}{\Delta t^2}$, Eq. 4 can be written in discrete-time domain as:

$$x[n] = y[n] + \left(\tau_f + \tau_s\right).\frac{y[n] - y[n-1]}{\Delta t} + \tau_f \tau_s.\frac{y[n] - 2y[n-1] + y[n-2]}{\Delta t^2} \tag{5}$$

Calibration experiments using the Nonin LifeSense CO_2 analyzer and Figaro CO_2 sensor were used to obtain values for τ_f, τ_s. MATLAB™ software's system identification toolbox was used to identify the time constants in the second order model as $\tau_f = 15.13$ and $\tau_s = 1.44$. The software computes the best fit between the predicted data and measured data to calculate these time constants. Trials with several model orders and time-constant values also indicated the correctness of the second order model and time constant values respectively. These time constants were used to estimate the input in other experiments.

Figure 5.11 shows the comparison between first and second order models in predicting the respiratory input due to a single breath. The error in estimating the input due to the first order model is clear from Figure 5.11. Figure 5.12 shows the effect of using Eq. 5 in correcting the drift observed in Figure 5.6.

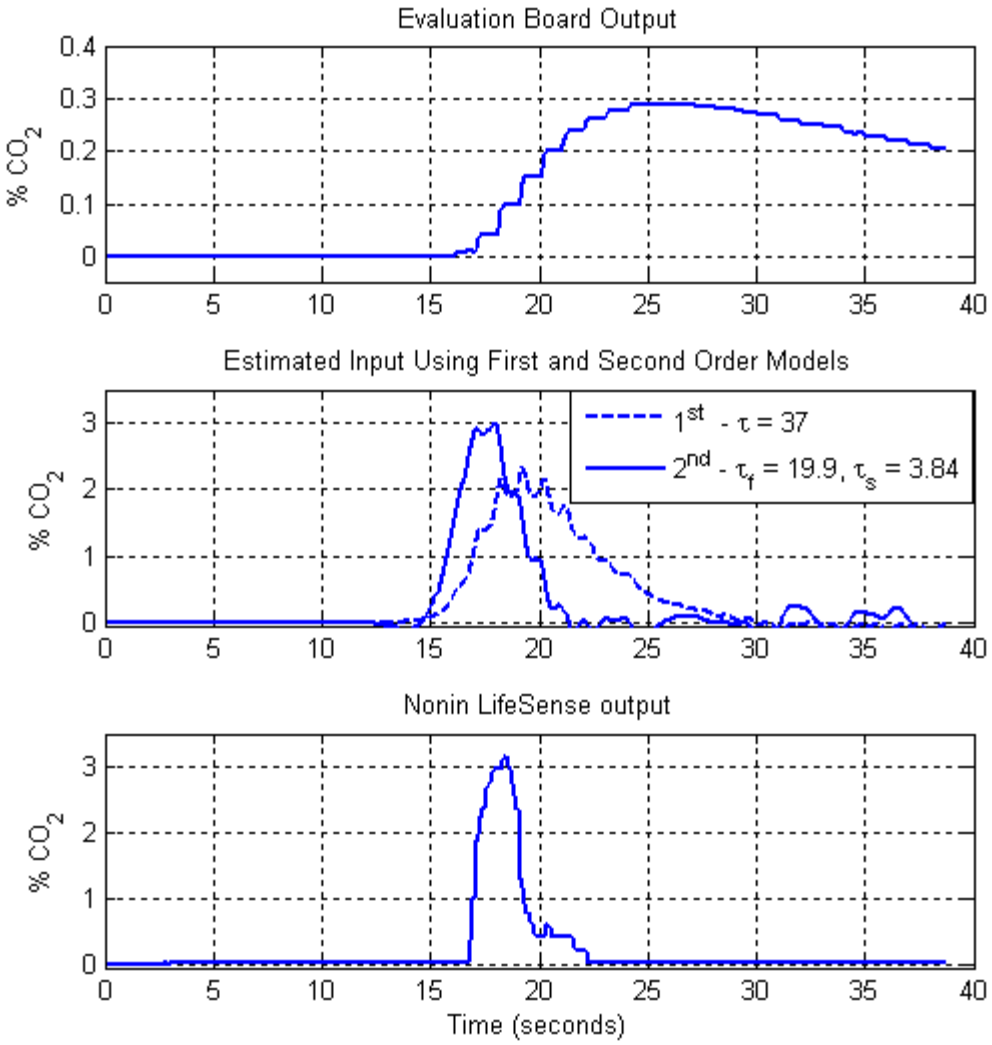

Figure 5.11. Comparison of estimated input using first and second order models for a single breath

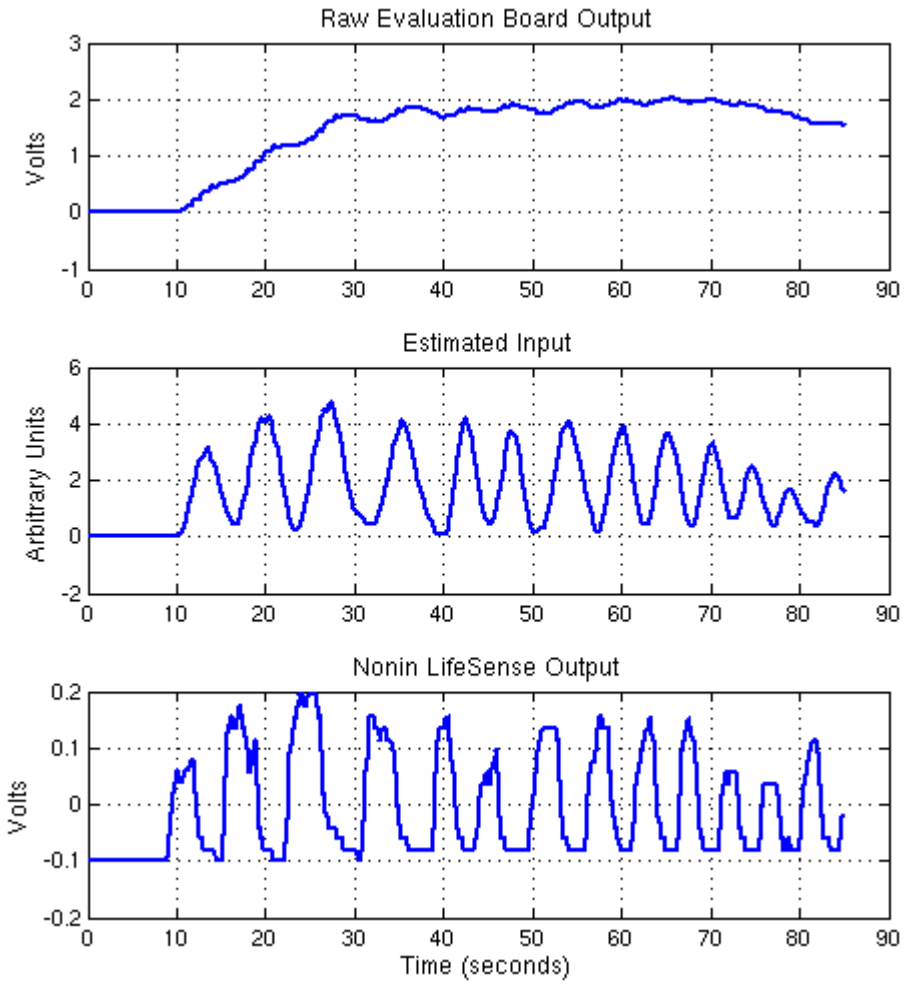

Figure 5.12. Drift-free estimate using second order model for CO_2 sensor

It may be seen from Figure 5.12 that the estimation algorithm reliably tracks variation in peak CO_2 concentration in every breath with little drift. However, the shape of the estimated capnogram is different, being affected by filtering to remove noise. In order to improve this shape, it is desirable to use filters with larger cut-off frequencies. However, low-frequency noise in the measured signal necessitates smaller cut-off frequencies. Hence, it is required to remove low-frequency noise from the measured signal.

5.3.1 NOISE REMOVAL

Upon investigation the frequency spectrum of the measured signal, a spurious low frequency tone (1 Hz) and its harmonics are found to be dominant. Since 1 Hz is close to

the CO_2 variation rate, filters designed to remove this frequency also cut off frequencies of interest in the estimated input. This in turn affects the shape of estimated capnogram. This low frequency tone can be traced to the 1 second update rate of the CO_2 sensor's evaluation board used in the experiment. Figure 5.13 shows that voltage measured from the evaluation board is updated once every second. This results in low-frequency chatter in the measured output voltage. This is an embodiment of the sensor used in this application and not of the estimation technique itself. Nevertheless, such noise affects the quality of estimated input because of the similarity in repetition rate with the true signal (respiratory CO2 concentration).

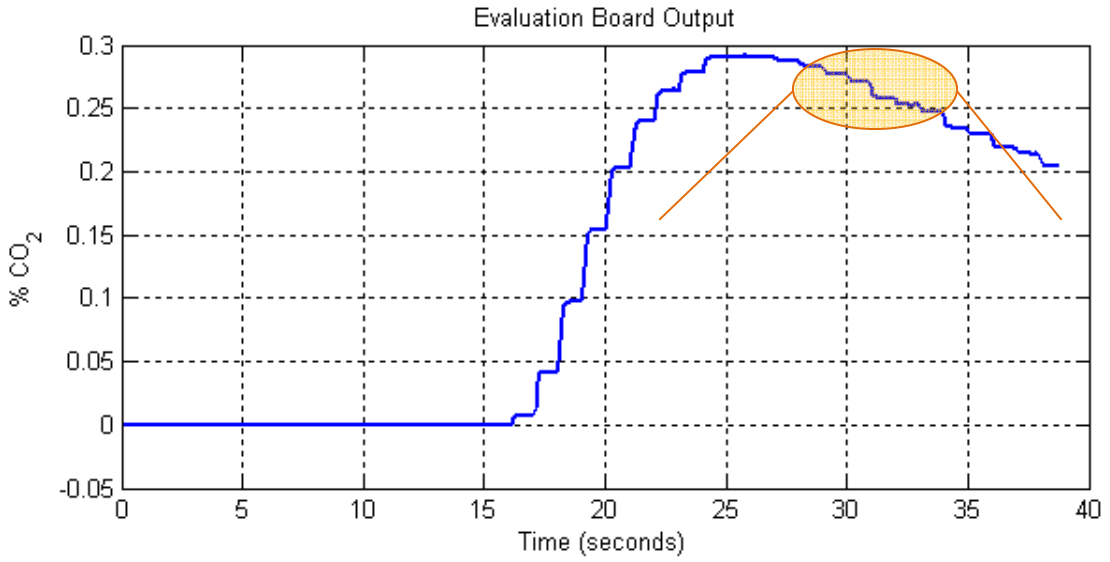

Figure 5.13. One second update rate of output from evaluation board; Inset: zoomed view

The update rate of the evaluation board is controlled by a factory-programmed microprocessor that measures the raw voltage from the sensor and converts it into CO_2 concentration while calibrating out temperature variation. Since the microprocessor cannot be reprogrammed, the sensor's raw output voltage is directly measured in this work to compute the CO_2 concentration without any delay. This is possible through the Nernst equation which relates the electromotive force generated by the electrolytic cell to the CO2 concentration. This equation is given by:

$$EMF = E_c - \frac{RT}{2F}\ln(P_{CO_2}) \tag{6}$$

where *EMF* is electromotive force, T is temperature, P_{CO_2} is partial pressure of CO_2 gas, E_c, R and F are constants.

Since EMF generated is typically small, the evaluation board contains amplifiers to boost the EMF into a measurable voltage. However, the amplification factor being unknown, it is not possible to predict CO_2 gas concentration from the amplified output using Eq. 6. Hence a least-squares-fit approach is used to identify parameters in Eq. 6.

From Eq. 6, the relation between measured voltage and CO_2 concentration can be written as:

$$V_{sensor} = kE_c - \frac{kR}{2F} T \ln(\chi_{CO_2}) \tag{7}$$

where V_{sensor} is voltage measured after amplification of EMF, *k* is amplification factor and χ_{CO_2} is mole fraction (concentration) of CO_2. Then,

$$V_{sensor} - V_{ref} = -\frac{kR}{2F}\left(T \ln(\chi_{CO_2}) - T_{ref} \ln(\chi_{CO_2-ref})\right) \tag{8}$$

or

$$V_{sensor} - V_{ref} = -\frac{kRT_{ref}}{2F}\left(\frac{T}{T_{ref}} \ln(\chi_{CO_2}) - \ln(\chi_{CO_2-ref})\right) \tag{9}$$

where V_{ref} is the voltage measured before breathing, χ_{CO_2-ref} is steady CO_2 concentration before breathing and T_{ref} is steady sensor temperature before breathing. The variables in Eq. 9 include V_{sensor}, χ_{CO_2} and T with all other terms being constant. Hence Eq. 9 may be rewritten as:

$$V_{sensor} - V_{ref} = a\frac{T}{T_{ref}} \ln(\chi_{CO_2}) + b \tag{10}$$

where $a = -\frac{kRT_{ref}}{2F}$ and $b = \frac{kRT_{ref}}{2F} \ln(\chi_{CO_2-ref})$. The ratio $\frac{T}{T_{ref}}$ can be computed by measurement of temperature using an inbuilt thermistor. Eq. 10 can then be used to compute values for constant *a* and *b* using a least-squares fit on the plot of

$\left(V_{sensor} - V_{ref}\right)$ vs. $\frac{T}{T_{ref}}.\ln(\chi_{CO_2})$. χ_{CO_2} itself is obtained from the slow voltage output of the evaluation board.

Upon estimation, constants *a* and *b* can be used to calculate the CO_2 concentration in real-time using the raw voltage output of the electrolytic sensor as shown in Eq. 11.

$$\chi_{CO_2} = \exp\left(\frac{V_{sensor} - V_{ref} - b}{a}.\frac{T_{ref}}{T}\right) \tag{11}$$

Figure 5.14 shows the linear relationship between $\left(V_{sensor} - V_{ref}\right)$ and $\frac{T}{T_{ref}}.\ln(\chi_{CO_2})$ indicating the correctness of the above analysis. Figure 5.15 further shows the comparison between CO_2 concentration estimated from sensor's voltage output and measured from the evaluation board.

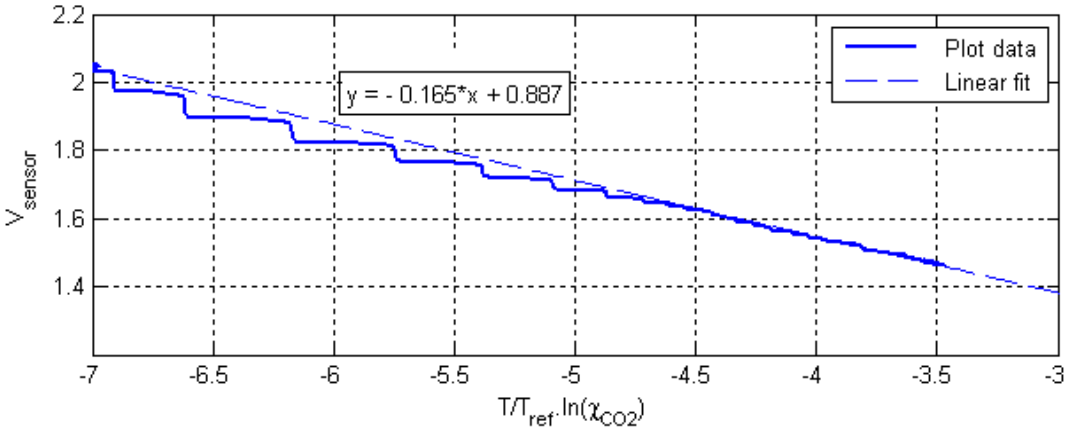

Figure 5.14. Linear relationship between raw sensor voltage and natural logarithm of CO_2 concentration

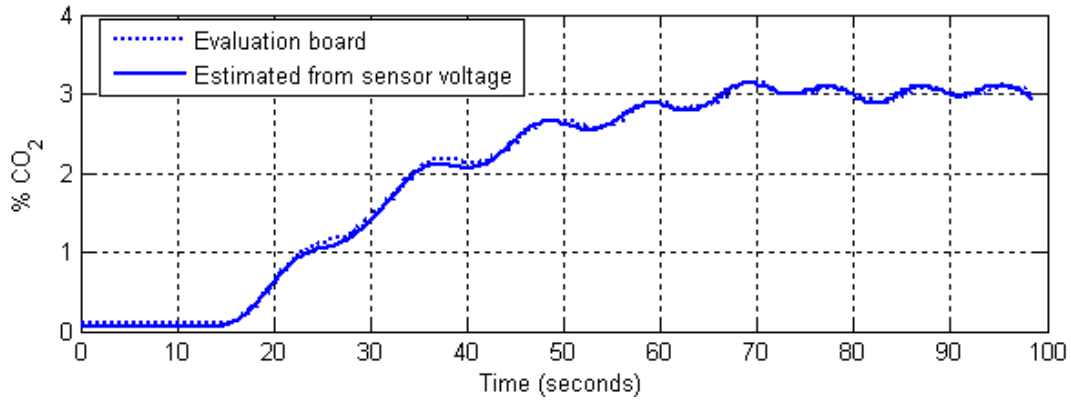

Figure 5.15. Comparison of CO_2 concentration predicted from raw sensor voltage with evaluation board's output

Eq. 5 is then used to estimate respiratory CO_2 input using the CO_2 concentration value obtained from Eq. 11. Figure 5.16 shows the resulting estimate of CO_2 input with a second-order low-pass filter having a cut-off frequency of 0.6 Hz. Note that the predicted CO_2 concentration from the sensor voltage is filtered with a low pass filter (cut-off frequency = 1.2Hz) prior to estimation. Figure 5.16 suggests that this estimate too has low frequency tones superimposed on the estimate. As discussed above, filters to remove such low frequency noise distort the shape of the capnogram.

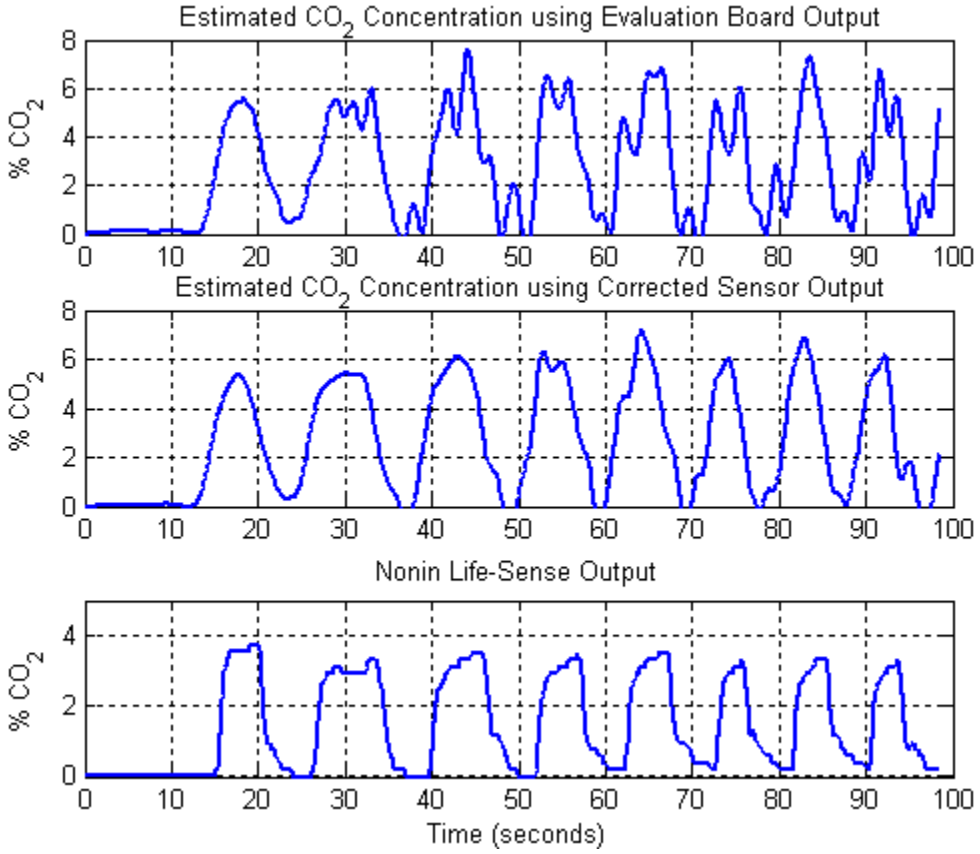

Figure 5.16. CO_2 concentration estimation using predicted CO_2 concentration from raw sensor voltage

Unlike the 1 second update rate in the earlier case, the source for such low frequency noise is different in this case. Examination of the estimated input in Figure 5.17 reveals that the noise becomes prominent in later breaths. This can be traced to lack of sufficient resolution during analog-to-digital conversion of the sensor's output. Figure 5.17 shows the step-wise change in the sensor's voltage with a step height of 2.45mV corresponding to the resolution of a 12-bit data acquisition (DAQ) system with a range of 10V (as used in this experiment). The step changes cause low-frequency chatter in the measured signal

resulting in low-frequency noise in the estimated input. Clearly, these steps due to discretization need to be avoided for noise-free CO_2 estimation.

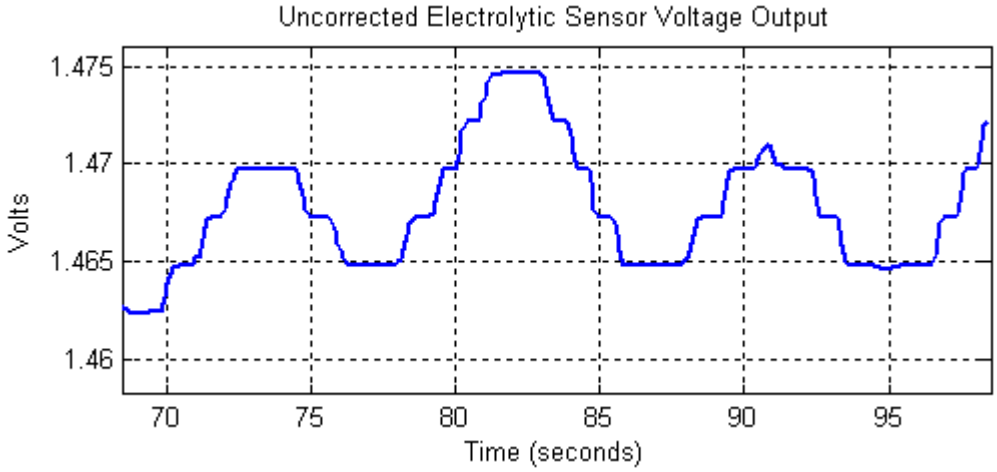

Figure 5.17. Discretization of sensor output voltage by 12-bit DAQ system

One solution to overcome this problem is to amplify the sensor's output further to suit the resolution of the DAQ card. In this work, a higher resolution data acquisition system is used instead to resolve this problem. Earlier a 12-bit DAQ system (National Instruments PCI6024e) had been used for all measurements. This is changed to a 16-bit DAQ system (Sensoray 626) with a voltage resolution of 0.15 mV to remove step-wise change due to inadequate resolution. It can be seen in Figure 5.18 that the estimated input represents the measured capnogram better using this technique. Low pass filters with cutoff frequencies of 1.5 Hz and 1.2 Hz were used before and after estimation respectively. These cut-off frequencies being larger than the ones used for earlier filters permit lesser distortion of the estimated CO_2 input. Figure 5.18 also shows the estimated input using the output from the evaluation board. A lower cut-off frequency of 0.7 Hz was used to filter the estimated input in this case due to larger noise in the estimate. It can be seen from Figure 5.18 that this estimate is smoother and less indicative of the true shape of the CO_2 breathing input.

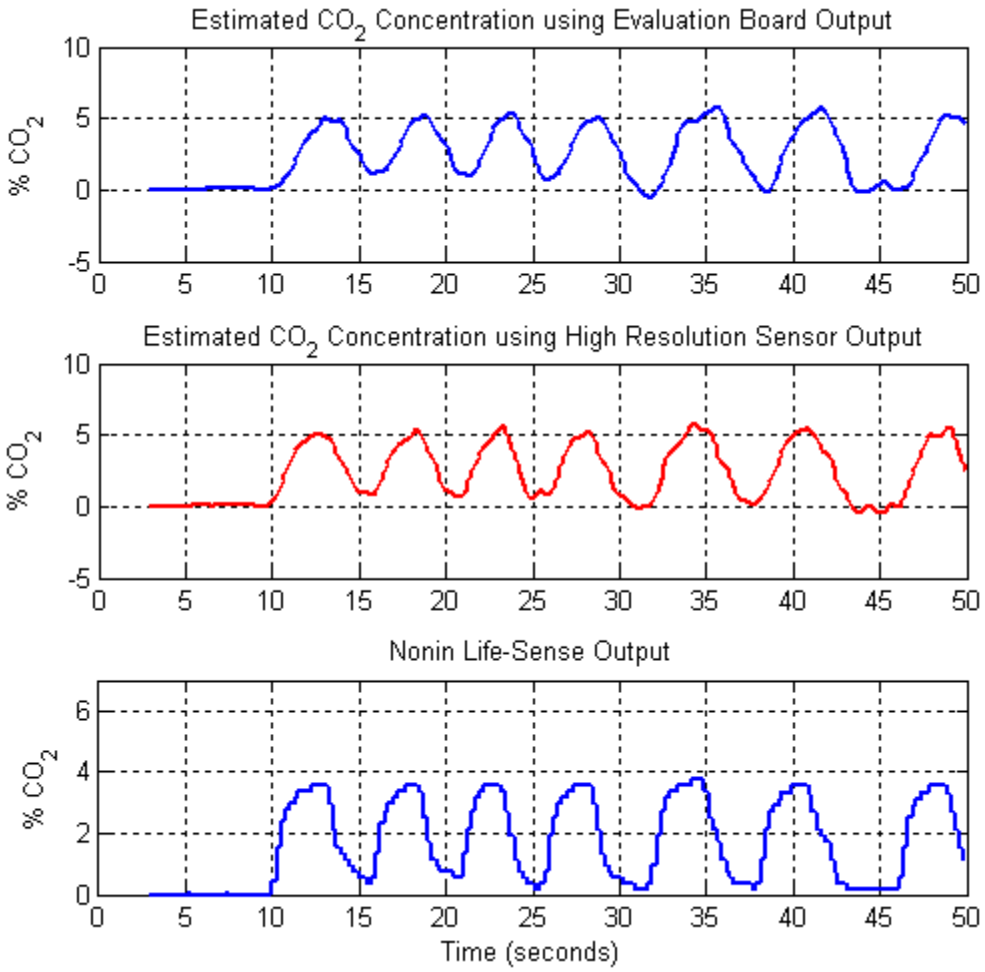

Figure 5.18. CO_2 concentration estimation using high resolution DAQ of sensor voltage

Figure 5.18 also suggests that the final estimate of respiratory CO_2 does not perfectly match that measured using the NDIR analyzer, notwithstanding improvements in modeling and measurement. The authors believe that this inaccuracy arises due to (a) suction pump in the NDIR analyzer, (b) inherent uncertainty in sensor's output, and (c) simplification of sensor's dynamics.

(a) The primary reason for the mismatch between predicted and measured capnograms could be suction of air by the NDIR analyzer's pump. The NDIR analyzer's sampling tube being closer to the incoming gas sample (Figure 5.5) removes gas before it reaches the electrolytic sensor. Such suction could alter the CO_2 concentration profile reaching the electrolytic sensor. Sec 5.4 describes the effect of experimental setup on the tracking

of peak CO_2 concentration. Results shown in Sec 5.4 suggest that the experimental procedure could cause significant variation in the accuracy of estimated CO_2 concentration. (b) Inaccuracy in the electrolytic CO_2 sensor's output is also a likely cause of mismatch between measured and predicted CO_2 concentration. The electrolytic sensor used in this work has an accuracy of ±20% [72] as compared to accuracy of ±2% of NDIR analyzer [73]. (c) Another reason for the mismatch in capnogram shapes could be the inherent assumption in using a second-order model that rising and falling response times are equal. However, the rising and falling times appear different in the sensor's datasheet [72] indicating that the sensor's response cannot be perfectly described by a second-order system.

5.4 COMPARISON OF PETCO_2 ESTIMATES

Normal capnograms show an initial CO_2 concentration close to zero before exhalation, due to the dead space in the non gas exchange airways. Then, the CO_2 concentration rises more steeply followed by a more gradual rise to a peak similar to the waveform shown in Figure 5.1. The peak value is referred as the end tidal CO_2 concentration or '$PetCO_2$'. $PetCO_2$ is a commonly used respiratory measure since it reflects alveolar CO_2 concentration which in turn is very close to arterial CO_2 concentration. This section provides a comparison of $PetCO_2$ values estimated using the model-inversion technique with measured values.

Figure 5.19 compares the estimated and measured $PetCO_2$ values using the estimated and measured capnograms respectively in Figure 5.18. It can be seen that the linear fit of the data is removed from the identity line, implying that the values do not match. However, the trend of the fit follows the identity line, indicating that the estimated $PetCO_2$ values correlates with the measured values.

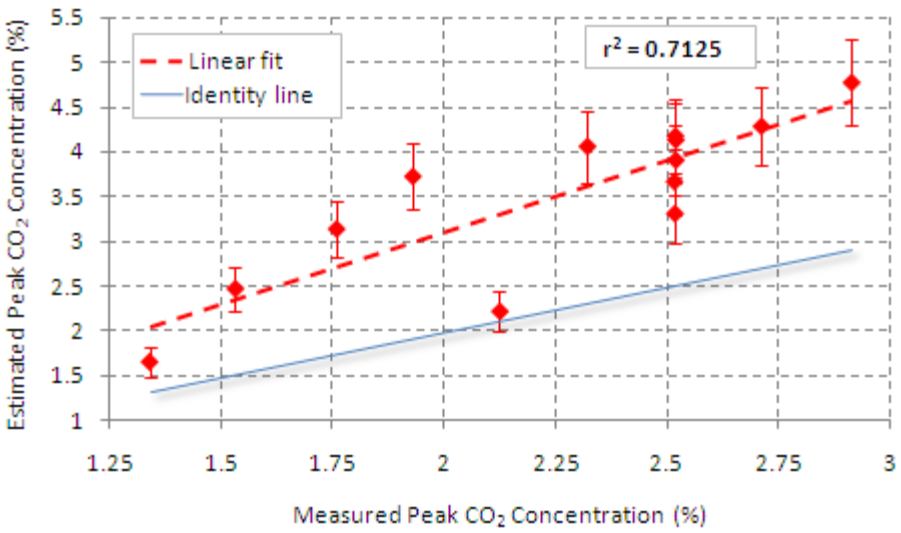

Figure 5.19. Comparison of estimated and measured $PetCO_2$ values with sampling tube stuck on Figaro sensor's wall

An important reason for this discrepancy could be the difference in CO_2 concentration profiles reaching the Figaro sensor and the (reference) Nonin LifeSense analyzer. The Nonin analyzer utilizes an internal suction pump that samples air at the rate of 75 ml/min through a sampling tube. It can be seen from Figure 5.5 that the pump would remove a fraction of the gas sample before it reaches the bottom of the Figaro sensor, where the sensing element is located. Hence, the gas concentration profile (and the peak CO_2 concentration) experienced by the two sensors will be different.

Figure 5.20 shows the comparison of $PetCO_2$ values when the gas sample flows over the Figaro sensor before reaching the Nonin analyzer (using an experimental setup shown in Figure 5.9). This ensures that the gas concentration profiles experienced by both sensors are similar. It can be seen that the estimated and measured CO_2 concentrations are much closer in this case. Further the regression coefficient (r^2) is also improved suggesting better linearity in the data. This suggests that the observed discrepancies in Figure 5.19 are likely due to the suction pump rather than inaccuracies in the model inversion technique.

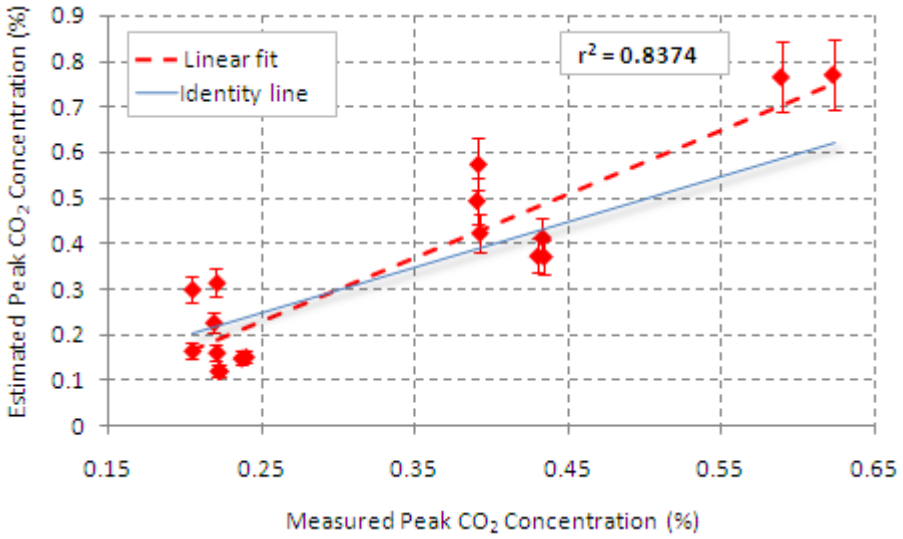

Figure 5.20. Comparison of estimated and measured $PetCO_2$ values with sampling tube inserted into Figaro sensor's wall

5.5 CONCLUSION

Results obtained show good correlation with measurements from standard-of-care NDIR respiratory CO_2 analyzers. The estimation algorithm reliably tracks the relative variation in peak CO_2 concentration with every breath.

It is noted that size and cost of current solid-state CO_2 sensors still remain above desired specifications for ambulatory respiratory CO_2 monitoring. Hence, a small low-cost sensor would need to be developed with comparable performance as current solid-state sensors. However, algorithms developed in this work will obviate the need for a fast response from custom-made sensors. This is an enormous benefit since most solid-state chemical reactions are slow compared to respiratory CO_2 changes. This could then lead to custom-made sensors that would be a small low-cost alternative for breath analysis.

The algorithms presented above are a first attempt to use signal processing to achieve high-speed gas sensing with slow CO_2 sensors. These modeling and measurement techniques allow use of any slow solid-state sensors for high-speed sensing. Thus, the developed method is potentially useful for a variety of sensing applications besides respiratory monitoring.

CHAPTER 6. CARBON NANOTUBE-CALCIUM CARBONATE NANOCOMPOSITE FOR ROOM TEMPERATURE CARBON DIOXIDE GAS SENSING

6.1 INTRODUCTION

As concluded in the previous chapter, though developed model inversion techniques allow use of slow CO_2 gas sensors for breath-by-breath monitoring, a small low-power carbon dioxide (CO_2) gas sensor is still unavailable for respiratory gas sensing. In order to satisfy this unmet requirement, a small low-power CO_2 sensor is explored in this chapter using a new nanocomposite made using single-walled carbon nanotubes (SWNTs) and calcium carbonate ($CaCO_3$). The resistance of the nanocomposite changes when CO_2 concentration changes. The SWNT-$CaCO_3$ nanocomposite structure is porous which results in high gas penetration and sensitivity at room temperature. Since no heating is used, the sensor has very low power requirements. The sensor shows cross-sensitivity to humidity due to the response of SWNTs to humidity. This is removed by using a bare SWNT film as a reference sensor. However, it is found that the response time of this sensor is too slow to be correctable by model inversion techniques. Hence, it is more appropriate for use in indoor air-quality sensing rather than respiratory CO_2 monitoring. But, other sensing techniques using the developed nanocomposite finally lead to a faster CO_2 sensor as described in the following chapter.

6.2 SENSING PRINCIPLE

The sensor demonstrated in this chapter uses a room temperature chemical equilibrium shown in Eq. (1), along with a sensitive method to monitor changes in the equilibrium. This is accomplished by forming a nanocomposite of $CaCO_3$ and single-walled carbon nanotubes (SWNTs) as shown in Figure 6.1.

$$BaCO_3 + CO_2 + H_2O \Leftrightarrow Ba\left(HCO_3\right)_2 \tag{2}$$

Eq. (1) has been proven in the past as the dominant mechanism for the reaction of barium carbonate ($BaCO_3$) with CO_2 at room temperature[34, 74]. In this chapter, the use of $BaCO_3$ is replaced with the use of $CaCO_3$.

The SWNTs have two functions in the sensor:

(a) They serve as a porous three-dimensional template to which nanoparticles of $CaCO_3$ are attached. For a given volume of $CaCO_3$, this structure allows large surface area for interaction between $CaCO_3$ and CO_2 gas.

(b) They are also used to detect changes in the calcium bicarbonate ($Ca(HCO_3)_2$) concentration. Conductivity of semi-conducting SWNTs is sensitive to the pH of its surrounding environment which is altered by the formation of $Ca(HCO_3)_2$. This can be measured by measuring the change in bulk conductivity of the nanocomposite film.

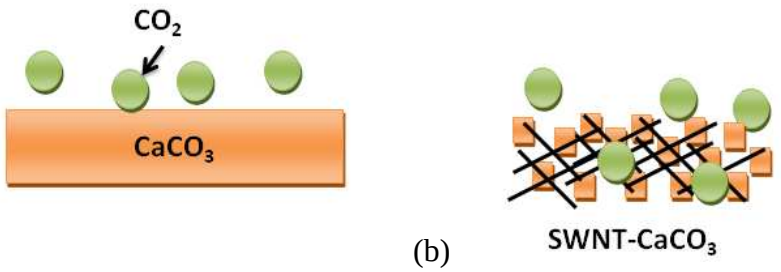

(a) (b)

Figure 6.1. (a) Surface interaction of CO_2 and $CaCO_3$ in electrolytic sensors and (b) bulk interaction in SWNT-$CaCO_3$ nanocomposite

In addition, semi-conducting SWNTs likely catalyze reaction (1) between $CaCO_3$ and CO_2 at room temperature. Such semiconductor-assisted CO_2 sensing has been shown earlier using barium titanate [75] and indium oxide [76] as catalysts. For a given volume of the nanocomposite, millions of interfaces between SWNTs and $CaCO_3$ can be expected. Given the porous structure of the nanocomposite, most of these interfaces are affected by changes in CO_2 concentration as shown in Figure 6.1. This enables measurement of very small changes in $Ca(HCO_3)_2$ concentration.

6.3 SENSOR FABRICATION

The SWNT-$CaCO_3$ composite material can be fabricated by a number of different methods. The SWNTs need to be first dispersed to form a solution. However, SWNTs are insoluble in most solvents and agglomerate when put in water due to Van der Waal's forces. Several chemical techniques have therefore been recently developed to disperse

SWNTs to enable coating of uniform SWNT films on surfaces [22, 68, 77]. Two SWNT dispersion techniques (acid treatment and alcohol dispersion) have been used in obtaining results on the performance of the new sensor material.

After dispersion of the SWNTs, the SWNT-$CaCO_3$ nanocomposite is prepared by a fabrication technique used for the development of field-emission displays [78]. Briefly, $CaCO_3$ nanoparticles are formed by in-situ precipitation through aqueous reaction of $CaCl_2$ and K_2CO_3. A negatively charged SWNT dispersion is immediately added to the solution causing the nanoparticles to bind to the surface of the SWNTs. Thus, the $CaCO_3$ nanoparticles are immediately harvested before they settle and crystallize into macro particles. Upon settling for 1-2 hours, SWNT-$CaCO_3$ nanocomposite crystallizes out of solution. The crystals are retrieved from solution using a syringe and drop coated onto a PCB and allowed to dry. The conductivity of a small area (approx 1mm x 5mm) of the nanocomposite is measured as CO_2 gas concentration is varied.

6.4 RESULTS AND DISCUSSION

Figure 6.2 shows results obtained using a nanocomposite material prepared by using acid treatment dispersed SWNTs while Figure 6.3 shows results obtained using a nanocomposite material prepared by using alcohol dispersed SWNTs. The upper half of the figure shows variation of the resistance of the SWNT-$CaCO_3$ material while the lower half of the figure shows the percentage of CO_2 in the sensing chamber as measured by a commercial Figaro electrolytic sensor. As seen in Figure 6.2 and Figure 6.3, the resistance change in the nanocomposite tracks the changes in CO_2 concentration. It should be noted that this particular commercial Figaro sensor measures only up to 4.5% in CO_2 concentration [33] and hence its signal is seen to saturate several times during the measurement while the new sensor material does not saturate in its response.

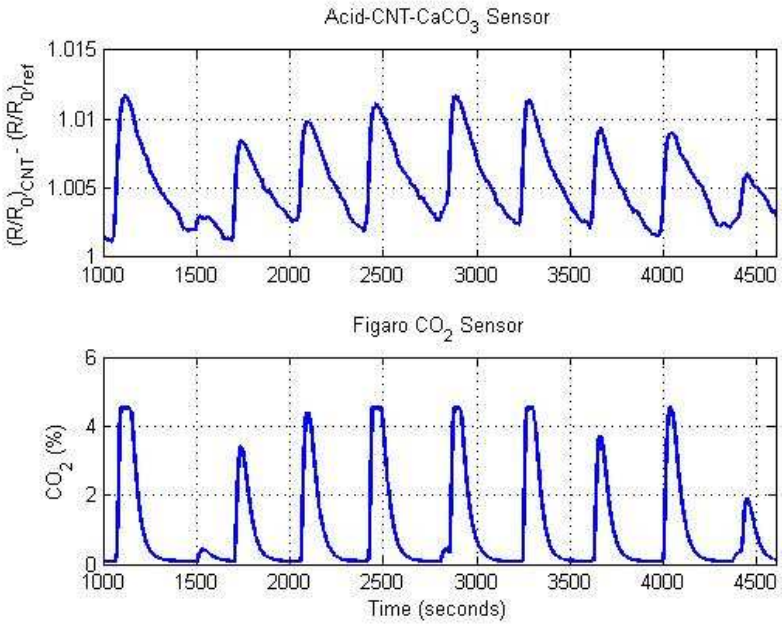

Figure 6.2. Acid-SWNT-CaCO3 sensor response and comparison with commercial Figaro sensor

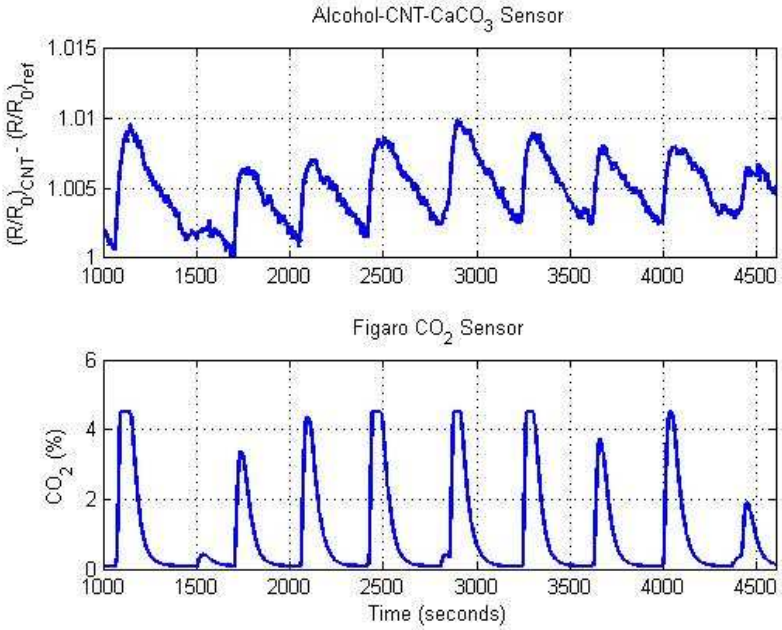

Figure 6.3. Alcohol-SWNT-CaCO3 sensor response and comparison with commercial Figaro sensor

It is found that the conductivity of the SWNT-$CaCO_3$ composite is affected by the humidity of the gas mixture, in addition to the concentration of the CO_2 in the mixture. In the data shown previously in Figure 6.2 and Figure 6.3, the humidity varied little

during the experiment. When the relative humidity varies significantly (5-10%), the change in humidity also influences the resistance of the SWNT-$CaCO_3$ material. Figure 6.4 shows the measured resistance of the SWNT-$CaCO_3$ material when the humidity varies. The lower third of the figure shows the measured humidity in the chamber. It can be seen that the CO_2 concentration measured by the new sensor is no longer a good match for the actual CO_2 concentration as measured from the commercial Figaro sensor.

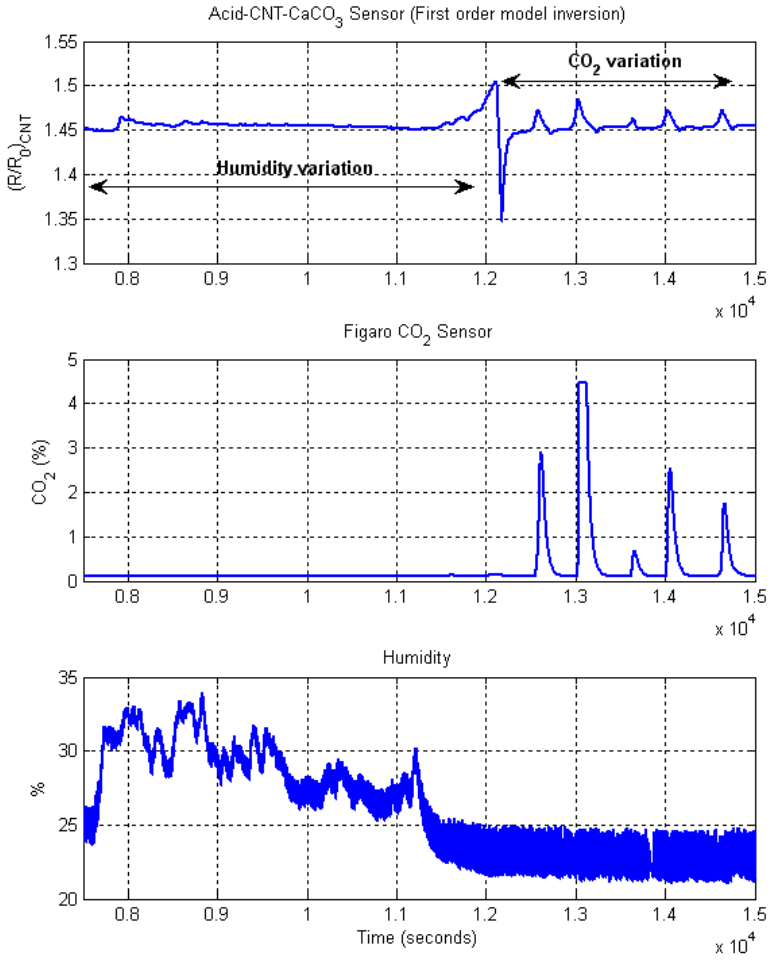

Figure 6.4. Acid-SWNT-$CaCO_3$ sensor response during humidity variation

However, the influence of humidity variation can be removed by carefully calibrating its influence, measuring humidity as a reference measurement in the sensor and using this measurement to compensate for changing humidity. The top portion of Figure 6.5 shows the resistance of the SWNT-CaCO3 composite sample after appropriate subtraction of the varying resistance of a reference bare SWNT film placed close to the sensor. The

reference SWNT film was prepared by the same acid treatment technique as the SWNT-$CaCO_3$ sample. The reference SWNT film is influenced by the humidity variations in the sensor environment but is not influenced by the variation of CO_2, since it does not have any $CaCO_3$.

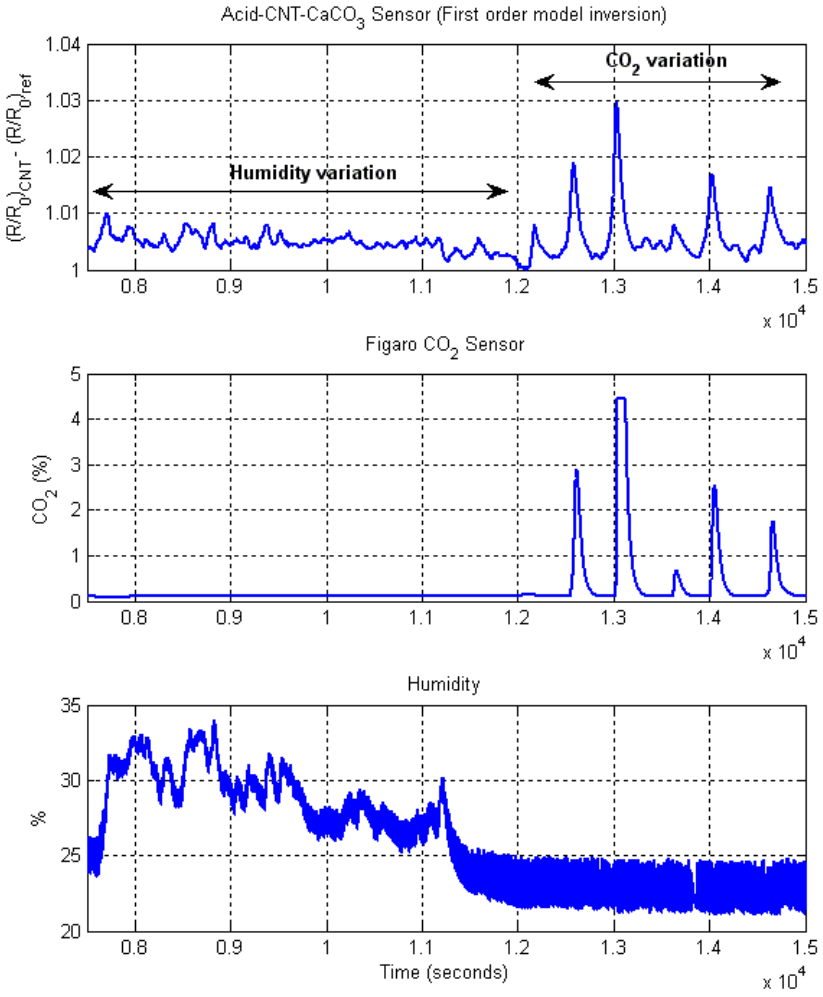

Figure 6.5. Sensor response with humidity compensation

6.5 CONCLUSION

It can be observed from Figure 6.2 and Figure 6.5 that the developed sensor is slow compared to the commercial Figaro sensor. This can be explained by the series resistor structure of the nanocomposite. The nanocomposite provides high sensitivity using millions of SWNT resistors connected as a random network. The bulk resistance of the structure is controlled by the resistance of SWNTs in the path of current flow. When the

resistance of a few resistors in this path changes, the bulk resistance is affected. Conversely, when the resistance of a few resistors in this network does not change due to chemisorbed CO_2, the bulk resistance is again affected [79]. This results in a slow response for the sensor.

In this case, chemisorption of CO_2 on SWNTs is enhanced due to chemical processes used to disperse SWNTs in solution. Future work could address identification of techniques for making SWNT-$CaCO_3$ nanocomposites that do not alter the wall structure of SWNTs. Such techniques could also extend the life of the sensing material, since long-term chemisorption can poison the sensor and prevent normal operation. Other less desirable alternatives could be using heat or ultraviolet light to refresh sensors on a periodic basis.

Another possible reason for the relatively slow response of the sensor could be the inherent kinetics of the solid-gas equilibrium reaction (Eq (1)). Alternative solutions to overcome this issue without using heating are currently unavailable. This will also be the subject of future work. It is noted however that the speed of response of the developed sensors make them suitable for low-speed indoor air-quality sensing. Thus, there is promise in using the developed sensors for critical energy-saving applications like demand controlled ventilation.

In summary, a new nanocomposite has been developed that has been shown to be sensitive to CO_2 at room temperature. The resulting low-power sensor is an important development since current CO_2 sensors consume significant power and thus are not suitable for long-term wireless monitoring. The proof-of-concept results show that cross-sensitivity to other environmental variables could be removed using a reference sensor. The speed of response however makes it unsuitable for respiratory CO_2 monitoring. It is discussed in the following chapter that the speed of response can be considerably increased by measuring the capacitance of the nanocomposite material. Combined with other design modifications, this is shown to lead to the development of a respiratory CO_2 sensor.

CHAPTER 7. FAST CAPACITIVE CO_2 SENSORS USING CARBON NANOTUBE-BARIUM CARBONATE NANOCOMPOSITE

7.1 INTRODUCTION

The SWNT-$CaCO_3$ nanocomposite sensor developed in the previous chapter suffers from the key disadvantage of slow response (>100s) since measurement of resistance of SWNTs was used to monitor changes in the equilibrium reaction between CO_2 and $CaCO_3$. Notwithstanding the use of model inversion techniques, it cannot be used for respiratory CO_2 monitoring where response times less than 100 ms are desirable. Slow response times have been reported earlier with other CNT sensors in a resistive configuration [79]. This is because a CNT-based resistive sensor is similar to a network of resistors whose resistance could be greatly affected by the resistance of a few resistors. Since, CNTs have a tendency to chemisorb gases on open/broken bonds, the resistance of a few CNTs takes a long time to return back to normal. If such slow-responding nanotubes were part of the current loop, the net resistance also takes a long time to reach back to the base level. Thus, the net response of the sensor becomes slow.

Snow et. al. have noted a similar problem with resistive carbon nanotube sensors and instead proposed capacitive sensing with CNTs as a fast sensing alternative[79]. In their embodiment of a capacitive sensor, nanotubes serve as one electrode of the sensor where gases get polarized. However, the SWNT-based nanocomposite is used as the dielectric itself in the developed sensor with metallic fingers serving as planar electrodes, as shown in Figure 7.1.

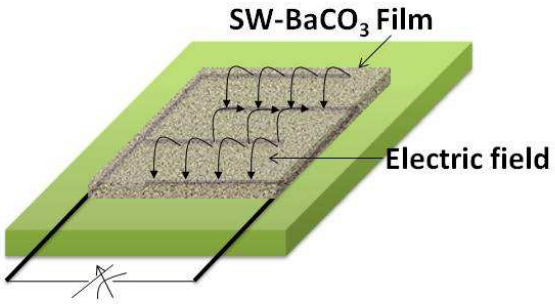

Figure 7.1. Schematic representation of a planar capacitive sensor with SWNT-$BaCO_3$ film as dielectric

This capacitive sensing configuration is explored in this work to increase the speed of response to CO_2 concentration variation.

7.2 SENSING PRINCIPLE

The sensing mechanism for the proposed CO_2 sensors is given by

$$BaCO_3(s) + CO_2 + H_2O \xleftrightarrow[Catalyst]{} Ba\left(HCO_3\right)_2(l) \quad (1)$$

A catalyst is required to promote reaction (1) since $BaCO_3$ shows negligibly small activity at room temperature. Such equilibria have been shown to occur at room temperature in the presence of semiconducting catalysts [75, 76]. It is noted that different reaction mechanisms are observable at higher temperatures (>400 ^oC) for pure $BaCO_3$ [21]. However, it is an objective of this work to design portable CO_2 sensors for respiratory monitoring; a key requirement for such sensors being low power consumption. Hence, power-consuming heaters for high temperature operation are not desirable in the design.

Semiconducting $BaTiO_3$ is a commonly used catalyst that promotes reaction (1) at room temperature [80]. However, the active region of $BaTiO_3$-based sensors is limited to the surface of thin film that is exposed to the gas. It was described in the previous chapter that single walled carbon nanotubes (SWNTs) are capable of catalyzing the equilibrium reaction between CO_2 and $CaCO_3$ while providing much large surface area for interaction between CO_2 and $CaCO_3$. The catalytic activity of SWNTs is believed to arise from the semiconducting CNTs present in the mixture. A large surface area of interaction can be obtained by making a nanocomposite of SWNTs and nanoparticles of $CaCO_3$. Such a

porous nanocomposite allows CO_2 to penetrate into the bulk of the material and interact with multiple $CaCO_3$ sites thereby providing a large sensitivity to CO_2. A similar technique can also be used to fabricate sensors based on the equilibrium reaction between CO_2 and $BaCO_3$. Figure 7.2 shows the capacitance of a pure $BaCO_3$ film responding slightly to change in CO_2 concentration while that of the SWNT-$BaCO_3$ nanocomposite tracking CO_2 concentration, in a pure nitrogen environment. The small spikes in capacitance of the pure $BaCO_3$ film can be attributed to small humidity changes due to change in CO_2 flow rate during the experiment.

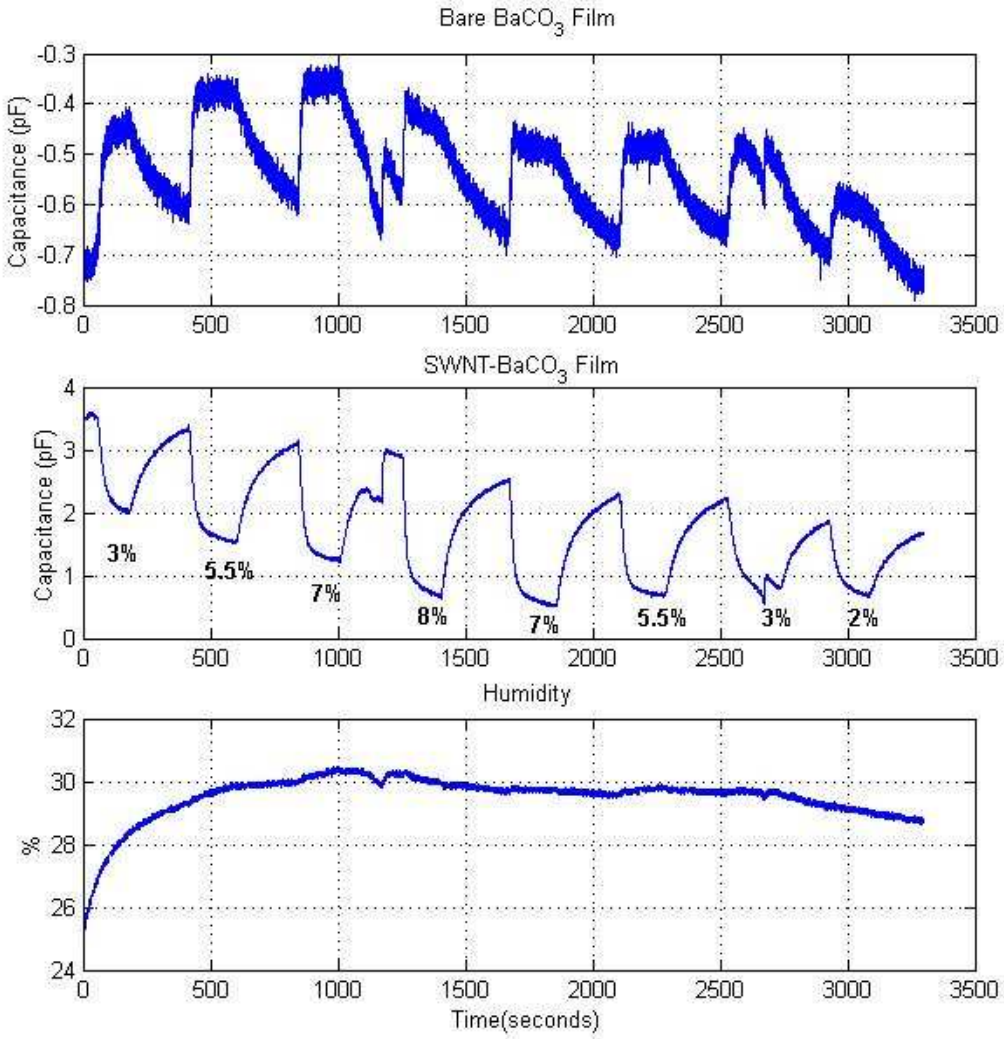

Figure 7.2. Comparative response of bare $BaCO_3$ film and SWNT-$BaCO_3$ nanocomposite to varying concentrations of CO_2

Figure 7.3 further shows that the capacitance of the $BaCO_3$ film can be used as reference to remove the humidity response of the SWNT-$BaCO_3$ nanocomposite. Thus, it can be concluded that pure $BaCO_3$ shows negligible response to CO_2 (in a pure nitrogen environment) while SWNT-$BaCO_3$ shows excellent sensitivity to CO_2. Thus, SWNTs are believed to catalyze Eq. (1) between $BaCO_3$ and CO_2.

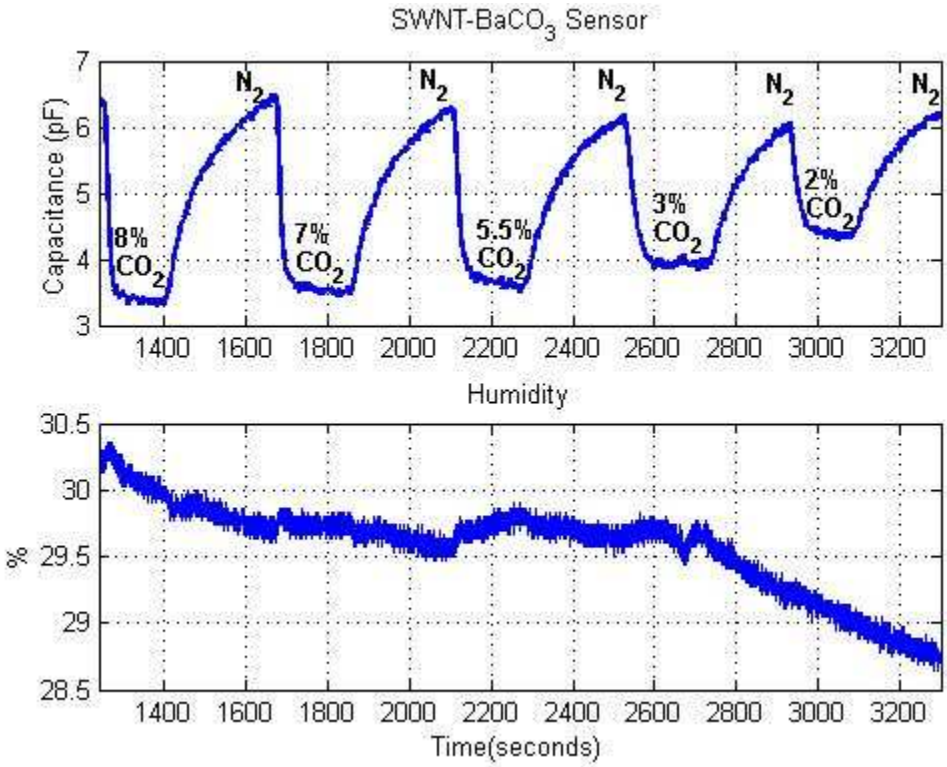

Figure 7.3. Corrected response of SWNT-$BaCO_3$ film with response of pure $BaCO_3$ film as reference

7.3 SENSOR DESIGN

With fast response times afforded by these capacitive sensors, a breath CO_2 sensor can be fabricated. However, a key challenge in breath CO_2 sensing involves the variation of humidity during breathing. Eq. (1) shows that the sensor responds to changes in humidity as well as CO_2 in the environment. This is an impediment for breath CO_2 sensing since the humidity level varies every breath along with CO_2 concentration. Complete removal of humidity from the breath is not a viable alternative since the CO_2 sensor requires humidity to function according to Eq. (1). In order to keep the humidity level constant

close to the sensor while removing the effect of the respiratory humidity, a new design (shown in Figure 7.1) is adopted.

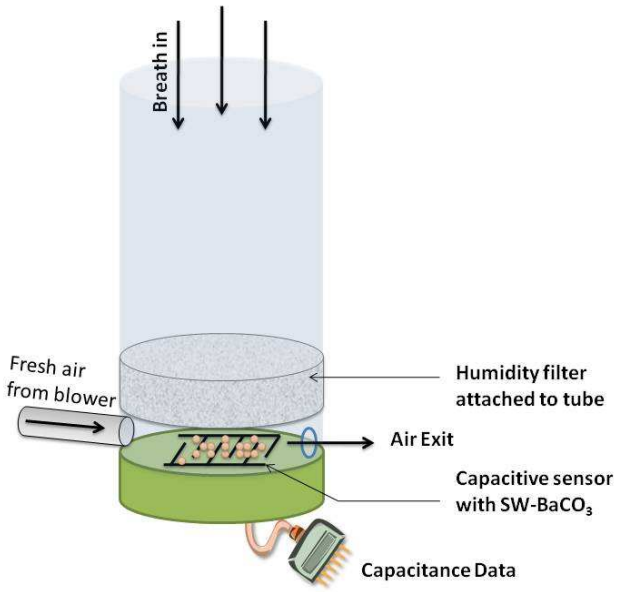

Figure 7.4. Schematic of respiratory CO_2 sensor design

In this design, the patient breathes through a preVent^{TM} Pneumotach (MedGraphics Inc.) tube to which a humidity filter is attached at the exit. The Pneumotach tube is designed to allow measurement of other respiratory variables and hence is used in cardiopulmonary measurements. With this design, breath passing through the filter is free of humidity but contains CO_2. The sensor is placed at the exit of the humidity filter in a chamber with inlet and exit holes as shown in Figure 7.4. The inlet hole is used to supply fresh air sampled well away from the sensor, using a low-flow pump into the sensing chamber (Parker Hargraves CTS air pump). By adjusting the air flow-rate, the humidity level in the chamber can be kept relatively constant.

The humidity in the chamber however varies slightly due to the arrival of dry air from the filter with every breath. This slight variation in humidity can be decreased by increasing the flow of fresh air through the chamber. However, a large flow rate can remove CO_2 from the chamber before it reaches the SWNT-$BaCO_3$ sensor. Thus, an optimal flow rate that maintains humidity while allowing sufficient CO_2 sensitivity is chosen through trial

and error. The air-flow also helps to quickly remove exhaled CO_2 from the chamber thus increasing the overall speed of response of the sensor.

Molecular sieve 3A is chosen as the humidity filter since its pore size allows selectively sorption of humidity while permitting flow of CO_2. The volume of the filter is chosen to be approximately $10cm^3$. A higher volume provides a longer filter life-time but higher resistance to flow. Since it is desirable to keep flow resistance to a minimum to minimize patient discomfort, higher filter volumes are not preferred. A lower filter volume may be used sacrificing life-time provided filtering efficiency is not compromised.

Figure 7.5. Photograph of respiratory CO_2 sensor with preVent^{TM} Pneumotach tube

It is noted that this design uses a humidity filter which gets consumed over time and loses efficiency after all molecular sieve cavities have been filled. Hence periodic replacement of the filter is necessary. The authors have observed that the filter lasts several 100 breath cycles if stored in a dry environment when unused. The flow through the filter may be expected to slow down the speed of response of the sensor. However, test data indicate that the tube configuration helps to focus the flow of breath into a narrow volume. This helps overcome the pressure drop associated with the humidity filter.

In order to further minimize resistance to flow and increase patient comfort, a perforated mouth-piece may be used as shown in Figure 7.6. Such mouth-pieces are commonly used

to securely hold the tube inside a patient's mouth. By introducing perforations in the mouth-piece, an additional path is provided for excess breath to escape from the tube as shown in Figure 7.7. This significantly reduces the resistance to breathing. Such perforations also enhance lifetime of the humidity filter since significant quantities of humid breath can be bypassed out of the breathing tube through perforations in the mouth-piece.

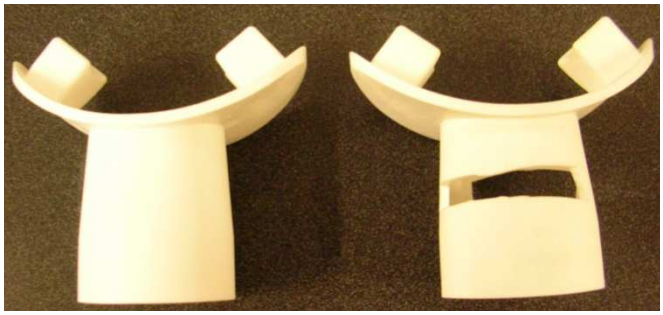

Figure 7.6. Photo of mouth-piece (left) and perforated mouth-piece(right)

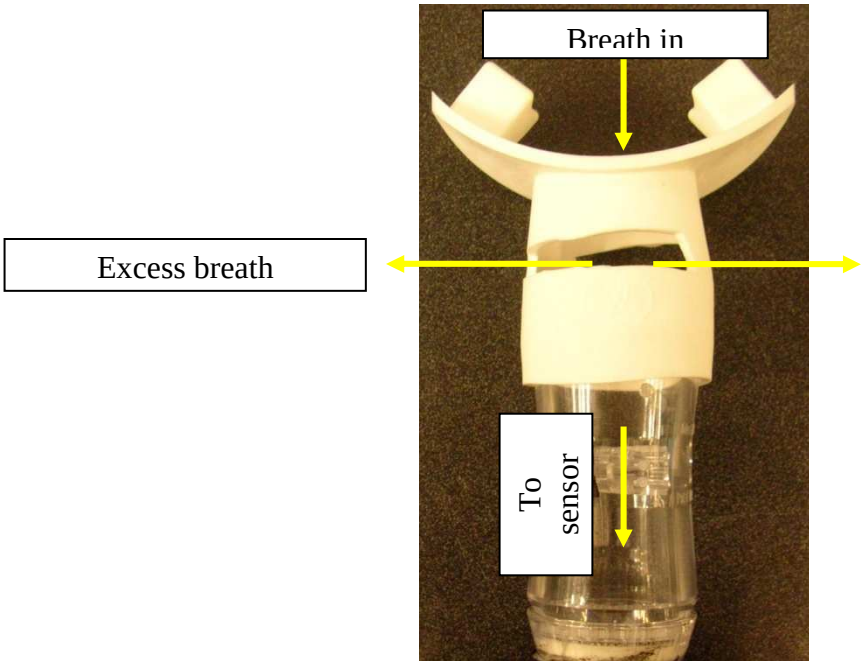

Figure 7.7. Photo of mouth-piece attached to breathing tube

The SWNT-$BaCO_3$ film itself is made by drop-coating the nanocomposite from solution and spreading it into a thin-film using the cylindrical surface of a needle. The composite preparation is similar to that of SWNT-$CaCO_3$ nanocomposite described in earlier work [81]. Briefly, equimolar aqueous solutions of barium chloride ($BaCl_2$) and potassium

carbonate (K_2CO_3) are mixed to form nanoparticles of insoluble $BaCO_3$. Acid-treated negatively charged SWNTs are immediately added to this solution to form a nanocomposite of SWNTs and $BaCO_3$. The nanocomposite is allowed to settle and crystallize for a few hours before used for drop-coating on the sensor.

The capacitive sensing structure is designed as a planar comb-like interdigital transducer on FR-4 epoxy glass substrate with finger spacing and width of 150 μm. The metal used for the electrodes is 43 μm copper coated with tin-lead reflow. An insulation layer of green LPI soldermask is used to electrically isolate the metallic electrodes from the coated SWNT-$BaCO_3$ thin film.

Finally, capacitance measurement is achieved by using an AD7746 two-channel capacitance-to-digital converter and evaluation board from Analog Devices Inc. A Labview™ program provided by Analog Devices Inc. is used to configure the measurement range, resolution and sampling speed for capacitance measurement. The chip along with a 5-pin header is soldered to the back-side of the capacitive sensor that is accessible externally. The 5-pin header is used to communicate between the evaluation board and the sensor PCB. Sampling speeds between 100 to 250 ms are used for respiratory CO_2 measurements. Figure 7.8 shows a photograph of the final sensor PCB with all the above components.

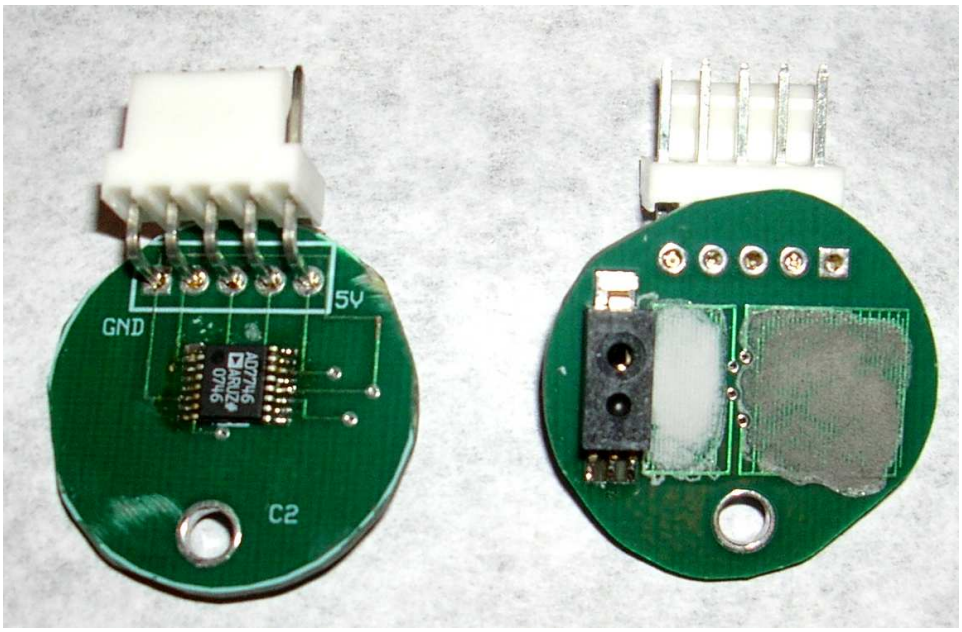

Figure 7.8. Photograph of top and bottom of sensor PCBs with sensing films, capacitance measurement chip and 5-pin connector

7.4 RESULTS AND DISCUSSION

The sensor design described above is used for respiratory CO_2 sensing. All reference CO_2 measurements are made using a MedGraphics CO_2/O_2 analyzer that is pre-calibrated and checked for linearity. This analyzer has a sampling tube connected to a vacuum pump that pulls gas into its CO_2/O_2 analyzers through a drying circuit. The sampling tube is placed inside the sensing chamber through the inlet hole for air flow shown in Figure 7.4. The analyzer uses a Datex CO_2 board that works based on the non-dispersive infra-red (NDIR) sensing principle. The CO_2 concentration is output as an analog voltage with a scaling factor of $1V/\%CO_2$. This voltage is sampled into a computer using a National Instruments PCI 6024E data acquisition card. The voltage acquisition is timed by the same Labview^{TM} program that also controls capacitance measurement of the CO_2 sensor.

Figure 7.9 shows the raw and calibrated response of the SWNT-$BaCO_3$ sensor to breathing cycles. CO_2 concentration measured by the reference MedGraphics CO_2 analyzer is shown in red. The capacitance of the SWNT-$BaCO_3$ sensor decreases with increasing CO_2 concentration. This capacitance change is found to be logarithmically

related to the CO_2 concentration upon plotting capacitance vs. logarithm of CO_2 concentration measured by the reference analyzer (Figure 7.10). The linear relationship obtained in Figure 7.10 is used to calibrate the SWNT-$BaCO_3$ sensor's response and obtain CO_2 concentration from the measured capacitance as shown in Figure 7.9.

Small discrepancies between the sensor and reference analyzer at lower CO_2 concentrations are attributed to the experimental setup. Since the setup uses a flow pump to supply fresh air, a fraction of the gas sample may be carried away before being sampled by the reference analyzer. At lower breathing volumes, this fraction can be significant and might explain the observed discrepancies. Further, the reference analyzer itself uses a vacuum pump to sample the incoming breath. The suction created by the analyzer's vacuum pump can also alter the concentration profile of CO_2 gas reaching the SWNT-$BaCO_3$ film. Notwithstanding these experimental limitations, the SWNT-$BaCO_3$ sensor can be seen to respond reliably to CO_2 changes in exhaled breath (Figure 7.9). Repeated tests also proved the reliability of the sensor's response.

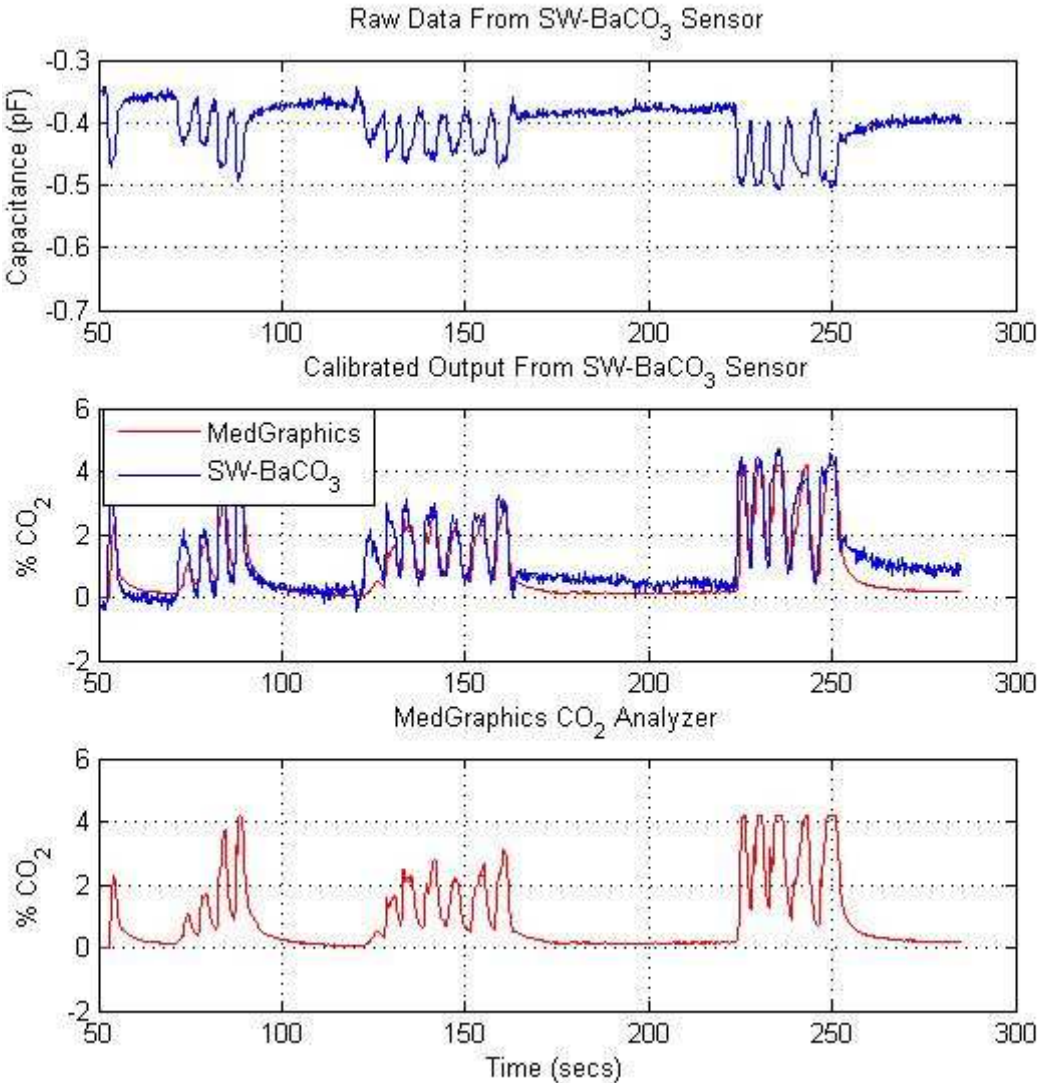

Figure 7.9. Raw and calibrated sensor response compared with MedGraphics CO_2 analyzer's response

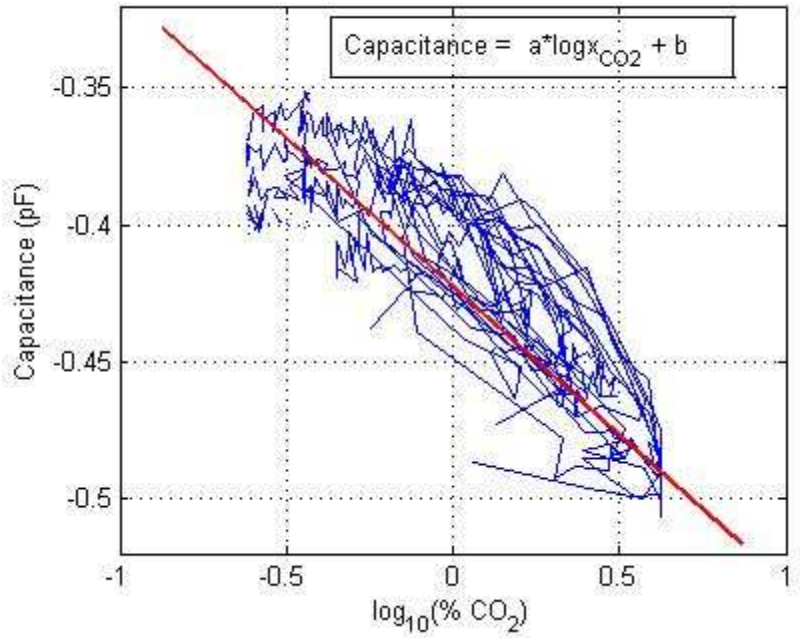

Figure 7.10. Linear relationship between capacitance change and logarithm of CO_2 concentration

The new sensing material based on SWNT-$BaCO_3$ nanocomposite is required to enhance sensitivity while keeping response time small. Other room-temperature solid-state CO_2 sensors have required a trade-off between sensitivity and response time because of the use of planar films for sensing. However, the three-dimensional network of CNTs and the sensing material ($BaCO_3$) enables large sensitivity while keeping the gas-penetration time small. Further, CO_2 sensors based on carbonates show inherent cross-sensitivity to humidity at room temperatures because of the sensing mechanism (Eq. (1)). Hence, room temperature sensing of CO_2 has not been possible with such sensors. CO_2 sensors are thus operated at high temperatures (>450^oC) where the reaction mechanism changes and cross-sensitivity to humidity is minimal [33]. However, designs to maintain constant humidity developed in this work enable room temperature respiratory CO_2 sensing with similar carbonate-based materials.

It is noted that this sensor design is based on CNTs which are challenging materials to use for gas sensing. CNTs themselves are sensitive to many gases and tend to chemisorb gases over time. This results in poor selectivity and long-term drift in the sensor. The issue of selectivity during respiratory CO_2 sensing is resolved in this design by using a

low CNT fraction in the nanocomposite and a molecular sieve filter that helps remove humidity. The nanocomposite is also insensitive to oxygen concentration thus making it usable for respiratory CO_2 sensing. However, cross-sensitivity to other relevant gas species must be tested before using similar SWNT-$BaCO_3$ films for other CO_2 sensing applications. The issue of long-term drift is reduced in this design by using capacitive sensing instead of resistive sensing. Future work could address real-time drift correction using a reference sensor insensitive to CO_2.

7.5 PARTICLE RELEASE TESTING

Sensors fabricated with CNT nanocomposites would require the sensing film to be exposed to the environment. However, use of such sensors for gas monitoring is possible only if no CNTs are released into the environment. The health implication of inhaling CNTs is currently the subject of investigation [82, 83]. However, the extremely long aspect ratio, similar to other lung carcinogens, could result in their trapping inside human lungs.

The tight intermingling of SWNTs and carbonates in the nanocomposite structure suggests that SWNTs should not be released individually. This is proven experimentally by testing the particle release from a SWNT-CaCO3 composite using a condensation particle counter (CPC; model 3025A, TSI Inc.). Figure 7.11 shows the schematic diagram of the CNT release test system.

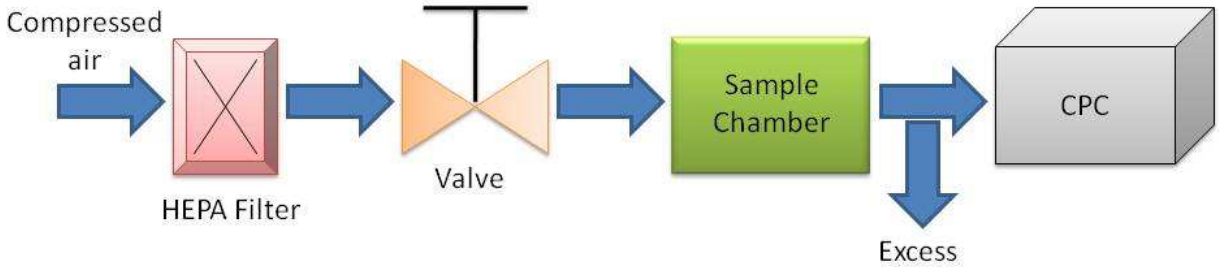

Figure 7.11. Schematic diagram of particle release testing setup

Particle free compressed air with flowrate of 5 lpm is flowed into the sample chamber, in which the sensors being tested are placed. The volume of the chamber is estimated to be 150 cm^3. The outlet from the chamber is connected to a CPC, which draws air at 1.5 lpm

with excess air being by-passed. The CPC is operated to display the total particle counts in 2 minutes.

Table 7.1. Observed particle count for CNT nanocomposite sensors

Testing Condition	Particle Counts in two Minutes
Empty chamber, no sensor placed	**2**
Sensor 1	**4**
Sensor 2	**1**
Glass substrate	**1**

From Table 7.1, no observable increase in particle count can be detected when sensors are placed inside the measurement chamber. In another experiment, films are fabricated by drop coating the nanocomposite on a clean silicon wafer and drying under heat. The wafer is placed inside a chamber which is constantly supplied with a flow of particle-free air as shown in Figure 7.12.

Figure 7.12. Photo of measurement chamber with sample holder and CPCs

Figure 7.13 shows the variation in particle count inside the chamber during multiple insertions and removal of the coated Si wafer. Prior to insertion of silicon wafer, small variations can be observed during the insertion of an uncoated glass dish. This indicates that observed changes were a result of hand movement in and out of the testing chamber.

Based on this observation, no consistent increase in particle count can be observed after insertion of the nanocomposite-coated silicon wafer.

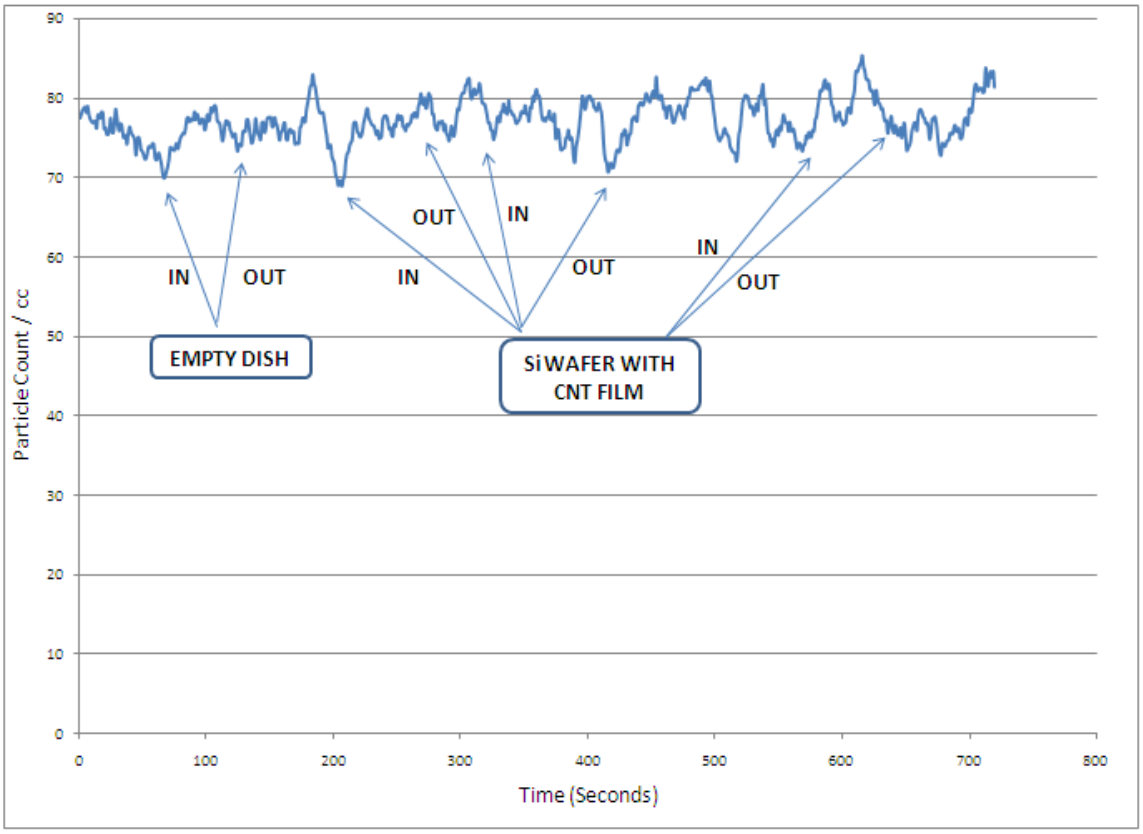

Figure 7.13. Variation in particle count due to introduction of CNT-nanocomposite coated silicon wafer

7.6 CONCLUSION

A fast portable respiratory CO_2 sensor is developed using SWNT-$BaCO_3$ as the sensing film. The nanocomposite structure allows a large surface area of interaction between CO_2 gas and $BaCO_3$ nanoparticles and fast gas-penetration into the sensing film. Capacitive sensing allows detection of fast CO_2 concentration changes despite the slow response of some CNTs due to chemisorption. Based on past reports of semiconducting catalysts for $BaCO_3$ sensors; the semiconducting nature of SWNTs seems to catalyze the reaction between $BaCO_3$ and CO_2.

Several design modifications to a standard breathing tube help the sensor respond to CO_2 in the presence of varying humidity in the breath. These modifications include a

molecular sieve filter to remove moisture in the breath, a low-power pump to supply humidified air into the sensing chamber and a perforated mouth-piece to bypass excess breath reaching the sensor. Finally, particle testing using a CPC shows that the nanocomposite is not released into the environment during breath sensing.

This design is a first investigation into the development of a portable and low-power solid-state CO_2 sensor for untethered respiratory CO_2 monitoring. Other portable respiratory CO_2 sensing designs developed in the past have used power-consuming designs based on NDIR analyzers [84] or electrolytic sensors [85] making them unsuitable for long-term wireless use. Several other sensing embodiments can be envisioned based on the developed idea to extend the use of respiratory CO_2 sensing to non-clinical monitoring applications. The low-cost and portability of the developed design could also make it attractive for clinical use.

CHAPTER 8. CONCLUSIONS

The objective of this work is to develop a portable, small and low-cost respiratory CO_2 analyzer for medical applications. Four types of solid-state sensors based on carbon nanotubes are examined for achieving the same:

1. PEI functionalized SWNTs coated on surface acoustic wave devices
2. Pure SWNTs coated on electret microphones
3. Resistive sensor based on SWNT-$CaCO_3$ nanocomposite
4. Capacitive sensor based on SWNT-BaCO3 nanocomposite

A thin film of PEI functionalized SWNTs responds to CO_2 by changing its conductivity which is measured with high precision using a surface acoustic wave (SAW) sensor. While showing a fast response time, the film and SAW sensor are found to be unacceptably sensitive to humidity – a key interfering species during respiratory monitoring. Hence, it is found unsuitable for use as a CO2 sensor.

Stiffness measurement of thin SWNT films using a novel stiffness measurement technique yields a CO_2 sensor. This measurement technique uses electret microphones (coated with SWNT films) as stiffness sensors. The acoustic sensitivity and geometry of the microphones greatly influence its stiffness sensitivity. Analytical techniques are developed to predict the sensitivity of commercial microphones to film stiffness changes. While sensitive to CO_2, the microphones show unreliable selectivity due to their construction. Selectivity tests on multiple samples of commercial electret microphone prove that such microphones are unreliable for gas sensing.

Investigation into selective carbonate-based CO_2 sensors then leads to a new nanocomposite material combining metal carbonates and SWNTs for CO_2 sensing. In this nanocomposite, metal carbonates function as the CO_2-sensitive material while SWNTs (a) catalyze the reaction, (b) increase the active surface area for sensing and (c) monitor carbonate activity. While highly sensitive to CO_2, the resistance of the nanocomposite is also found sensitive to humidity. This cross-sensitivity is corrected by using a bare-SWNT film as a reference sensor. However, the response time of this resistive sensor is

found to be unacceptably large for breath-by-breath CO_2 monitoring. Mathematical model inversion techniques developed to extract fast CO_2 input concentration data from the sensor's slow output do not work for such large response times.

A variation in the sensing methodology then helps improve the sensing speed of the nanocomposite film. In this variation, the capacitance of the nanocomposite film is measured rather than its resistance. However, this sensor too is found to be sensitive to humidity. Indeed, the sensing mechanism requires humidity to detect CO_2. Along with designs to decrease humidity fluctuations during respiratory monitoring, this sensor results in a portable, small and low-cost respiratory CO_2 sensor.

Future work on this sensor could involve:

1. Correcting long term drift in the sensor's response and increasing operation life-time using hardware/software techniques.
2. Development of an indoor air-quality CO_2 sensor based on the nanocomposite.
3. Development of nanocomposite sensors for other gases using SWNT and metal sulphate/nitrate composites.

REFERENCES

[1] American Society of Anesthesiologists, "Standards for basic anesthetic monitoring (approved by the ASA house of delegates on october 21, 1986, and last amended on october 25, 2005.) park ridge (IL):"

[2] D. M. Coventry, "Anaesthesia for laparoscopic surgery," *J. R. Coll. Surg. Edinb.,* vol. 40, pp. 151-160, Jun. 1995.

[3] M. S. Takrouri, "Anesthesia for laparoscopic general surgery. A special review," *Middle East J. Anesthesiol.,* vol. 15, pp. 39-62, Feb. 1999.

[4] K. Zwerneman, "End-Tidal Carbon Dioxide Monitoring: A VITAL Sign Worth Watching," *Crit. Care Nurs. Clin. North Am.,* vol. 18, pp. 217-225, 2006.

[5] B. D. Johnson, B. Whipp, R. J. Zeballos, I. M. Weisman, K. C. Beck, D. Mahler, J. Cotes, K. Sietsema and K. Killian, "Conceptual and physiological basis of cardiopulmonary exercise testing measurement," *Am. J. Respir. Crit. Care Med.,* vol. 167, pp. 228-238, 2003.

[6] M. Folke, L. Cernerud, M. Ekstrom and B. Hok, "Critical review of non-invasive respiratory monitoring in medical care," *Medical & Biological Engineering & Computing,* vol. 41, pp. 377-383, Jul. 2003.

[7] www.oridion.com, "Oridion Capnography," 2007.

[8] P. Gauthama and E. A. J. Morris, "Checking the capnograph before anaesthesia: a survey of national practice in the UK," *Eur. J. Anaesthesiol.,* vol. 23, pp. 160-164, 2006.

[9] P. BurdettSmith, "A patient who changed my practice - Always check the respiratory rate," *British Medical Journal,* vol. 314, pp. 1549-1549, May 24. 1997.

[10] P. B. Lovett, J. M. Buchwald, K. Sturmann and P. Bijur, "The vexatious vital: Neither clinical measurements by nurses nor an electronic monitor provides accurate measurements of respiratory rate in triage," *Annals of Emergency Medicine,* vol. 45, pp. 68-76, Jan. 2005.

[11] J. Butler, S. Hanumanthu, D. Chomsky and J. R. Wilson, "Frequency of low-risk hospital admissions for heart failure," *Am. J. Cardiol.,* vol. 81, pp. 41-44, 1998.

[12] J. B. O'Connell and M. R. Bristow, "Economic impact of heart failure in the United States: time for a different approach," *J. Heart Lung Transplant.,* vol. 13, pp. S107-12, Jul-Aug. 1994.

[13] D. Dodds, J. Purdy and C. Moulton, "The PEP transducer: a new way of measuring respiratory rate in the non-intubated patient," *Journal of Accident & Emergency Medicine,* vol. 16, pp. 26-28, Jan. 1999.

[14] D. Sankar and K. J. Kini, "Respiratory monitoring of non-intubated patients using the 'PIPPA' breathing monitor," *British Journal of Anaesthesia,* vol. 89, pp. 677P-677P, Oct. 2002.

[15] A. E. Hoyt, A. J. Ricco, J. W. Bartholomew and G. C. Osbourn, "SAW Sensors for the Room-Temperature Measurement of CO2 and Relative Humidity," *Anal. Chem.,* vol. 70, pp. 2137-2145, 1998.

[16] P. L. Kebabian and A. Freedman, "Fluoropolymer-based capacitive carbon dioxide sensor," *MEASUREMENT SCIENCE AND TECHNOLOGY,* vol. 17, pp. 703, 2006.

[17] A. Star, T. R. Han, V. Joshi, J. C. P. Gabriel and G. Gruener, "Nanoelectronic Carbon Dioxide Sensors," *Adv Mater,* vol. 16, pp. 2049-2052, 2004.

[18] S. Sivaramakrishnan, R. Rajamani, C. S. Smith, K. A. McGee, K. R. Mann and N. Yamashita, "Carbon nanotube-coated surface acoustic wave sensor for carbon dioxide sensing," *Sens. Act. B:Chem.,* vol. 132, pp. 296-304, 2008.

[19] A. Zribi, A. Knobloch, W. C. Tian and S. Goodwin, "Micromachined resonant multiple gas sensor," *Sensors & Actuators: A.Physical,* vol. 122, pp. 31-38, 2005.

[20] S. Chen, H. Hadano, Y. Ishiguro, M. Nakayama and K. Watanabe, "A NASICON CO2 gas sensor with drift-detection electrode," in *Instrumentation and Measurement Technology Conference, 2002. IMTC/2002. Proceedings of the 19th IEEE,* 2002,

[21] K. Kaneyasu, K. Otsuka, Y. Setoguchi, S. Sonoda, T. Nakahara, I. Aso and N. Nakagaichi, "A carbon dioxide gas sensor based on solid electrolyte for air quality control," *Sensors & Actuators: B.Chemical,* vol. 66, pp. 56-58, 2000.

[22] H. Yu, T. Cao, L. Zhou, E. Gu, D. Yu and D. Jiang, "Layer-by-Layer assembly and humidity sensitive behavior of poly (ethyleneimine)/multiwall carbon nanotube composite films," *Sensors and Actuators.B, Chemical,* vol. 119, pp. 512-515, 2006.

[23] M. Penza, F. Antolini and M. V. Antisari, "Carbon nanotubes as SAW chemical sensors materials," *Sensors and Actuators B,* vol. 100, pp. 47-59, 2004.

[24] H. E. Endres, R. Hartinger, M. Schwaiger, G. Gmelch and M. Roth, "A capacitive CO 2 sensor system with suppression of the humidity interference," *Sensors Actuators B: Chem.,* vol. 57, pp. 83-87, 1999.

[25] T. Baimpos, I. G. Giannakopoulos, V. Nikolakis and D. Kouzoudis, "Effect of Gas Adsorption on the Elastic Properties of Faujasite Films Measured Using Magnetoelastic Sensors," *Chem.Mater,* vol. 20, pp. 1470-1475, 2008.

[26] M. Matsui, "Carbon dioxide gas sensor with Li2TiSiO5 solid electrolyte and NiO-Li2CO3 as sensing electrode," *J.Ceram.Soc.Jap.,* vol. 111, pp. 848-851, 2003.

[27] F. Picaud, R. Langlet, M. Arab, M. Devel, C. Girardet, S. Natarajan, S. Chopra and A. M. Rao, "Gas-induced variation in the dielectric properties of carbon nanotube bundles for selective sensing," *J. Appl. Phys.,* vol. 97, pp. 114316, 2005.

[28] J. D. Adams, G. Parrott, C. Bauer, T. Sant, L. Manning, M. Jones, B. Rogers, D. McCorkle and T. L. Ferrell, "Nanowatt chemical vapor detection with a self-sensing, piezoelectric microcantilever array," *Appl. Phys. Lett.,* vol. 83, pp. 3428, 2003.

[29] C. Vancura, M. Ruegg, Y. Li, C. Hagleitner and A. Hierlemann, "Magnetically actuated complementary metal oxide semiconductor resonant cantilever gas sensor systems," *Anal. Chem.,* vol. 77, pp. 2690-2699, May 1. 2005.

[30] D. Lange, C. Hagleitner, A. Hierlemann, O. Brand and H. Baltes, "Complementary metal oxide semiconductor cantilever arrays on a single chip: mass-sensitive detection of volatile organic compounds," *Anal. Chem.,* vol. 74, pp. 3084-3095, Jul 1. 2002.

[31] C. L. Britton Jr, R. L. Jones, P. I. Oden, Z. Hu, R. J. Warmack, S. F. Smith, W. L. Bryan and J. M. Rochelle, "Multiple-input microcantilever sensors," *Ultramicroscopy,* vol. 82, pp. 17-21, Feb. 2000.

[32] J. Thaysen, A. D. Yalcinkaya, P. Vettiger and A. K. Menon, "Polymer-based stress sensor with integrated readout," *Journal of Physics D Applied Physics,* vol. 35, pp. 2698-2703, 2002.

[33] Figaro Engineering Inc., "Technical information for CDM 4160," 2007.

[34] B. Ostrick, J. Mühlsteff, M. Fleischer, H. Meixner, T. Doll and C. D. Kohl, "Adsorbed water as key to room temperature gas-sensitive reactions in work function type sensors: the carbonate–carbon dioxide system," *Sensors & Actuators: B.Chemical,* vol. 57, pp. 115-119, 1999.

[35] J. Herrán, G. G (a) Mandayo and E. Castaño, "Semiconducting BaTiO3-CuO mixed oxide thin films for CO2 detection," *Thin Solid Films,* vol. 517, pp. 6192-6197, 2009.

[36] E. J. Staples and S. Viswanathan, "Ultrahigh-speed chromatography and virtual chemical sensors for detecting explosives and chemical warfare agents," *IEEE Sensors Journal,* vol. 5, pp. 622-631, 2005.

[37] W. P. Jakubik, M. W. Urbanczyk and E. Maciak, "Palladium and metal-free phthalocyanine bilayer structures for hydrogen detection in the SAW sensor system based on interaction speed," *Ieee Sensors Journal,* vol. 6, pp. 1178-1185, OCT. 2006.

[38] A. Ricco, R. Crooks and G. Osbourn, "Surface acoustic wave chemical sensor arrays: new chemically sensitive interfaces combined with novel cluster analysis to detect volatile organic com pounds and mixture," *Acc. Chem. Res.,* vol. 31, pp. 289-296, 1998.

[39] G. Fischerauer, F. Dickert and R. Sikorski, "Telemetric surface acoustic wave chemical sensors," *Frequency Control Symposium, 1998.Proceedings of the 1998 IEEE International,* pp. 608-614, 1998.

[40] A. Pohl, "Review of wireless SAW sensors," *IEEE Trans. Ultrason. Ferroelectr. Freq. Control,* vol. 47, pp. 317-332, 2000.

[41] L. Reindl, G. Scholl, T. Ostertag, H. Scherr, U. Wolff and F. Schmidt, "Theory and application of passive SAW radio transponders as sensors," *Ultrasonics, Ferroelectrics and Frequency Control, IEEE Transactions on,* vol. 45, pp. 1281-1292, 1998.

[42] A. J. Ricco and S. J. Martin, "Thin metal film characterization and chemical sensors: Monitoring electronic conductivity, mass loading and mechanical properties with surface acoustic wave devices," *Metallurgical Coatings and Thin Films; Proceedings of the International Conference, 18th, San Diego, CA, Apr.22-26, 1991.Vols.1 & 2.A95-79256, p.94-101,* 1991.

[43] B. A. Auld, *Acoustic Fields and Waves in Solids. Vol. 2.* Wiley, 1990,

[44] www.sandia.gov/mstc/technologies/microsensors/paws.html, "Portable acoustic wave sensor systems (PAWS),"

[45] R. Zhou, A. Hierlemann, U. Weimar, D. Schmeizer and W. Gopel, "Mass Sensitive Detection Of CO/sub 2/By Aminogroup-functionalized Polymers," *Solid-State Sensors and Actuators, 1995 and Eurosensors IX.Transducers' 95.the 8th International Conference on,* vol. 1, 1995.

[46] J. Galipeau, L. LeGore, J. Caron, J. Vetelino, K. Snow and J. Andle, "The integration of a chemiresistive film overlay with a surface acoustic wave microsensor," *Sensors Actuators B: Chem.,* vol. 35, pp. 158-163, 1996.

[47] A. Ricco, S. Martin and T. Zipperian, "Surface acoustic wave gas sensor based on film conductivity changes," *International Conference on Solid-State Sensors and Actuators/Transducers' 85/, 3rd, Philadelphia, PA, June 11-14, 1985) Sensors and Actuators (ISSN 0250-6874),* vol. 8, pp. 319-333, 1985.

[48] O. Varghese, P. Kichambre, D. Gong, K. Ong, E. Dickey and C. Grimes, "Gas sensing characteristics of multi-wall carbon nanotubes," *Sensors and Actuators B,* vol. 81, pp. 32-41, 2001.

[49] A. Star, T. R. Han, V. Joshi and J. R. Stetter, "Sensing with Nafion Coated Carbon Nanotube Field-Effect Transistors," *Electroanalysis,* vol. 16, pp. 108-112, 2004.

[50] T. Zhang, S. Mubeen, E. Bekyarova, B. Y. Yoo, R. C. Haddon, N. V. Myung and M. A. Deshusses, "Poly (m-aminobenzene sulfonic acid) functionalized single-walled carbon nanotubes based gas sensor," *Nanotechnology,* vol. 18, pp. 165504, 2007.

[51] K. G. Ong, K. Zeng and C. Grimes, "A wireless, passive carbon nanotube-based gas sensor," *IEEE Sensors Journal,* vol. 2, pp. 82-88, 2002.

[52] P. Avouris, J. Appenzeller, R. Martel and S. J. Wind, "Carbon nanotube electronics," *Proc IEEE,* vol. 91, pp. 1772-1784, 2003.

[53] T. Ozel, A. Gaur, J. A. Rogers and M. Shim, "Polymer electrolyte gating of carbon nanotube network transistors," *Nano Lett.,* vol. 5, pp. 905-911, May. 2005.

[54] M. Penza, M. Tagliente, P. Aversa, M. Re and G. Cassano, "The effect of purification of single-walled carbon nanotube bundles on the alcohol sensitivity of nanocomposite Langmuir–Blodgett films for SAW sensing applications," *Nanotechnology,* vol. 18, pp. 185502, 2007.

[55] N. Saran, K. Parikh, D. S. Suh, E. Munoz, H. Kolla and S. K. Manohar, "Fabrication and characterization of thin films of single-walled carbon nanotube bundles on flexible plastic substrates," *J. Am. Chem. Soc.,* vol. 126, pp. 4462-4463, 2004.

[56] X. Yu, R. Rajamani, K. A. Stelson and T. Cui, "Carbon nanotube based transparent conductive thin films," *Journal of Nanoscience and Nanotechnology,* vol. 6, pp. 1939-1944, JUL. 2006.

[57] S. Martin and A. Ricco, "Effective utilization of acoustic wave sensor responses: simultaneous measurement of velocity and attenuation," *Ultrasonics Symposium, 1989.Proceedings., IEEE 1989,* pp. 621-625, 1989.

[58] B. Chachulski, J. Gebicki, G. Jasinski, P. Jasinski and A. Nowakowski, "Properties of a polyethyleneimine-based sensor for measuring medium and high relative humidity," *Measurement Science and Technology,* vol. 17, pp. 12-16, 2006.

[59] A. Zribi, A. Knobloch and R. Rao, "CO2 detection using carbon nanotube networks and micromachined resonant transducers," *Appl. Phys. Lett.,* vol. 86, pp. 203112, 2005.

[60] S. H. Lim, "Chemical vapor detection using nanomechanical platform," *Journal of Mechanical Science and Technology,* vol. 21, pp. 1876-1880, 2007.

[61] K. M. Hansen, H. F. Ji, G. Wu, R. Datar, R. Cote, A. Majumdar and T. Thundat, "Cantilever-based optical deflection assay for discrimination of DNA single-nucleotide mismatches," *Anal. Chem.*, vol. 73, pp. 1567-1571, Apr 1. 2001.

[62] S. Satyanarayana, D. T. McCormick and A. Majumdar, "Parylene micro membrane capacitive sensor array for chemical and biological sensing," *Sensors & Actuators: B.Chemical*, vol. 115, pp. 494-502, 2006.

[63] Y. Chen, R. C. Jaeger and J. C. Suhling, "Delta-Sigma Based CMOS Stress Sensor with RF Output," *Solid-State Circuits Conference, 2006.ASSCC 2006.IEEE Asian*, pp. 243-246, 2006.

[64] S. J. Martin, G. C. Frye and S. D. Senturia, "Dynamics and Response of Polymer-Coated Surface Acoustic Wave Devices: Effect of Viscoelastic Properties and Film Resonance," *Anal. Chem.*, vol. 66, pp. 2201-2219, 1994.

[65] R. Rodriguez, J. Chung, K. Lee and J. Lee, "Bio/chemical Sensing by Thin Membrane Transducers," *ASME International Mechanical Engineering Congress and Exposition, Anaheim*, 2004.

[66] V. Tsouti, S. Chatzandroulis, D. Goustouridis, P. Normand and D. Tsoukalas, "Design and fabrication of a Si micromechanical capacitive array for DNA sensing," *Microelectronic Engineering*, vol. doi:10.1016/j.mee.2007.12.075, 2008.

[67] D. Piyabongkarn, Y. Sun, R. Rajamani, A. Sezen and B. J. Nelson, "Travel range extension of a MEMS electrostatic microactuator," *Control Systems Technology, IEEE Transactions on*, vol. 13, pp. 138-145, 2005.

[68] P. R. L. Malenfant, W. V. Cicha, P. A. Bui and D. L. Simone, "Nanotubes and methods of dispersing and separating nanotubes," *U. S. Pat. 72476702007*, 2007.

[69] R. S. Loewe, S. M. Khersonsky and R. D. McCullough, "A Simple Method to Prepare Head-to-Tail Coupled, Regioregular Poly (3-alkylthiophenes) Using Grignard Metathesis," *Adv Mater*, vol. 11, pp. 250-253, 1999.

[70] M. Z. Jacobson, *Fundamentals of Atmospheric Modeling.* Cambridge University Press, 2005,

[71] P. C. P. Watts, N. Mureau, Z. Tang, Y. Miyajima, J. D. Carey and S. R. P. Silva, "The importance of oxygen-containing defects on carbon nanotubes for the detection of polar and non-polar vapours through hydrogen bond formation," *Nanotechnology*, vol. 18, pp. 175701, 2007.

[72] Figaro Engineering Inc., "TGS 4160 product information," 2006.

[73] Nonin Medical Inc., "LifeSense brochure," 2007.

[74] B. Ostrick, M. Fleischer, H. Meixner and C. D. Kohl, "Investigation of the reaction mechanisms in work function type sensors at room temperature by studies of the cross-sensitivity to oxygen and water: the carbonate–carbon dioxide system," *Sensors & Actuators: B.Chemical,* vol. 68, pp. 197-202, 2000.

[75] B. Liao, Q. Wei, K. Wang and Y. Liu, "Study on CuO–BaTiO3 semiconductor CO2 sensor," *Sensors & Actuators: B.Chemical,* vol. 80, pp. 208-214, 2001.

[76] A. Prim, E. Pellicer, E. Rossinyol, F. Peiró, A. Cornet and J. R. Morante, "A novel mesoporous CaO-loaded In2O3 material for CO2 sensing," *Advanced Functional Materials,* vol. 17, pp. 2957, 2007.

[77] M. Penza, P. Aversa, G. Cassano, W. Wlodarski and K. Kalantar-Zadeh, "Layered SAW gas sensor with single-walled carbon nanotube-based nanocomposite coating," *Sensors & Actuators: B.Chemical,* vol. 127, pp. 168-178, 2007.

[78] W. E. Ford, A. Yasuda and J. M. Wessels, "Microcrystalline Composite Particles of Carbon Nanotubes and Calcium Carbonate," *Langmuir,* vol. 24, pp. 3479-3485, 2008.

[79] E. S. Snow, F. K. Perkins, E. J. Houser, S. C. Badescu and T. L. Reinecke, "Chemical detection with a single-walled carbon nanotube capacitor," *Science,* vol. 307, pp. 1942-1945, 2005.

[80] J. Herrán, G. Mandayo, N. Pérez, E. Castano, A. Prim, E. Pellicer, T. Andreu, F. Peiró, A. Cornet and J. R. Morante, "On the structural characterization of BaTiO3–CuO as CO2 sensing material," *Sensors & Actuators: B.Chemical,* vol. 133, pp. 315-320, 2008.

[81] W. E. Ford, A. Yasuda and J. M. Wessels, "Microcrystalline Composite Particles of Carbon Nanotubes and Calcium Carbonate," *Langmuir,* vol. 24, pp. 3479-3485, 2008.

[82] C. W. Lam, J. T. James, R. McCluskey and R. L. Hunter, "Pulmonary toxicity of single-wall carbon nanotubes in mice 7 and 90 days after intratracheal instillation," *Toxicological Sciences,* vol. 77, pp. 126, 2004.

[83] J. Muller, F. Huaux, N. Moreau, P. Misson, J. F. Heilier, M. Delos, M. Arras, A. Fonseca, J. B. Nagy and D. Lison, "Respiratory toxicity of multi-wall carbon nanotubes," *Toxicol. Appl. Pharmacol.,* vol. 207, pp. 221-231, 2005.

[84] http://capnostat.respironics.com, "Capnostat, Philips Respironics,"

[85] T. Kirschke and J. Heisig, "Respiratory sensor system (RSS) for in situ breath measurement: O2, CO2 and flow, based on a MSP430F149,"